Journal of Dynamics and Differential Equations (2019) 31:153–203
https://doi.org/10.1007/s10884-018-9694-7

Pinned Solutions in a Heterogeneous Three-Component FitzHugh–Nagumo Model

Peter van Heijster[1] · Chao-Nien Chen[2] · Yasumasa Nishiura[3] · Takashi Teramoto[4]

Received: 28 April 2017 / Revised: 26 May 2018 / Published online: 11 August 2018

Abstract
We analyse pinned front and pulse solutions in a singularly perturbed three-component FitzHugh–Nagumo model with a small jump-type heterogeneity. We derive explicit conditions for the existence and stability of these type of pinned solutions by combining geometric singular perturbation techniques and an action functional approach. Most notably, in certain parameter regimes we can explicitly compute the pinning distance of a localised solution to the defect.

Keywords Reaction–diffusion equations · Defects · Calculus of variations · Singular perturbations · Existence · Stability · Localised defect solutions

Mathematics Subject Classification 34A34 · 34A36 · 34C37 · 35B25 · 35B35 · 35K57 · 49J40

1 Introduction

Systems of partial differential equations (PDEs) with spatial heterogeneities, i.e. defect systems, have received a lot of attention in the literature over the past few decades [1,3,17,18,30,34–37,50,54,59–62, e.g.] and defect systems have been mentioned as potentially being used in device applications [27,43, e.g.]. In this manuscript, we study a singularly

PvH was supported under the Australian Research Councils Discovery Early Career Researcher Award funding scheme DE140100741. Part of the work was done when CNC was visiting QUT and he is grateful for the support by the Ministry of Science and Technology of Taiwan. YN is partially supported by KAKENHI 26247015 and JSPS A3 Foresight Program. TT is partially supported by KAKENHI Grant-in-Aid for Scientific Research 17K05355.

✉ Peter van Heijster
petrus.vanheijster@qut.edu.au

1 School of Mathematical Sciences, Queensland University of Technology, Brisbane, QLD 4001, Australia

2 Department of Mathematics, National Tsing Hua University, Hsinchu 300, Taiwan

3 WPI Advanced Institute for Materials Research, Tohoku University, Sendai 980-8577, Japan

4 School of Medicine, Asahikawa Medical University, Asahikawa 078-8510, Japan

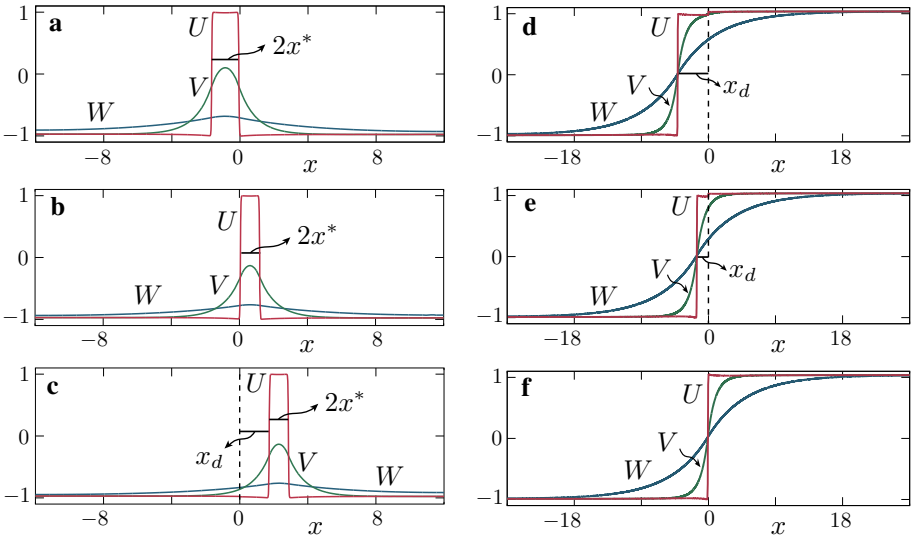

Fig. 1 Pinned defect pulse and front solutions supported by (1) obtained by simulating the time-independent version of (1), i.e. by simulating (10), on a domain of length 24. The system parameters used for the simulations in panels **a–c** are $(\alpha, \beta, D, \gamma_1, \gamma_2, \varepsilon) = (3, 2, 5, 2, 2.5, 0.02)$, while the system parameters used in the panels **d–f** are $(\alpha, \beta, D, \gamma_1, \gamma_2, \varepsilon) = (3, -2, 5, 0.02, -5, 0.02)$

perturbed three-component FitzHugh–Nagumo defect model

$$\begin{cases} U_t = \varepsilon^2 U_{xx} + U - U^3 - \varepsilon(\alpha V + \beta W + \gamma(x)) \,, \\ \tau V_t = V_{xx} + U - V \,, \\ \theta W_t = D^2 W_{xx} + U - W \,, \end{cases} \tag{1}$$

with a small jump-type heterogeneity, or defect, at $x = 0$:

$$\gamma(x) = \begin{cases} \gamma_1 \,, & \text{for } x \leq 0 \,, \\ \gamma_2 \,, & \text{for } x > 0 \,. \end{cases} \tag{2}$$

Here, $0 < \varepsilon \ll 1$; $D > 1$; $\tau, \theta > 0$; $(x, t) \in \mathbb{R} \times \mathbb{R}^+$; $\alpha, \beta, \gamma_{1,2} \in \mathbb{R}$ and all parameters are *a priori* assumed to be $\mathcal{O}(1)$ with respect to ε. We are particularly interested in stationary localised solutions supported by (1) whose interfaces are pinned away from the defect, see, for instance, panels "c–e" of Fig. 1. Following [24], we call this type of pinned solutions *local defect solutions* and we call the distance of the interface to the defect the *pinning distance*.

For completeness, we first recall the definitions of the big-$\mathcal{O}$-notation and the big-Θ-notation.

Definition 1 *(Adapted from* [29]*)*

- $h_1 = \mathcal{O}(\phi_1)$ as $\varepsilon \downarrow \varepsilon_0$ if there are constants $k_0 > 0$ and ε_1 such that $|h_1(\varepsilon)| \leq k_0 |\phi_1(\varepsilon)|$ for $\varepsilon_0 < \varepsilon < \varepsilon_1$.
- $h_2 = \Theta(\phi_2)$ as $\varepsilon \downarrow \varepsilon_0$ if there are constants $k_0, k_1 > 0$ and ε_1 such that $k_1 |\phi_2(\varepsilon)| \leq |h_2(\varepsilon)| \leq k_0 |\phi_2(\varepsilon)|$ for $\varepsilon_0 < \varepsilon < \varepsilon_1$.

By combining Geometrical Singular Perturbation Theory (GSPT) [25,31,32] with an action functional approach [52], we derive the following result related to the the existence and stability of local defect front and pulse solutions.

Main Result 1 *Let ε be small enough and let τ and θ be bounded by some $\mathcal{O}(1)$-constant.*[1]

If $\gamma_1 = \varepsilon\tilde{\gamma}_1$, with $\tilde{\gamma}_1 = \Theta(1)$, $(\alpha, \beta, D, \gamma_2)$ are $\Theta(1)$ such that $\tilde{\gamma}_1 - \gamma_2 = \Theta(1)$ and if there exist an $x_d > 0$ solving

$$2\tilde{\gamma}_1 - \frac{1}{2}\gamma_2 f(x_d) = 0\,, \quad \text{with} \quad f(x_d) := \alpha e^{-x_d} + \beta e^{-x_d/D}\,, \tag{3}$$

then (1) supports a local defect front solution $Z^{\ell}_{f,ld} = (U^{\ell}_{f,ld}, V^{\ell}_{f,ld}, W^{\ell}_{f,ld})$ that asymptotes to $\pm 1 + \mathcal{O}(\varepsilon)$ as $x \to \pm\infty$ and which is pinned to the left of the defect with leading order pinning distance x_d. The local defect front solution $Z^{\ell}_{f,ld}$ is stable if and only if

$$\gamma_2 g(x_d) > 0\,, \quad \text{with} \quad g(x_d) := \alpha e^{-x_d} + \frac{\beta}{D} e^{-x_d/D}\,. \tag{4}$$

If $(\alpha, \beta, D, \gamma_1, \gamma_2)$ are $\Theta(1)$ such that $\gamma_1 - \gamma_2 = \Theta(1)$ and if there exist an $x^* > 0$ and $x_d > 0$ solving

$$f(2x^*) = \gamma_2\,, \qquad f(x_d) = f(x_d + 2x^*), \tag{5}$$

then (1) supports a local defect pulse solution $Z^{r}_{p,ld} = (U^{r}_{p,ld}, V^{r}_{p,ld}, W^{r}_{p,ld})$ that asymptotes to $-1 + \mathcal{O}(\varepsilon)$ as $x \to \pm\infty$ and which is pinned to the right of the defect with leading order width[2] *$2x^*$ and leading order pinning distance x_d. The local defect pulse solution $Z^{r}_{p,ld}$ is stable if and only if*

$$g(2x^*) > 0\,, \quad \text{and} \quad (\gamma_2 - \gamma_1)(g(x_d) - g(x_d + 2x^*)) > 0\,. \tag{6}$$

To understand the implications of Main Result 1, we take a closer look at the existence conditions (3) and (5), and stability conditions (4) and (6). If α and β have the same sign, then f is monotonic. Consequently, the existence condition (3) for local defect front solutions pinned to the left of the defect has at most one solution, while the existence conditions (5) for local defect pulse solutions pinned to the right of the defect has no solutions. In other words, if α and β have the same sign—and if the other system parameters are chosen appropriately—then Main Result 1 gives the existence of a local defect front solutions pinned to the left of the defect. After noting that $g(x_d) = -f'(x_d)$, we get from (4) that this solution is stable only if α and γ_2 have the same sign.

If α and β have opposite signs (however, see Remark 2), then, by the particulars of f, (3) has at most two distinct solutions. Consequently, and if the other system parameters are chosen appropriately, Main Result 1 gives the existence of (at most) two local defect front solutions pinned to the left of the defect and with different pinning distances. If $\alpha\gamma_2 > 0$, then the local defect front solution with the smaller pinning distance is stable, while the other local defect front solution is unstable. The opposite holds for $\alpha\gamma_2 < 0$. Main Result 1 also gives, if the other system parameters are chosen appropriately, the existence of (at most) two local defect pulse solutions pinned to the right of the defect and with different pinning distances. If $\beta < 0 < \alpha$ and $\gamma_2 > \gamma_1$, then the local defect pulse solution with the smaller

[1] Whilst the parameters τ and θ do not explicitly appear anywhere in the derivation of the results of Main Result 1, the $\mathcal{O}(1)$-bounds on them are needed to ensure that the stability framework of [7,9,10] carries over, see also [53].

[2] For historical reasons we represent the width of the pulse by $2x^*$, rather than by x^* [23,53].

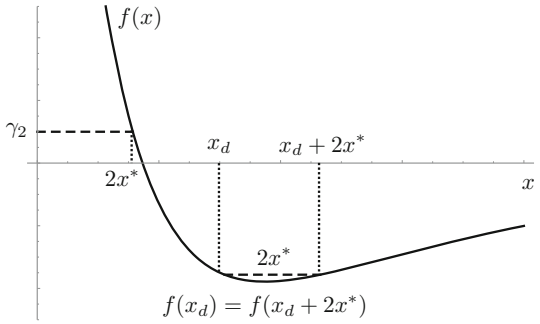

Fig. 2 Graphical representation of the existence condition (5) and the stability condition (6) of Main Result 1 related to local defect pulse solutions $Z^r_{p,ld}$. Here, the first existence condition $f(2x^*) = \gamma_2$ (5) has a unique solution $2x^*$ and since $g(x) = -f'(x)$, we have that $g(2x^*) > 0$ (6). The second existence condition $f(x_d) = f(x_d + 2x^*)$ (5) yields a unique pinning distance x_d and $g(x_d) - g(x_d + 2x^*) > 0$. Thus, by (6), the related local defect pulse solution $Z^r_{p,ld}$ is stable if $\gamma_2 > \gamma_1$ and unstable if $\gamma_2 < \gamma_1$

width is stable, while the other local defect front solution is unstable. Both local defect pulse solutions are unstable if $\beta < 0 < \alpha$ and $\gamma_2 < \gamma_1$. The opposite holds for $\alpha < 0 < \beta$. See also Fig. 2. More details are given in the remainder of this manuscript, see, in particular, Sect. 3.2, Sect. 4.2, and Tables 1 and 2.

For $x \neq 0$, (1) has the symmetries

$$(U, V, W, x, \gamma_1, \gamma_2) \mapsto -(U, V, W, x, \gamma_2, \gamma_1), \tag{7}$$

and

$$(x, \gamma_1, \gamma_2) \mapsto (-x, \gamma_2, \gamma_1). \tag{8}$$

From Main Result 1 and the symmetries one can directly derive existence and stability conditions for local defect front and pulse solutions that asymptote to $1 + \mathcal{O}(\varepsilon)$ as $x \to -\infty$ and/or local defect front and pulse solutions that are pinned in the opposite γ_i-region (so on the other side of the defect). For brevity of presentation, we do not explicitly state these additional results. Furthermore, we assume, without loss of generality, that defect solutions asymptote to $-1 + \mathcal{O}(\varepsilon)$ as $x \to -\infty$ in the remainder of the manuscript (unless stated otherwise).

Remark 1 The results presented in Main Result 1 are not rigorous since not all the functional analytic details of the methodology of combining geometric singular perturbation techniques and an action functional approach have been fully worked out. Many of the functional analytic details of the approach are given in all detail in series of papers by Chen and collaborators [5–12] for slightly different problems and these methods can be generalised to the setting of the current manuscript, see also [52]. However, these generalisations are a nontrivial exercise and we decided to not proceed this direction (for the readability of the manuscript). Instead, we explain the essentials of the approach in some detail in Sect. 2, see, in particular, Sect. 2.2, and we test the results of Main Result 1 against numerical simulations and we get excellent agreement, see, in particular, Figs. 5, 6, 10, and 11. Further, in [52] we introduced this methodology for the homogeneous version of (1) and used it to explicitly replicate known rigorous results regarding the existence and stability of localised solutions from [23,53,55].

1.1 Background of the Model

A dimensional homogeneous version of (1)—so with $\gamma_1 = \gamma_2 = \gamma(x)$—was introduced in the nineties to study gas-discharge systems [42,48]. Versions of the dimensional—and nondimisionalised—homogeneous model have been studied intensively afterwards, see [2, 15,23,28,39,46,51–53,55–58, e.g.] and references therein. From a mathematical point of view, the homogeneous version of (1) is arguably the most mathematically rigorously studied singularly perturbed three-component reaction–diffusion equation. It is not a surprise that the homogeneous version of (1) supports stable slowly travelling front solutions with speed $c = \frac{3}{2}\sqrt{2}\varepsilon^2\gamma$ [55], since the homogeneous model can be seen as a weakly perturbed Allen-Cahn type equation [4,15,26]. Consequently, stationary front solutions exist only for $\gamma \equiv 0$. In [23], it was shown there exist a (family of) stationary pulse solution(s) with leading order width $2x^*$ if there is an $x^* > 0$ solving $f(2x^*) = \gamma$, where f is defined in (3). By using the NonLocal Eigenvalue Problem approach for Evans functions [20–22], it was shown in [53] that the critical part of the spectrum associated with a stationary pulse solution consists of a translation invariance eigenvalue at the origin and a critical eigenvalue $\lambda = -3\sqrt{2}\varepsilon^2 g(2x^*)$, where g is defined in (4). The remaining subset of the spectrum is contained in the left half-plane bounded away from the imaginary axis with an $\mathcal{O}(1)$-bound and there are no complex-valued eigenvalues for τ and θ of $\mathcal{O}(1)$. Thus, the stationary pulse solution is stable if $g(2x^*) > 0$. In other words, the existence and stability conditions for homogeneous stationary pulse solutions coincide with the first conditions for the existence and stability of local defect pulse solutions of Main Result 1.

In [52], we reproduced the above mentioned existence and stability results for homogeneous stationary front and pulse solutions by combining GSPT techniques with an action functional approach. The action functional approach for a mono-stable or a bi-stable two-component FitzHugh–Nagumo model without small diffusion was pioneered by Chen and collaborators in a series of papers [5–7,9,10,12]. In [52] it was shown that the action functional J for a stationary homogeneous pulse solution (u, v, w)—whose profile with unknown width is computed by GSPT—is given by

$$\begin{aligned} J(u) = \int_{-\infty}^{\infty} \Big(&\frac{1}{2}\varepsilon^2 u_x^2 + F(u) - F(\bar{u}_\gamma) + \frac{1}{2}\varepsilon\alpha(u\mathcal{L}_1 u - \bar{u}_\gamma^2) \\ &+ \frac{1}{2}\varepsilon\beta(u\mathcal{L}_2 u - \bar{u}_\gamma^2) + \varepsilon\gamma(u - \bar{u}_\gamma)\Big)\, dx, \end{aligned} \tag{9}$$

with antiderivative $F(u) = \frac{1}{4}u^4 - \frac{1}{2}u^2$, $\bar{u}_\gamma$ the steady state of the system near -1 (see (11)), $\mathcal{L}_1 := (-\frac{d^2}{dx^2} + 1)^{-1}$, $\mathcal{L}_2 := (-D^2\frac{d^2}{dx^2} + 1)^{-1}$. Consequently, the existence condition determining the width of the pulse solution follows from the critical points of J (with respect to the unknown width) and the stability condition follows from the minimisers of J. We derive Main Result 1 for the heterogeneous model (1) by utilising, and extending, this action functional approach of [52] (however, see Remark 1).

(Versions of) the heterogeneous model (1), and the effect of the defect, have also been studied [24,41,54,61,62, e.g.]. We shortly discuss the results of [24,54] as they are most relevant for this manuscript. Since the heterogeneous model (1) is, in contrast to the homogeneous model, not translation invariant, a stationary solution is typically isolated and does not come as a family of solutions. Moreover, since the defect is small it does not alter the spectrum in a leading order fashion and the perturbed translation invariant eigenvalue (at the origin for the homogeneous case) will determine the fate of the stability of a defect solution (there are no leading complex-valued eigenvalues since τ and θ are $\mathcal{O}(1)$ [53]). In [54] it was

shown that, under certain parameter conditions, (1) supports so-called stable pinned *global defect solutions* [24]. That is, stationary front and pulse solutions with one of the interfaces pinned at the defect (this in contrast to local defect solutions were the interfaces are pinned away from the defect). In particular, it was shown that global defect front solutions exist if $\gamma_1\gamma_2 < 0$ and that they are stable if, in addition, $\gamma_1 > 0$, see also panel "e" of Fig. 1. For the global defect pulse solutions it was shown that the widths of the pinned pulse solutions are, to leading order, given by $2x^*$, where $2x^*$ solves $f(2x^*) = \min\{\gamma_1, \gamma_2\}$, see also panel "a" of Fig. 1. That is, they correspond to the widths of the pulse solutions in the homogeneous case with $\gamma = \min\{\gamma_1, \gamma_2\}$.

Local defect solutions were investigated numerically in [54] since the analytic methods employed in [54] cannot be used directly to study local defect solutions. This is due to the fact that the interaction of the defect with the localised interfaces is weak—due to the $\Theta(1)$-distance between them—and higher order computations are needed. For instance, a leading order GSPT analysis appended with a Melnikov integral [47] gives that the leading order width $2x^*$ of a local defect pulse solution is—again—given by the roots of $f(2x^*) = \gamma_i$, see also panels "b" and "c" of Fig. 1. In other words, the widths of the pinned pulse solutions are in essence not affected by the introduction of the small defect. However, the pinning distance x_d cannot be determined from this leading order analysis.

Since the system parameters used for the simulations of the pinned pulse (front) solutions in Fig. 1 are all the same, we have the co-existence of local and global defect pulse (front) solutions. Moreover, the numerically stable local defect pulse solution shown in panel "c" of Fig. 1 is pinned in the region to the right of the defect (where $\gamma(x) = \gamma_2$), while the numerically stable global defect pulse solution shown in panel "a" of Fig. 1 is pinned in the opposite region to the left of the defect (where $\gamma(x) = \gamma_1$). The two stable pinned pulse solutions are separated by a numerically unstable pinned pulse solution shown in panel "b" of Fig. 1. This unstable pulse is pinned at the defect in the γ_2-region and has a width similar as the stable local defect pulse solution. This unstable pinned pulse solution acts as the *separatrix* between the two stable pinned pulse solutions and is called the *scatter solution* [39–41,50,62].

In [24], the authors used geometric methods to study the persistence of heteroclinic and homoclinic orbits for a general system of ordinary differential equations (ODEs) with a weak defect and under generic conditions on the nonlinearities. The ODE associated to pinned defect solutions of (1) (see (10)) fits into an extended version of this general system, see also Remark 1.13 of [24]. Consequently, some of the results of [24] are directly applicable here.

Theorem 2 (adopted from Thms. 4.7 and 4.8 of [24]) *Let $\gamma(x)$ be as in (2) and let ε be small enough. Moreover, let $\alpha > 0$, $\beta > 0$, $\gamma_2 \in \mathbb{R}$ be $\mathcal{O}(1)$ with respect to ε.*

- *If $\gamma_1 = 0$, then (1) supports a local defect front solution $Z^\ell_{f,ld} = (U^\ell_{f,ld}, V^\ell_{f,ld}, W^\ell_{f,ld})$ that asymptotes to $\pm 1 + \mathcal{O}(\varepsilon)$ as $x \to \pm\infty$ and with its front pinned to the left of the defect.*
- *If $0 < \gamma_1 < \alpha + \beta$, then (1) supports a local defect pulse solution $Z^\ell_{p,ld} = (U^\ell_{p,ld}, V^\ell_{p,ld}, W^\ell_{p,ld})$ that asymptotes to $-1 + \mathcal{O}(\varepsilon)$ as $x \to -\infty$ and with its pulse pinned to the left of the defect.*

Whilst Theorem 2 partly settles the question related to the existence of local defect front and pulse solutions supported by (1), it has several limitations. Firstly, it requires that both α and β are positive and does not provide any insights for α and/or β negative. See, however, Remark 2. Secondly, Theorem 2 does not provide any information regarding the profiles—and thus also not regarding the pinning distances—of the local defect solutions. Thirdly,

for the existence of local defect front solutions it is required that $\gamma_1 = 0$—this to ensure the existence of a stationary front solution in the homogeneous case [55]—while one would also expect local defect front solutions for γ_1 small, but not zero. Finally, Theorem 2 does not provide any information regarding the stability of the local defect solutions. The results of this manuscript as stated in Main Result 1 (partly) address the above issues and thus significantly extend the results of [24]. In particular, we put *a priori* no additional restrictions on the parameters and determine leading order expressions for the pinning distances x_d. In addition, we also determine the stability of the local defect solutions.

Remark 2 From Main Result 1 it follows that the most interesting results of this manuscript relate to the case where $\alpha\beta < 0$. For instance, the second existence condition of (5) implies that, in this case only, the pinning distance $x_d = \Theta(1)$ (since f is monotonic for $\alpha\beta > 0$). The original activator–inhibitor framework of the homogeneous version of (1) [42,48, e.g.] actually required that both α and β were positive. However, this restriction is mathematically not necessary and the dynamics of the homogeneous and heterogeneous model is much richer without it. See, for instance, [23,24,58].

1.2 Outlook

We derive Main Result 1 by combining GSPT techniques with the action functional approach of [52]. In short, GSPT techniques will provide the profile of a local defect solution—with unknown width (for a pulse) and unknown pinning distance (for both a front and a pulse). The critical points of the action functional landscape of the derived profile determine the potential widths and pinning distances of the local defect solution under consideration and only the minimisers of the action functional yield stable local defect solutions. In Sect. 2, we discuss this action functional approach in more detail and show how to append the action functional (9) of the homogeneous case as to deal with the heterogeneity of (1).

Besides local and global defect solutions, another type of defect solutions—the *trivial defect solution* – was introduced in [24]. This type of defect solution is characterised by the fact that it stays $\mathcal{O}(\varepsilon)$-close to both asymptotic end states over the whole spatial domain. That is, a trivial defect solution is—in some sense—a small perturbation of a steady state solution and can thus be seen as the heterogeneous equivalent of a homogeneous steady state solution. It was shown in [24] that, under generic conditions, trivial defect solutions exist and are unique—in the sense that there is exactly one trivial defect solution near each of the steady states. The homogenous version of (1) has two steady state solutions (near $(U, V, W) = \pm(1, 1, 1)$) that fulfil these generic conditions, and, consequently, (1) has two trivial defect solutions $Z_{td}^{\pm} = (U_{td}^{\pm}, V_{td}^{\pm}, W_{td}^{\pm})$. Whilst pinned local defect solutions are the main subject of interest of this manuscript, we also explicitly determine the profiles of these trivial defect solutions $Z_{td}^{\pm}$ in "Appendix A". We add the derivation of these profiles for completeness, but also to illustrate how the region around the defect should be handled from an asymptotic perspective.[3] Specifically, we show that the defect introduces two new *fast regions* where the dynamics of the U-component dominates, one just to the left of the defect and one just to the right of the defect. To leading order, these additional fast regions do not contribute to the profile of the trivial defect solutions, i.e. the profiles are to leading order ± 1 in both fast regions, but they do contribute at an $\mathcal{O}(\varepsilon)$-level. Heuristically, local defect solutions can be seen as a concatenation of the equivalent stationary solution to the

[3] Observe that the trivial defect solutions $Z_{td}^{\pm}$ can also be studied with variational methods.

homogenous model with one of the trivial defect solutions.[4] Therefore, obtaining insights in these trivial defect solutions is also a first crucial step towards understanding local defect solutions.

In Sect. 3, we derive the part of Main Result 1 related to local defect front solutions $Z^{\ell}_{f,ld}$ pinned to the left of the defect and determine the profile—up to and including $\mathcal{O}(\varepsilon)$-terms—of these solutions. We also use the action functional approach to study global defect front solutions $Z_{f,gd}$ and reproduce the key results of [54] related to the existence ($\gamma_1\gamma_2 < 0$) and stability ($\gamma_1 > 0 > \gamma_2$) of these global defect front solutions (note that only leading order computations are needed to obtain these results). Finally, we combine the results for local and global defect front solutions and we numerically investigate the stationary version of (1) to confirm the asymptotic findings.

In Sect. 4, we follow the same procedure as in Sect. 3 but now for defect pulse solutions. That is, we derive the part of Main Result 1 related to local defect pulse solutions $Z^{r}_{p,ld}$ pinned to the right of the defect and determine the profile—up to and including $\mathcal{O}(\varepsilon)$-terms—of these solutions. Most of this derivation has been placed in "Appendix B" since it is very similar to the derivation in Sect. 3 and it is only algebraically more involved (the GSPT procedure now determines the profiles up to two unknowns, the pinning distance x_d and the pulse width $2x^*$). We also discuss the connection of the action functional approach and the results for global defect pulse solutions $Z_{p,gd}$ from [54] and combine these results to obtain a broader picture for pinned pulse solutions. Finally, we numerically investigate the stationary version of (1) to confirm the asymptotic findings.

We end this manuscript with a summary and a short outlook on future projects.

2 GSPT and the Action Functional Approach

Pinned solutions to (1) solve the following system of ODEs

$$\begin{cases} 0 = \varepsilon^2 u_{xx} + u - u^3 - \varepsilon(\alpha v + \beta w + \gamma(x)), \\ 0 = v_{xx} + u - v, \\ 0 = D^2 w_{xx} + u - w, \end{cases} \tag{10}$$

and they asymptote to the *asymptotic end states* $(\bar{u}_{\gamma_i}, \bar{u}_{\gamma_i}, \bar{u}_{\gamma_i})$ and/or $(\hat{u}_{\gamma_i}, \hat{u}_{\gamma_i}, \hat{u}_{\gamma_i})$ of (1). These are solutions of (1) in the regions $|x| \gg 1$ that are to leading order constant in time and space and they are determined by two of the roots of the cubic polynomial $u^3 - u + \varepsilon((\alpha+\beta)u + \gamma_i) = 0$.[5] In particular, $\bar{u}_{\gamma_i}$ and $\hat{u}_{\gamma_i}$ are given by

$$\bar{u}_{\gamma_i} := -1 + \frac{1}{2}\varepsilon(\alpha + \beta - \gamma_i) + \mathcal{O}(\varepsilon^2), \hat{u}_{\gamma_i} := 1 - \frac{1}{2}\varepsilon(\alpha + \beta + \gamma_i) + \mathcal{O}(\varepsilon^2), \tag{11}$$

see, for instance, [23].

2.1 GSPT

The leading order profiles of trivial and local defect solutions to (1) (i.e. solutions of (10)) are relatively straightforward to determine. In short, we divide the spatial domain in $N + 2$,

[4] This concatenation idea has been employed before for various types of Hamiltonian systems, see, for instance, [13,14] and the references therein.

[5] The third root relates to an unstable homogeneous steady state solution (in PDE sense) and is not of interest for localised structures, see [23] for more details.

asymptotically small, fast regions I_f and $N+2$ slow regions I_s: a fast region around each of the N interfaces of the local defect solution, two fast regions around the defect at $x=0$ and $N+2$ slow regions away from the N interfaces and the defect. In particular, for a trivial defect solution $Z_{td}^{\pm}$ we have $N=0$, while $N=1$ for a local defect front solution $Z_{f,ld}$ and $N=2$ for a local defect pulse solution $Z_{p,ld}$. In the slow regions away from the interfaces and defect, the *fast* u-component of (10) is, due to the asymptotic smallness of its diffusion coefficient, close to one of its asymptotic end states (11). Consequently, the equations for the *slow* (v,w)-components can be solved to leading order. In the fast, asymptotically small, regions, the fast u-component of (10) is dominant, while the slow (v,w)-components are to leading order constant. To study the fast u-equation in these fast regions, we introduce the fast scaling $\xi := x/\varepsilon$ and rewrite (10) in ξ:

$$\begin{cases} 0 = u_{\xi\xi} + u - u^3 - \varepsilon(\alpha v + \beta w + \gamma(\xi)), \\ 0 = v_{\xi\xi} + \varepsilon^2(u - v), \\ 0 = D^2 w_{\xi\xi} + \varepsilon^2(u - w), \end{cases} \tag{12}$$

where we note that (10) and (12) are equivalent as long as $\varepsilon \neq 0$. The u-equation is to leading order solved by $\pm\tanh((\xi-\hat{\xi})/\sqrt{2})$, where $\hat{\xi}$ is an arbitrary translational constant that is determined by the location of the interface. Finally, we concatenate the solutions in the different slow and fast regions to construct the leading order profiles of the trivial and local defect solutions. For more details, see, in particular, "Appendix A", the upcoming sections and [23,54,55].

Remark 3 The defining difference between a local defect solution Z_{ld} and a global defect solution Z_{gd} is the location of the interfaces of the solution with respect to the defect at $x=0$. If this pinning distance is $\Theta(1)$ in the slow scaling x, then we have a local defect solution Z_{ld}, while we have a global defect solution Z_{gd} if the pinning distance is $\mathcal{O}(1)$ in the fast scaling $\xi := x/\varepsilon$. In other words, for global defect solutions Z_{gd} the defect and one of the interfaces lie in the same fast field, while they lie in different fast fields—and are separated by a slow field—for local defect solutions Z_{ld}. So, the spatial domain has to be divided in $N+1$ fast and $N+1$ slow regions to study global defect solutions.

2.2 The Action Functional Approach

The Lagrangian associated with the homogenous version of (10) is a skew-gradient system [8] and is given by

$$\begin{aligned} L_0(u,v,w) := {} & \frac{1}{2}\varepsilon^2 u_x^2 + F(u) + \varepsilon\alpha\left(uv - \frac{1}{2}v_x^2 - \frac{1}{2}v^2\right) \\ & + \varepsilon\beta\left(uw - \frac{1}{2}D^2 w_x^2 - \frac{1}{2}w^2\right) + \varepsilon\gamma u + c_0 . \end{aligned} \tag{13}$$

Here, $F(u) = \frac{1}{4}u^4 - \frac{1}{2}u^2$ and c_0 is a normalising constant so that we deal with finite critical values. With the second and third equations of (10) being linear, the associated Lagrangians are convex, which provide natural coercivity. Furthermore, straightforward calculations yield

$$\int_{-\infty}^{\infty}(uv - v_x^2 - v^2)dx = 0, \quad \int_{-\infty}^{\infty}(uw - D^2 w_x^2 - w^2)dx = 0, \tag{14}$$

if $u \in \mathcal{C}_0^\infty(\mathbb{R})$ or $\mathbb{H}^1(\mathbb{R})$, and where v, respectively w, is the unique bounded solution of the second, respectively third, equation of (10). The solutions of the homogeneous version of (10) can be found from the critical points of a variational functional associated with the Lagrangian $L_0(u, v, w)$ [8]. This functional is strongly indefinite, which requires min-max arguments to show the existence of critical points. However, we may take advantage of the linearity of the second and third equations of (10). That is, we introduce $\mathcal{L}_1 := (-\frac{d^2}{dx^2}+1)^{-1}$ and $\mathcal{L}_2 := (-D^2\frac{d^2}{dx^2}+1)^{-1}$, such that $\mathcal{L}_1 u$ exactly solves the linear v-equation $0 = v_{xx}+u-v$ for any given u, while $\mathcal{L}_2 u$ exactly solves the linear w-equation $0 = D^2 w_{xx} + u - w$, and use (14) to employ an action functional J defined by (9) to investigate the stationary solutions of the homogenous version of (10). From (14) it is clear that

$$\int_{-\infty}^{\infty} u\mathcal{L}_i u dx \geq 0\,, \qquad i = 1, 2,$$

a coercivity which enables us to seek minimisers of J. See also [5,10,11,52], and references therein, for more details.

As in [52], the idea of Lyapunov-Schmidt reduction helps us to investigate the pinned front and pulse solutions; however, we need to further refine the argument to deal with the defect imposed on (10). Knowing that the defect is located at $x = 0$, we adjust L_0 (13) for the different γ-values and split the integral associated to the action functional over the two domains $x < 0$ and $x > 0$. In particular, for a defect pulse solution we use the following action functional

$$J_p(u) = \int_{-\infty}^{0} L(u; \bar{u}_{\gamma_1}) dx + \int_{0}^{\infty} L(u; \bar{u}_{\gamma_2}) dx\,, \tag{15}$$

with

$$\begin{aligned} L(u; \bar{u}_{\gamma_i}) := \frac{1}{2}\varepsilon^2 u_x^2 + F(u) - F(\bar{u}_{\gamma_i}) + \frac{1}{2}\varepsilon\alpha(u\mathcal{L}_1 u - \bar{u}_{\gamma_i}^2) \\ + \frac{1}{2}\varepsilon\beta(u\mathcal{L}_2 u - \bar{u}_{\gamma_i}^2) + \varepsilon\gamma_i(u - \bar{u}_{\gamma_i})\,, \end{aligned} \tag{16}$$

and with $F(u)$, $\bar{u}_{\gamma_i}$ and $\mathcal{L}_{1,2}$ as before. The admissible functions u are the profiles of the defect pulse solutions with unknown widths and pinning distances determined by the GSPT procedure outlined in Sect. 2.1. Thus, $u \in \mathbb{H}^1 + \hat{u}$, where $\hat{u}$ is a C^∞ function and

$$\hat{u} = \begin{cases} \bar{u}_{\gamma_1}\,, & \text{for } x < -1\,, \\ \bar{u}_{\gamma_2}\,, & \text{for } x > 1\,. \end{cases}$$

Stationary front solutions are not studied in [52][6], but it is not hard to adapt the above action functional for defect pulse solutions to an action functional for defect front solutions. The main difference is that a defect front solution asymptotes to $(\hat{u}_{\gamma_2}, \hat{u}_{\gamma_2}, \hat{u}_{\gamma_2})$ as $x \to \infty$, hence, the action functional for a defect front solution becomes

$$J_f(u) = \int_{-\infty}^{0} L(u; \bar{u}_{\gamma_1}) dx + \int_{0}^{\infty} L(u; \hat{u}_{\gamma_2}) dx\,, \tag{17}$$

[6] This is due to the fact that stationary front solutions exist only for $\gamma = 0$ and they are trivially stable in the homogeneous case [55].

with L given by (16) and $\hat{\bar{u}}_{\gamma_{1,2}}$ given by (11). The admissible functions u are now the profiles of the defect front solutions with unknown pinning distances, and, hence, $u \in \mathbb{H}^1 + \breve{u}$, where $\breve{u}$ is a C^∞ function and

$$\breve{u} = \begin{cases} \bar{u}_{\gamma_1}\,, & \text{for } x < -1\,, \\ \hat{u}_{\gamma_2}\,, & \text{for } x > 1\,. \end{cases}$$

The Maslov index derived in [7] can be used to study the stability of stationary pulse solutions of skew-gradient systems; in particular of FitzHugh–Nagumo equations [5,9]. This index plays a similar role as the Morse index for the solutions of gradient systems and the Maslov index of a minimiser of J_p is zero. In view of the skew-gradient structure for (10), the fact that the second and third equations are linear reduces the complexity of the calculations in the spectral analysis. For instance, both $-\frac{d^2}{dx^2} + 1$ and $-D^2\frac{d^2}{dx^2} + 1$ are positive operators. In addition, suitably small τ and θ precludes the existence of non-real eigenvalues in the right half-plane [9, Lemma 4.1] and [53]. This assumption on τ and θ can thus be construed as keeping the system away from a strongly excitable situation, as might result, for instance, in Hopf bifurcations. So, similar to the results established in [7,9], the minimisers of J_p will correspond to stable pinned pulse solutions. Likewise, we can adapt the approach of [10] to assert that the minimisers of J_f will correspond to stable pinned front solutions.

We now take a closer look to the individual terms of L (16) inside the action functionals (15) and (17). As discussed above, to construct the profiles of the defect front and pulse solutions we split the spatial domain into slow regions I_s—that are away from the defect and away from the interfaces—and fast regions I_f—near the defect and interfaces. In the slow regions I_s, the slow (v, w)-components are dominant and the fast u-component is slaved to the slow components. In particular, the fast u-component, as well as $\hat{\bar{u}}_{\gamma_{1,2}}$ (11), are to leading order ± 1 (see also the upcoming sections and appendices). Consequently, the $\frac{1}{2}\varepsilon^2 u_x^2$-terms in L of (15) and (17) are $\mathcal{O}(\varepsilon^4)$ in the slow regions. For the antiderivative $F(u)$, we have

$$F(\pm 1 + \varepsilon K_1 + \varepsilon^2 K_2 + \mathcal{O}(\varepsilon^3)) = -\frac{1}{4} + \varepsilon^2 K_1^2 + \mathcal{O}(\varepsilon^3). \tag{18}$$

Hence, the $F(u) - F(\hat{\bar{u}}_{\gamma_{1,2}})$-terms in L of (15) and (17) are $\mathcal{O}(\varepsilon^2)$ in the slow regions. Consequently, the leading order terms of the action functionals in the slow region I_s are actual $\mathcal{O}(\varepsilon)$. By using regular expansions for $u = u_0 + \varepsilon u_1 + \mathcal{O}(\varepsilon^2) = \pm 1 + \varepsilon u_1 + \mathcal{O}(\varepsilon^2)$ and $\hat{\bar{u}}_{\gamma_i} = \hat{\bar{u}}_{\gamma_i,0} + \varepsilon\hat{\bar{u}}_{\gamma_i,1} + \mathcal{O}(\varepsilon^2) = \pm 1 + \varepsilon\hat{\bar{u}}_{\gamma_i,1} + \mathcal{O}(\varepsilon^2)$ (11), we get that in the slow regions I_s

$$L(u; \hat{\bar{u}}_{\gamma_i})|_{I_s} = \varepsilon L_1(u; \hat{\bar{u}}_{\gamma_i}) + \varepsilon^2 L_2(u; \hat{\bar{u}}_{\gamma_i}) + \mathcal{O}(\varepsilon^3)\,,$$

with

$$L_1(u; \hat{\bar{u}}_{\gamma_i}) := \frac{1}{2}\alpha(u_0\mathcal{L}_1 u_0 - 1) + \frac{1}{2}\beta(u_0\mathcal{L}_2 u_0 - 1) + \gamma_i(u_0 - \hat{\bar{u}}_{\gamma_i,0})\,, \tag{19}$$

and

$$\begin{aligned} L_2(u; \hat{\bar{u}}_{\gamma_i}) := u_1^2 - (\hat{\bar{u}}_{\gamma_i,1})^2 + \frac{1}{2}\alpha(u_1\mathcal{L}_1 u_0 + u_0\mathcal{L}_1 u_1 - 2\hat{\bar{u}}_{\gamma_i,0}\hat{\bar{u}}_{\gamma_i,1}) \\ + \frac{1}{2}\beta(u_1\mathcal{L}_2 u_0 + u_0\mathcal{L}_1 u_1 - 2\hat{\bar{u}}_{\gamma_i,0}\hat{\bar{u}}_{\gamma_i,1}) + \gamma_i(u_1 - \hat{\bar{u}}_{\gamma_i,1})\,. \end{aligned} \tag{20}$$

In the fast, asymptotically small, regions I_f the fast component is dominant and the slow components are effectively constant, see (12) and [23]. We use the fast scaling $\xi = x/\varepsilon$ to study the action functional in these fast regions. That is,

$$J_{f,p}(u) = \varepsilon \int_{-\infty}^{0} \bar{L}(u; \bar{u}_{\gamma_1}) d\xi + \varepsilon \int_{0}^{\infty} \bar{L}(u; \hat{\bar{u}}_{\gamma_2}) d\xi \,, \tag{21}$$

with

$$\begin{aligned} \bar{L}(u; \hat{\bar{u}}_{\gamma_i}) = \frac{1}{2} u_\xi^2 + F(u) - F(\hat{\bar{u}}_{\gamma_i}) + \frac{1}{2} \varepsilon \alpha (u \mathcal{L}_1 u - \hat{\bar{u}}_{\gamma_i}^2) \\ + \frac{1}{2} \varepsilon \beta (u \mathcal{L}_2 u - \hat{\bar{u}}_{\gamma_i}^2) + \varepsilon \gamma (u - \hat{\bar{u}}_{\gamma_i}) \,, \end{aligned}$$

where $F, \mathcal{L}_{1,2}$, and $\hat{\bar{u}}_{\gamma_i}$ (11) are as before and where we note the ε-term premultiplying the integrals of (21). By using a regular expansion in ξ for the different components of $\bar{L}$, we get that in the fast regions I_f

$$\bar{L}(u; \hat{\bar{u}}_{\gamma_i})|_{I_f} = \bar{L}_0(u; \hat{\bar{u}}_{\gamma_i}) + \varepsilon \bar{L}_1(u; \hat{\bar{u}}_{\gamma_i}) + \mathcal{O}(\varepsilon^2) \,,$$

with

$$\bar{L}_0(u; \hat{\bar{u}}_{\gamma_i}) := \frac{1}{2} (u_0)_\xi^2 + F(u_0) + \frac{1}{4} \,, \tag{22}$$

and

$$\begin{aligned} \bar{L}_1(u; \hat{\bar{u}}_{\gamma_i}) := (u_0)_\xi (u_1)_\xi + u_0 u_1 (u_0^2 - 1) + \frac{1}{2} \alpha (u_0 \mathcal{L}_1 u_0 - 1) \\ + \frac{1}{2} \beta (u_0 \mathcal{L}_2 u_0 - 1) + \gamma_i (u_0 - \hat{\bar{u}}_{\gamma_{i,0}}) \,, \end{aligned} \tag{23}$$

where we used (18) and the observation that $F(u_0 + \varepsilon u_1 + \mathcal{O}(\varepsilon^2)) = F(u_0) + \varepsilon u_0 u_1 (u_0^2 - 1) + \mathcal{O}(\varepsilon^2)$.

3 Pinned Front Solutions

In this section, we focus on pinned front solutions supported by (1) and we first derive the part of Main Result 1 related to the existence and stability of local defect front solutions $Z_{f,ld}^{\ell}$ pinned to the left of the defect. In particular, we explicitly derive the relationship (3) determining the pinning distance of the interface of the local defect front solution to the defect. In Sect. 3.2, we combine these results with the results of [54] related to global defect front solutions to obtain a broader picture for pinned front solutions. Finally, we confirm our asymptotic findings by numerically investigating the stationary version of (1), that is, by investigating (10).

3.1 Local Defect Front Solutions $Z_{f,ld}^{\ell}$ Pinned to the Left of the Defect

In order to study local defect front solutions $Z_{f,ld}^{\ell}$ pinned to the left of the defect and as outlined in Sect. 2.1, we split the spatial domain into three slow regions $I_s^{1,3,6}$ and three fast regions $I_f^{2,4,5}$. In particular,

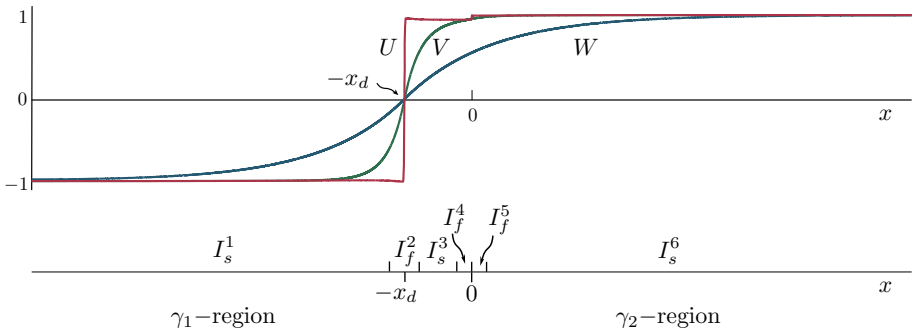

Fig. 3 Schematic depiction of the three slow regions $I_s^{1,3,6}$ and three fast regions $I_f^{2,4,5}$ (24) used to study local defect front solutions $Z_{f,ld}^{\ell}$ pinned to the left of the defect

$$\begin{aligned} I_s^1 &:= (-\infty, -x_d - \sqrt{\varepsilon}\,], & I_s^3 &:= [-x_d + \sqrt{\varepsilon}, -\sqrt{\varepsilon}\,], & I_s^6 &:= [\sqrt{\varepsilon}, \infty)\,, \\ I_f^2 &:= (-x_d - \sqrt{\varepsilon}, -x_d + \sqrt{\varepsilon})\,, & I_f^4 &:= (-\sqrt{\varepsilon}, 0]\,, & I_f^5 &:= (0, \sqrt{\varepsilon})\,, \end{aligned} \tag{24}$$

with $0 < x_d = \Theta(1)$ the, currently undetermined, pinning distance and with the defect located in between the fast fields I_f^4 and I_f^5. See also Fig. 3. We use a regular expansion in ε and expand the profile of a local defect front solution $Z_{f,ld}^{\ell}(x)$

$$\begin{aligned} Z_{f,ld}^{\ell}(x) = (U_{f,ld}^{\ell}, V_{f,ld}^{\ell}, W_{f,ld}^{\ell})(x) &= (U_{f,ld,0}^{\ell}, V_{f,ld,0}^{\ell}, W_{f,ld,0}^{\ell})(x) \\ &+ \varepsilon(U_{f,ld,1}^{\ell}, V_{f,ld,1}^{\ell}, W_{f,ld,1}^{\ell})(x) + \mathcal{O}(\varepsilon^2)\,. \end{aligned} \tag{25}$$

Since the defect is small, it has no leading order influence on the profile and we can thus use the results from the homogeneous case. In particular, we have that

$$U_{f,ld,0}^{\ell}(x) = \begin{cases} -1\,, & \text{in } I_s^1\,, \\ \tanh\left(\dfrac{x + x_d}{\sqrt{2\varepsilon}}\right), & \text{in } I_f^2\,, \\ 1\,, & \text{in } I_s^3 \cup I_f^4 \cup I_f^5 \cup I_s^6\,, \end{cases} \tag{26}$$

see, for instance, [15,54,55] (and recall that $\tanh((\xi - \hat{\xi})/\sqrt{2})$ solves $u_{\xi\xi} + u - u^3 = 0$). The leading order components of the slow components are given by

$$V_{f,ld,0}^{\ell}(x) = \begin{cases} e^{x+x_d} - 1\,, & \text{in } I_s^1\,, \\ 0\,, & \text{in } I_f^2\,, \\ -e^{-(x+x_d)} + 1\,, & \text{in } I_s^3 \cup I_f^4 \cup I_f^5 \cup I_s^6\,, \end{cases} \tag{27}$$

and

$$W_{f,ld,0}^{\ell}(x) = \begin{cases} e^{(x+x_d)/D} - 1\,, & \text{in } I_s^1\,, \\ 0\,, & \text{in } I_f^2\,, \\ -e^{-(x+x_d)/D} + 1\,, & \text{in } I_s^3 \cup I_f^4 \cup I_f^5 \cup I_s^6\,. \end{cases} \tag{28}$$

Before we compute the higher order correction terms of $Z_{f,ld}^{\ell}$, we first look at the contribution of the leading order profile to the action functional J_f (17). That is, we compute $J_{f,1}^{1,3} :=$

$\int_{I_s^{1,3}} L_1(U^\ell_{f,ld};\bar{u}_{\gamma_1})dx$, $J^6_{f,1} := \int_{I_s^6} L_1(U^\ell_{f,ld};\hat{u}_{\gamma_2})dx$, $J^{2,4}_{f,1} := \int_{I_f^{2,4}} \bar{L}_0(U^\ell_{f,ld};\bar{u}_{\gamma_1})d\xi$, and $J^5_{f,1} := \int_{I_f^5} \bar{L}_0(U^\ell_{f,ld};\hat{u}_{\gamma_2})d\xi$, see (19), respectively (22), for the definition of L_1, respectively $\bar{L}_0$. These computations will be similar in spirit to the computations in [52] for homogeneous pulse solutions (since the contributions of the weak defect enter only at the next level of the action functional). We first compute the leading order contributions of the three slow integrals $J^{1,3,6}_{f,1}$. We get

$$\begin{aligned} J^1_{f,1} &= \int_{I_s^1} L_1(U^\ell_{f,ld};\bar{u}_{\gamma_1})dx \\ &= \int_{I_s^1} \left(\frac{1}{2}\alpha\left(U^\ell_{f,ld,0}V^\ell_{f,ld,0}-1\right)+\frac{1}{2}\beta\left(U^\ell_{f,ld,0}W^\ell_{f,ld,0}-1\right)\right. \\ &\quad \left.+\gamma_1\left(U^\ell_{f,ld,0}+1\right)\right)dx \\ &= -\int_{-\infty}^{-x_d}\left(\frac{1}{2}\alpha e^{x+x_d}+\frac{1}{2}\beta e^{(x+x_d)/D}\right)dx+\mathcal{O}(\sqrt{\varepsilon}) \\ &= -\frac{1}{2}(\alpha+\beta D)+\mathcal{O}(\sqrt{\varepsilon}), \end{aligned} \tag{29}$$

where the $\mathcal{O}(\sqrt{\varepsilon})$-term stems from the fact that we shifted the limit of the integral from $-x_d-\sqrt{\varepsilon}$ to $-x_d$. Likewise, we get

$$J^3_{f,1} = \frac{1}{2}\left(\alpha\left(e^{-x_d}-1\right)+\beta D\left(e^{-x_d/D}-1\right)\right)+2\gamma_1 x_d+\mathcal{O}(\sqrt{\varepsilon}),$$

where we remark that the explicit γ_1-dependence follows from the fact that $U^\ell_{f,ld,0}=1$ in I_s^3 while $\bar{u}_{\gamma_1}=-1$ in I_s^3, see Fig. 3. Similarly,

$$J^6_{f,1} = -\frac{1}{2}\left(\alpha e^{-x_d}+\beta D e^{-x_d/D}\right)+\mathcal{O}(\sqrt{\varepsilon}).$$

The integral over the first fast region I_f^2 gives

$$\begin{aligned} J^2_{f,1} &= \int_{I_f^2}\bar{L}_0(U^\ell_{f,ld};\bar{u}_{\gamma_1})d\xi = \int_{I_f^2}\left(\frac{1}{2}(U^\ell_{f,ld,0})^2_\xi+F(U^\ell_{f,ld,0})+\frac{1}{4}\right)d\xi \\ &= \int_0^{1/\sqrt{\varepsilon}}\operatorname{sech}^4\left(\frac{\xi}{\sqrt{2}}\right)d\xi = \frac{2\sqrt{2}}{3}+\mathcal{O}(e^{-1/\sqrt{\varepsilon}}), \end{aligned} \tag{30}$$

where we used that $\tanh^4(\cdot)-2\tanh^2(\cdot)+1=(\tanh^2(\cdot)-1)^2=\operatorname{sech}^4(\cdot)$, see also [52], and the correction term again arises from changing the limit of the integral. The other two fast integrals do not yield a leading order contribution to the action functional since the U-profile is to leading order constant $+1$ over $I_f^{4,5}$, see (26). In particular, over these fields we have that $(U^\ell_{f,ld,0})_\xi=0$ and $F(U^\ell_{f,ld,0})=-1/4$ and, hence, $\bar{L}_0(U^\ell_{f,ld,0},\hat{\bar{u}}_{\gamma_i})=0$ (22). So, by adding $J^{1,2,3}_{f,1}$ and $J^6_{f,1}$ we get that the action functional for a local defect front solution $Z^\ell_{f,ld}$ pinned to the left of the defect is given by

$$J_f(U^\ell_{f,ld}) = \left(2\gamma_1 x_d + \frac{2\sqrt{2}}{3} - (\alpha + \beta D)\right)\varepsilon + \mathcal{O}(\varepsilon\sqrt{\varepsilon})\,. \tag{31}$$

As long as $\gamma_1 = \Theta(1)$ (and thus unequal to 0), the critical points of $J_f(U^\ell_{f,ld})$ with respect to the pinning distance x_d are—to leading order—given by $x_d \to 0$ and $x_d \to \infty$. In other words, they approach the boundaries of the slow region I^1_s. Consequently, local defect front solutions $Z^\ell_{f,ld}$ pinned to the left of the defect do not exist if $\gamma_1 = \Theta(1)$, and, as expected, the pinning distance x_d of $Z^\ell_{f,ld}$ cannot be determined from the leading order computation.

Remark 4 By the symmetry (7) of (1), the action functional for a local defect front solution $Z^r_{f,ld}$ pinned to the right of the defect is given by

$$J_f(U^r_{f,ld}) = \left(-2\gamma_2 x_d + \frac{2\sqrt{2}}{3} - (\alpha + \beta D)\right)\varepsilon + \mathcal{O}(\varepsilon\sqrt{\varepsilon})\,,$$

where $x_d > 0$ is again the pinning distance. So, combining the results following from the action functionals for $U^\ell_{f,ld}$ and $U^r_{f,ld}$ also hints to the results for the existence and stability of global defect front solutions $Z_{f,gd}$ pinned at the defect as obtained in [54]: global defect front solutions exist if $\gamma_1\gamma_2 < 0$, and they are stable if and only if $\gamma_2 < 0 < \gamma_1$. In more detail, for $\gamma_1 > 0$ the action functional $J_f(U^\ell_{f,ld})$ indicates that a front solution to the left of the defect wants to move towards the defect (towards smaller $x_d > 0$) to minimise its action functional, while it moves away from the defect for $\gamma_1 < 0$. Similarly, for $\gamma_2 < 0$ the action functional $J_f(U^r_{f,ld})$ indicates that a front solution to the right of the defect wants to move towards the defect (towards smaller $x_d > 0$) to minimise the action functional, while it moves away from the defect for $\gamma_2 > 0$.

3.1.1 The Next Order

As eluded to above, it is clear from (31) that, to leading order, we necessarily need that $\gamma_1 = 0$ for the existence of a local defect front solution $Z^\ell_{f,ld}$ pinned to the left of the defect. So, we set $\gamma_1 = \varepsilon\tilde{\gamma}_1$ with, *a priori*, $\tilde{\gamma}_1 = \Theta(1)$. To be able to determine the next order term of the action functional J_f (17), we first compute the higher order correction terms $(U^\ell_{f,ld,1}, V^\ell_{f,ld,1}, W^\ell_{f,ld,1})(x)$ (25) of $Z^\ell_{f,ld}$. In the slow fields $I^{1,3,6}_s$, we substitute the regular expansion (25)—with $U^\ell_{f,ld,0}$, $V^\ell_{f,ld,0}$ and $W^\ell_{f,ld,0}$ respectively given by (26)–(28)—into (10), to obtain

$$\begin{cases} \mathcal{O}(\varepsilon) = U^\ell_{f,ld,1} - 3(U^\ell_{f,ld,0})^2 U^\ell_{f,ld,1} - (\alpha V^\ell_{f,ld,0} + \beta W^\ell_{f,ld,0} + \gamma(x))\,, \\ \mathcal{O}(\varepsilon) = (V^\ell_{f,ld,1})_{xx} + U^\ell_{f,ld,1} - V^\ell_{f,ld,1}\,, \\ \mathcal{O}(\varepsilon) = D^2(W^\ell_{f,ld,1})_{xx} + U^\ell_{f,ld,1} - W^\ell_{f,ld,1}\,. \end{cases} \tag{32}$$

Since $(U^\ell_{f,ld,0})^2 = 1$ in all three slow fields, the first equation yields that the higher order correction term $U^\ell_{f,ld,1}$ in the slow fields is given by

$$U^\ell_{f,ld,1} = -\frac{1}{2}\left(\alpha V_{f,ld,0} + \beta W_{f,ld,0} + \gamma(x)\right),$$

with $V^{\ell}_{f,ld,0}$, respectively $W^{\ell}_{f,ld,0}$, given by (27), respectively (28) and $\gamma(x)$ given by (2) with $\gamma_1 = 0$ (since $\gamma_1 = \varepsilon\tilde{\gamma}_1$ is a higher order term). This allows us to solve the second and third equations of (32) explicitly. In I^1_s we obtain

$$I^1_s : \begin{cases} U^{\ell}_{f,ld,1} = \frac{1}{2}(\alpha+\beta) - \frac{1}{2}\left(\alpha e^{x+x_d} + \beta e^{(x+x_d)/D}\right), \\ V^{\ell}_{f,ld,1} = \frac{1}{2}(\alpha+\beta) + C_{1,V}e^{x} + \frac{1}{8}\alpha(2x-1)e^{x+x_d} \\ \qquad\qquad - \frac{1}{2}\beta\left(\frac{D^2}{D^2-1}\right)e^{(x+x_d)/D}, \\ W^{\ell}_{f,ld,1} = \frac{1}{2}(\alpha+\beta) + C_{1,W}e^{x/D} + \frac{1}{2}\alpha\left(\frac{1}{D^2-1}\right)e^{x+x_d} \\ \qquad\qquad + \frac{1}{8}\beta\left(\frac{2x}{D}-1\right)e^{(x+x_d)/D}, \end{cases}$$

where we used that both slow components need to be bounded as x approaches $-\infty$ and the fact that $\gamma_1 = 0$ to leading order. In I^3_s we obtain

$$I^3_s : \begin{cases} U^{\ell}_{f,ld,1} = -\frac{1}{2}(\alpha+\beta) + \frac{1}{2}\left(\alpha e^{-(x+x_d)} + \beta e^{-(x+x_d)/D}\right), \\ V^{\ell}_{f,ld,1} = -\frac{1}{2}(\alpha+\beta) + C_{3,V}e^{x} + D_{3,V}e^{-x} + \frac{1}{8}\alpha(2x+1)e^{-(x+x_d)} \\ \qquad\qquad + \frac{1}{2}\beta\left(\frac{D^2}{D^2-1}\right)e^{-(x+x_d)/D}, \\ W^{\ell}_{f,ld,1} = -\frac{1}{2}(\alpha+\beta) + C_{3,W}e^{x/D} + D_{3,W}e^{-x/D} \\ \qquad\qquad - \frac{1}{2}\alpha\left(\frac{1}{D^2-1}\right)e^{-(x+x_d)} + \frac{1}{8}\beta\left(\frac{2x}{D}+1\right)e^{-(x+x_d)/D}, \end{cases}$$

and in I^6_s we have

$$I^6_s : \begin{cases} U^{\ell}_{f,ld,1} = -\frac{1}{2}(\alpha+\beta+\gamma_2) + \frac{1}{2}\left(\alpha e^{-(x+x_d)} + \beta e^{-(x+x_d)/D}\right), \\ V^{\ell}_{f,ld,1} = -\frac{1}{2}(\alpha+\beta+\gamma_2) + D_{6,V}e^{-x} + \frac{1}{8}\alpha(2x+1)e^{-(x+x_d)} \\ \qquad\qquad + \frac{1}{2}\beta\left(\frac{D^2}{D^2-1}\right)e^{-(x+x_d)/D}, \\ W^{\ell}_{f,ld,1} = -\frac{1}{2}(\alpha+\beta+\gamma_2) + D_{6,W}e^{-x/D} - \frac{1}{2}\alpha\left(\frac{1}{D^2-1}\right)e^{-(x+x_d)} \\ \qquad\qquad + \frac{1}{8}\beta\left(\frac{2x}{D}+1\right)e^{-(x+x_d)/D}, \end{cases}$$

where we used that both slow components need to be bounded as x approaches ∞.

In the three fast regions $I_f^{2,4,5}$, we use the fast scaling ξ and substitute the regular expansion (25)—as function of ξ—into (12). By using the expressions of $U^\ell_{f,ld,0}$, $V^\ell_{f,ld,0}$ and $W^\ell_{f,ld,0}$, given by respectively (26)–(28), we obtain

$$\begin{cases} \mathcal{O}(\varepsilon) = \left(U^\ell_{f,ld,1}\right)_{\xi\xi} + U^\ell_{f,ld,1} - 3\left(U^\ell_{f,ld,0}\right)^2 U^\ell_{f,ld,1} \\ \qquad\qquad - \left(\alpha V^\ell_{f,ld,0} + \beta W^\ell_{f,ld,0} + \gamma(x)\right), \\ \mathcal{O}(\varepsilon) = \left(V^\ell_{f,ld,1}\right)_{\xi\xi}, \\ \mathcal{O}(\varepsilon) = D^2\left(W^\ell_{f,ld,1}\right)_{\xi\xi}, \end{cases} \tag{33}$$

where we used that both $(V^\ell_{f,ld,0})_{\xi\xi}$ and $(W^\ell_{f,ld,0})_{\xi\xi}$ are $\mathcal{O}(\varepsilon^2)$ in the fast fields. So, the slow components are solved by linear functions. However, the solutions have to stay bounded and therefore they are to leading order constant, see also "Appendix A". Furthermore, since the fast fields are *too small* for the slow components to change significantly, see, for instance, [54], these slow components—as well as their derivatives—need to match over the fast fields. This gives

$$C_{1,V} = -\frac{1}{4}\gamma_2 + \frac{1}{8}\alpha(-3+2x_d)e^{x_d} + \frac{1}{2}\beta\left(\frac{1}{D^2-1}\right)e^{x_d}, \quad C_{3,V} = -\frac{1}{4}\gamma_2,$$
$$D_{3,V} = \frac{1}{8}\alpha(3+2x_d)e^{-x_d} - \frac{1}{2}\beta\left(\frac{1}{D^2-1}\right)e^{-x_d}, \quad D_{6,V} = \frac{1}{4}\gamma_2 + D_{3,V},$$

and

$$C_{1,W} = -\frac{1}{4}\gamma_2 - \frac{1}{2}\alpha\left(\frac{D^2}{D^2-1}\right)e^{x_d/D} + \frac{1}{8}\beta\left(-3+\frac{2x_d}{D}\right)e^{x_d/D},$$
$$C_{3,W} = -\frac{1}{4}\gamma_2,$$
$$D_{3,W} = \frac{1}{2}\alpha\left(\frac{D^2}{D^2-1}\right)e^{-x_d/D} + \frac{1}{8}\beta\left(3+\frac{2x_d}{D}\right)e^{-x_d/D},$$
$$D_{6,W} = \frac{1}{4}\gamma_2 + D_{3,W}.$$

So, we have completely determined the correction terms $V^\ell_{f,ld,1}$ and $W^\ell_{f,ld,1}$.

In the first fast field I_f^2, the U-equation of (33) reduces to

$$\mathcal{O}(\varepsilon) = (U^\ell_{f,ld,1})_{\xi\xi} + \left(1 - 3\tanh^2\left(\frac{\xi+\xi_d}{\sqrt{2}}\right)\right)U^\ell_{f,ld,1},$$

where we used that the leading order computation implied that $\gamma_1 = \Theta(\varepsilon)$. The above equation is explicitly solved by

$$U^\ell_{f,ld,1}(\xi) = D_{2,U}\left(2\sinh\left(\frac{\xi+\xi_d}{\sqrt{2}}\right)\cosh\left(\frac{\xi+\xi_d}{\sqrt{2}}\right) + 3\tanh\left(\frac{\xi+\xi_d}{\sqrt{2}}\right)\right.$$
$$\left. + 3\left(\frac{\xi+\xi_d}{\sqrt{2}}\right)\operatorname{sech}^2\left(\frac{\xi+\xi_d}{\sqrt{2}}\right)\right) + C_{2,U}\operatorname{sech}^2\left(\frac{\xi+\xi_d}{\sqrt{2}}\right),$$

see Sect. 2 of [54]. However, to ensure that $U^{\ell}_{f,ld,1}$ stays bounded as ξ approaches the boundaries of the fast field, which are to leading order in ξ given by $\xi \to \pm\infty$, we have $D_{2,U} = 0$. Moreover, also $C_{2,U}$ can be taken identically zero since the original U-equation, upon substituting the leading order expressions of the slow components in the first fast field I^2_f (see (27) and (28)), has no $\mathcal{O}(\varepsilon)$-terms. In particular, the u-equation of (12) in I^2_f reduces to $\mathcal{O}(\varepsilon^2) = u_{\xi\xi} + u - u^3$ and so no $\mathcal{O}(\varepsilon)$-correction term is expected, see also [53]. Thus,

$$U^{\ell}_{f,ld,1}(\xi) = 0\,, \qquad \xi \in I^2_f.$$

In the other two fast fields $I^{4,5}_f$, the U-equation of (33) reduces to

$$\mathcal{O}(\varepsilon) = (U^{\ell}_{f,ld,1})_{\xi\xi} - 2U^{\ell}_{f,ld,1} - (\alpha(-e^{-x_d}+1) + \beta(-e^{-x_d/D}+1) + \gamma(\xi))\,.$$

This equation is solved, see also "Appendix A", by

$$U^{\ell}_{f,ld,1}(\xi) = \begin{cases} -\frac{1}{2}(\alpha+\beta) + C_{4,U}e^{\sqrt{2}\xi} + D_{4,U}e^{-\sqrt{2}\xi} \\ \quad + \frac{1}{2}\left(\alpha e^{-x_d} + \beta e^{-x_d/D}\right), & \xi \in I^4_f\,, \\ -\frac{1}{2}(\alpha+\beta+\gamma_2) + C_{5,U}e^{\sqrt{2}\xi} + D_{5,U}e^{-\sqrt{2}\xi} \\ \quad + \frac{1}{2}\left(\alpha e^{-x_d} + \beta e^{-x_d/D}\right), & \xi \in I^5_f\,. \end{cases}$$

These two terms—as well as their derivatives—have to match at the defect point $x = 0$. This gives $C_{4,U} + D_{4,U} = C_{5,U} + D_{5,U} - \frac{1}{2}\gamma_2$ and $C_{4,U} - D_{4,U} = C_{5,U} - D_{5,U}$. Moreover, matching with the slow fields gives $D_{4,U} = 0 = C_{5,U}$. Combining these gives $C_{4,U} = -\frac{1}{4}\gamma_2 = -D_{5,U}$. Hence, the correction term $U^{\ell}_{f,ld,1}$ is now also completely determined and given by

$$U^{\ell}_{f,ld,1}(x) = \begin{cases} \frac{1}{2}(\alpha+\beta) - \frac{1}{2}\left(\alpha e^{x+x_d} + \beta e^{(x+x_d)/D}\right), & x \in I^1_s\,, \\ 0\,, & x \in I^2_f\,, \\ -\frac{1}{2}(\alpha+\beta) + \frac{1}{2}\left(\alpha e^{-(x+x_d)} + \beta e^{-(x+x_d)/D}\right), & x \in I^3_s\,, \\ -\frac{1}{2}(\alpha+\beta) - \frac{1}{4}\gamma_2 e^{\sqrt{2}x/\varepsilon} + \frac{1}{2}\left(\alpha e^{-x_d} + \beta e^{-x_d/D}\right), & x \in I^4_f\,, \\ -\frac{1}{2}(\alpha+\beta+\gamma_2) + \frac{1}{4}\gamma_2 e^{-\sqrt{2}x/\varepsilon} \\ \quad + \frac{1}{2}\left(\alpha e^{-x_d} + \beta e^{-x_d/D}\right), & x \in I^5_f\,, \\ -\frac{1}{2}(\alpha+\beta+\gamma_2) + \frac{1}{2}\left(\alpha e^{-(x+x_d)} + \beta e^{-(x+x_d)/D}\right), & x \in I^6_s\,. \end{cases} \tag{34}$$

We are now in the position to compute the higher order correction term of the action functional J_f (17) for a front solution $Z^{\ell}_{f,ld}$ pinned to the left of the defect. We start by computing the higher order contributions to the action functional coming from the first slow region I^1_s. Recall that to obtain the leading order contribution from the first slow region I^1_s, i.e. (29), we shifted the upper limit of the integral of $J^1_{f,1}$ and this resulted in an $\mathcal{O}(\sqrt{\varepsilon})$-error.

Since we are now interested in the higher order contributions, we actually need to explicitly compute this error-term. From (29) we deduce

$$\begin{aligned} J^1_{f,1} &= -\frac{1}{2}(\alpha+\beta D) + \int_{-x_d-\sqrt{\varepsilon}}^{-x_d} \left(\frac{1}{2}\alpha e^{x+x_d} + \frac{1}{2}\beta e^{(x+x_d)/D}\right) dx \\ &= -\frac{1}{2}(\alpha+\beta D) + \frac{1}{2}\left(\alpha\left(1-e^{-\sqrt{\varepsilon}}\right) + \beta D\left(1-e^{\sqrt{\varepsilon}/D}\right)\right) \\ &= -\frac{1}{2}(\alpha+\beta D) + \frac{1}{2}(\alpha+\beta)\sqrt{\varepsilon} - \frac{1}{4}\left(\alpha+\frac{\beta}{D}\right)\varepsilon + \mathcal{O}(\varepsilon\sqrt{\varepsilon})\,. \end{aligned}$$

Next, we compute the contribution of the remaining correction terms of the profile in I^1_s. That is, we compute

$$\begin{aligned} J^1_{f,2} :&= \int_{I^1_s} L_2(U^\ell_{f,ld}; \bar{u}_{\varepsilon\tilde{\gamma}_1}) dx \\ &= \int_{I^1_s} \left(\left(U^\ell_{f,ld,1}\right)^2 - \left(\bar{u}_{0,1}\right)^2 + \frac{1}{2}\alpha\left(U^\ell_{f,ld,1}\mathcal{L}_1 U^\ell_{f,ld,0} + U^\ell_{f,ld,0}\mathcal{L}_1 U^\ell_{f,ld,1}\right.\right. \\ &\quad \left. + 2\bar{u}_{0,1}\right) + \frac{1}{2}\beta\left(U^\ell_{f,ld,1}\mathcal{L}_2 U^\ell_{f,ld,0} + U^\ell_{f,ld,0}\mathcal{L}_1 U^\ell_{f,ld,1} + 2\bar{u}_{0,1}\right) \\ &\quad \left. + \tilde{\gamma}_1\left(U^\ell_{f,ld,0}+1\right)\right) dx \\ &= \int_{I^1_s} \left(\left(U^\ell_{f,ld,1}\right)^2 - \left(\bar{u}_{0,1}\right)^2 + \frac{1}{2}\alpha\left(U^\ell_{f,ld,1}\mathcal{L}_1 U^\ell_{f,ld,0} + U^\ell_{f,ld,0}\mathcal{L}_1 U^\ell_{f,ld,1}\right.\right. \\ &\quad \left. \left. + 2\bar{u}_{0,1}\right) + \frac{1}{2}\beta\left(U^\ell_{f,ld,1}\mathcal{L}_2 U^\ell_{f,ld,0} + U^\ell_{f,ld,0}\mathcal{L}_1 U^\ell_{f,ld,1} + 2\bar{u}_{0,1}\right)\right) dx\,, \end{aligned}$$

where we used the asymptotic scaling $\gamma_1 = \varepsilon\tilde{\gamma}_1$ and recall that $\bar{u}_{0,1}$ is the $\mathcal{O}(\varepsilon)$-term of the asymptotic end state near -1, see (11). For the clarity of the presentation, we compute the different components of the integral separately. We get

$$\begin{aligned} &\int_{I^1_s} \left((U^\ell_{f,ld,1})^2 - (\bar{u}_{0,1})^2\right) dx \\ &= \int_{I^1_s} \frac{1}{4}\left(\alpha e^{x+x_d} + \beta e^{(x+x_d)/D}\right)\left(-2(\alpha+\beta) + \left(\alpha e^{x+x_d} + \beta e^{(x+x_d)/D}\right)\right) dx \\ &= -\frac{3}{8}(\alpha^2+\beta^2 D) - \frac{1}{2}\alpha\beta\left(\frac{D^3-1}{D^2-1}\right) + \mathcal{O}(\sqrt{\varepsilon})\,, \end{aligned}$$

where the $\mathcal{O}(\sqrt{\varepsilon})$-term again appears due to the error made by shifting the limit of the integral. Similarly,

$$
\begin{aligned}
&\frac{1}{2}\alpha\int_{I_s^1}\left(U^\ell_{f,ld,1}\mathcal{L}_1U^\ell_{f,ld,0}+U^\ell_{f,ld,0}\mathcal{L}_1U^\ell_{f,ld,1}+2\bar{u}_{0,1}\right)dx\\
&\quad=\frac{1}{2}\alpha\int_{I_s^1}\left(U^\ell_{f,ld,1}V^\ell_{f,ld,0}-V^\ell_{f,ld,1}+(\alpha+\beta)\right)dx\\
&\quad=\frac{1}{2}\alpha\int_{I_s^1}\left(\left(\frac{1}{2}(\alpha+\beta)-\frac{1}{2}\left(\alpha e^{x+x_d}+\beta e^{(x+x_d)/D}\right)\right)(e^{x+x_d}-1)-\right.\\
&\qquad\left(\frac{1}{2}(\alpha+\beta)+\left(-\frac{1}{4}\gamma_2+\frac{1}{8}\alpha e^{x_d}(-3+2x_d)+\frac{1}{2}\beta\frac{1}{D^2-1}e^{x_d}\right)e^x\right.\\
&\qquad\left.\left.+\frac{1}{8}\alpha e^{x+x_d}(2x-1)-\frac{1}{2}\beta\frac{D^2}{D^2-1}e^{(x+x_d)/D}\right)+(\alpha+\beta)\right)dx\\
&\quad=\frac{1}{2}\alpha\int_{I_s^1}\left(\frac{1}{4}\gamma_2e^x+\frac{1}{4}\alpha\left(6-(x+x_d)\right)e^{x+x_d}-\frac{1}{2}\alpha e^{2(x+x_d)}\right.\\
&\qquad+\frac{1}{2}\beta\left(1-\frac{1}{D^2-1}\right)e^{x+x_d}+\frac{1}{2}\beta\left(1+\frac{D^2}{D^2-1}\right)e^{(x+x_d)/D}\\
&\qquad\left.-\frac{1}{2}\beta e^{x+x_d}e^{(x+x_d)/D}\right)dx\\
&\quad=\frac{1}{2}\alpha\left(\frac{1}{4}\gamma_2e^{-x_d}+\frac{3}{2}\alpha+\beta\left(\frac{D^3-1}{D^2-1}\right)\right)+\mathcal{O}(\sqrt{\varepsilon})\,,
\end{aligned}
$$

and

$$
\begin{aligned}
&\frac{1}{2}\beta\int_{I_s^1}\left(U^\ell_{f,ld,1}\mathcal{L}_2U^\ell_{f,ld,0}+U^\ell_{f,ld,0}\mathcal{L}_2U^\ell_{f,ld,1}+2\bar{u}_{0,1}\right)dx\\
&\qquad=\frac{1}{2}\beta\left(\frac{1}{4}\gamma_2De^{-x_d/D}+\alpha\left(\frac{D^3-1}{D^2-1}\right)+\frac{3}{2}\beta D\right)+\mathcal{O}(\sqrt{\varepsilon})\,.
\end{aligned}
$$

So, the total contribution to the action functional coming from the first slow field I_s^1 is given by

$$
\begin{aligned}
J_f|_{I_s^1}&=\varepsilon J^1_{f,1}+\varepsilon^2J^1_{f,2}+\mathcal{O}(\varepsilon^3)\\
&=-\frac{1}{2}(\alpha+\beta D)\varepsilon+\frac{1}{2}(\alpha+\beta)\varepsilon\sqrt{\varepsilon}+\left(-\frac{1}{4}\left(\alpha+\frac{\beta}{D}\right)+\frac{1}{8}\gamma_2\left(\alpha e^{-x_d}\right.\right.\\
&\qquad\left.\left.+\beta De^{-x_d/D}\right)+\frac{3}{8}\left(\alpha^2+\beta^2D\right)+\frac{1}{2}\alpha\beta\left(\frac{D^3-1}{D^2-1}\right)\right)\varepsilon^2+\mathcal{O}(\varepsilon^2\sqrt{\varepsilon})\,.
\end{aligned}
$$

Observe that the pinning distance x_d and γ_2—but not $\tilde{\gamma}_1$—enter the $\mathcal{O}(\varepsilon^2)$-term. We also expect that, after adding the contributions to the action functional from the other slow and fast regions, the $\mathcal{O}(\varepsilon\sqrt{\varepsilon})$-term above disappears (since the boundaries between the slow and fast fields are artificial in the sense we could have used any $\varepsilon^a, a\in(0,1)$, as boundary instead of $\sqrt{\varepsilon}$, see also [23]).

We also compute the contributions to the action functional over the other two slow regions $I_s^{3,6}$. Using the same notation as above, i.e. $J_f|_{I_s^{3,6}} = \varepsilon J_{f,1}^{3,6} + \varepsilon^2 J_{f,2}^{3,6} + \mathcal{O}(\varepsilon^3)$, we get for I_s^3

$$\begin{aligned} J_{f,1}^3 = &\frac{1}{2}\left(\alpha\left(e^{-x_d}-1\right)+\beta D\left(e^{-x_d/D}-1\right)\right)+\frac{1}{2}\left(\alpha\left(1+e^{-x_d}\right)\right.\\ &\left.+\beta\left(1+e^{-x_d/D}\right)\right)\sqrt{\varepsilon}+\frac{1}{4}\left(\alpha\left(e^{-x_d}-1\right)+\frac{\beta}{D}\left(e^{-x_d/D}-1\right)\right)\varepsilon\\ &+\mathcal{O}(\varepsilon\sqrt{\varepsilon}), \end{aligned}$$

and

$$\begin{aligned} J_{f,2}^3 :&= \int_{I_s^3} L_2(U_{f,ld}^{\ell};\bar{u}_{\varepsilon\tilde{\gamma}_1})dx\\ &= 2\tilde{\gamma}_1 x_d+\frac{1}{8}\gamma_2\left(\alpha(e^{-x_d}-1)+\beta D\left(e^{-x_d/D}-1\right)\right)+\frac{1}{8}\alpha^2\left(3-3e^{-x_d}\right.\\ &\quad\left.-x_d e^{-x_d}\right)+\frac{1}{8}\beta^2\left(3D-3De^{-x_d/D}-x_d e^{-x_d/D}\right)+\frac{1}{2}\alpha\beta\left(\frac{D^3-1}{D^2-1}\right)\\ &\quad+\frac{1}{2}\alpha\beta\left(\frac{e^{-x_d}-D^3e^{-x_d/D}}{D^2-1}\right)+\mathcal{O}(\sqrt{\varepsilon}). \end{aligned}$$

Observe that this term does explicitly depend on $\tilde{\gamma}_1$. Similarly, For I_s^6 we get

$$\begin{aligned} J_{f,1}^6 = &-\frac{1}{2}(\alpha e^{-x_d}+\beta De^{-x_d/D})+\frac{1}{2}\left(\alpha e^{-x_d}+\beta e^{-x_d/D}\right)\sqrt{\varepsilon}\\ &-\frac{1}{4}\left(\alpha e^{-x_d}+\frac{\beta}{D}e^{-x_d/D}\right)\varepsilon+\mathcal{O}(\varepsilon\sqrt{\varepsilon}), \end{aligned}$$

and

$$\begin{aligned} J_{f,2}^6 :&= \int_{I_s^6} L_2(U_{f,ld}^{\ell};\hat{u}_{\gamma_2})dx\\ &= \frac{1}{8}\gamma_2\left(\alpha\left(1+2e^{-x_d}\right)+\beta D\left(1+2e^{-x_d/D}\right)\right)+\frac{1}{8}\alpha^2\left(3+x_d\right)e^{-x_d}\\ &\quad+\frac{1}{8}\beta^2\left(3D+x_d\right)e^{-x_d/D}+\frac{1}{2}\alpha\beta\left(\frac{D^3e^{-x_d/D}-e^{-x_d}}{D^2-1}\right)+\mathcal{O}(\sqrt{\varepsilon}). \end{aligned}$$

Next, we compute the higher order contribution of the action functional over the fast fields $I_f^{2,4,5}$. Unlike the case for the slow fields, the error terms of the leading order contributions arising from shifting the limits of the fast integrals are exponentially small and we thus do not have to revisit $I_{f,1}^{2,4,5}$. We start with computing the correction term $J_{f,2}^2$ coming from the first fast field I_f^2. There is no $\mathcal{O}(\varepsilon)$-correction term to the fast component in I_f^2, see (34), and, in addition, the slow components in I_f^2 are to leading order zero, see (27) and (28). So, since $\gamma_1 = \Theta(\varepsilon)$, (23) reduces, to leading order, to

$$J_{f,2}^2 := \int_{I_f^2}\bar{L}_1(U_{f,ld}^{\ell};\bar{u}_{\varepsilon\gamma_1})d\xi = -\frac{1}{2}(\alpha+\beta)\int_{I_f^2}d\xi = -\frac{1}{\sqrt{\varepsilon}}(\alpha+\beta),$$

and we have

$$J_f|_{I_f^2} = \frac{2\sqrt{2}}{3}\varepsilon-(\alpha+\beta)\varepsilon\sqrt{\varepsilon}+\mathcal{O}(\varepsilon^2\sqrt{\varepsilon}).$$

The fast component is to leading order constant $+1$ over the two fast fields $I_f^{4,5}$ around the defect. So, $(U^\ell_{f,ld,0})_\xi = 0$ and $(U^\ell_{f,ld,0})^2 - 1 = 0$ in both I_f^4 and I_f^5. In addition, since $\gamma(x) = \gamma_1 = \Theta(\varepsilon)$ in I_f^4, (23) becomes

$$\begin{aligned} J^4_{f,2} :&= \int_{I_f^4} \bar{L}_1(U^\ell_{f,ld}; \bar{u}_{\varepsilon\gamma_1}) d\xi = -\frac{1}{2}\left(\alpha e^{-x_d} + \beta e^{-x_d/D}\right) \int_{I_f^4} d\xi \\ &= -\frac{1}{2}\frac{1}{\sqrt{\varepsilon}}\left(\alpha e^{-x_d} + \beta e^{-x_d/D}\right). \end{aligned}$$

In I_f^5, $\gamma(x) = \gamma_2$ but $U^\ell_{f,ld,0} - \hat{u}_{\gamma_2,0} = 0$, and (23) again reduces to

$$J^5_{f,2} :\, = \int_{I_f^5} \bar{L}_1(U^\ell_{f,ld}; \hat{u}_{\gamma_2}) d\xi = -\frac{1}{2}\frac{1}{\sqrt{\varepsilon}}\left(\alpha e^{-x_d} + \beta e^{-x_d/D}\right).$$

Combining the contributions from the slow and fast regions to the action functional gives—as expected—that the $\mathcal{O}(\varepsilon\sqrt{\varepsilon})$-terms from the fast regions cancel out with the $\mathcal{O}(\varepsilon\sqrt{\varepsilon})$-terms from the slow regions, and the total action functional of a local defect front solution $Z^\ell_{f,ld}$ pinned to the left of the defect becomes

$$\begin{aligned} J_f(U^\ell_{f,ld}) = &\left(\frac{2\sqrt{2}}{3} - (\alpha + \beta D)\right)\varepsilon + \left(2\tilde{\gamma}_1 x_d + \frac{1}{2}\gamma_2\left(\alpha e^{-x_d} + \beta D e^{-x_d/D}\right)\right. \\ &\left. -\frac{1}{2}\left(\alpha + \frac{\beta}{D}\right) + \frac{3}{4}\left(\alpha^2 + \beta^2 D\right) + \alpha\beta\left(\frac{D^3 - 1}{D^2 - 1}\right)\right)\varepsilon^2 \\ &+ \mathcal{O}(\varepsilon^2\sqrt{\varepsilon}). \end{aligned} \tag{35}$$

3.1.2 The Derivation of the First Part of Main Result 1

We study the critical points of the action functional $J_f(U^\ell_{f,ld})$ (35) to derive the results for local defect front solutions $Z^\ell_{f,ld}$ pinned to the left of the defect as stated in Main Result 1. For more details regarding this approach, we refer to Sect. 2, [5–7,9–12,52] and references therein, however, see also Remark 1. In particular, expression (3) determining the pinning distance x_d is obtained from the critical points of the action functional $J_f(U^\ell_{f,ld})$ (35), and only the critical points that are minima yield stable solutions. That is, the minima of the action functional coincide with the stability condition (4). To this purpose, we differentiate the action functional $J_f(U^\ell_{f,ld})$ (35) with respect to the unknown pinning distance x_d

$$\frac{d}{dx_d}(J_f(U^\ell_{f,ld})) = 2\tilde{\gamma}_1 - \frac{1}{2}\gamma_2\left(\alpha e^{-x_d} + \beta e^{-x_d/D}\right) = 2\tilde{\gamma}_1 - \frac{1}{2}\gamma_2 f(x_d),$$

and the second derivative is

$$\frac{d^2}{dx_d^2}(J_f(U^\ell_{f,ld})) = \frac{1}{2}\gamma_2\left(\alpha e^{-x_d} + \frac{\beta}{D}e^{-x_d/D}\right) = \frac{1}{2}\gamma_2 g(x_d).$$

So, the critical points of the action functional $J_f(U^\ell_{f,ld})$ (35) with respect to the pinning distance x_d are exactly given by the existence condition (3) of Main Result 1, and a critical point is a minimum if the stability condition (4) of Main Result 1 holds.

3.2 Pinned Front Solutions

We further investigate the results of Main Result 1 related to local defect front solutions, and we combine these results with the results of [54] related to global defect front solutions, see also Remark 4. So, we aim to get a broad picture of pinned front solutions supported by (1). For this reason, we first shortly discuss the essential properties of f (as defined in (3)) and $g = -f'$ (as defined in (4)). For $\alpha\beta > 0$ the function $\alpha f(x)$ is monotonically decreasing and strictly positive, while $f(x)$ has an extremum f_{ex} at x_{ex} for $\alpha\beta < 0$ and $|\alpha D| > |\beta|$ (recall that $D > 1$ by assumption). In particular,

$$f_{ex} := -\alpha(D-1)\left(-\frac{\alpha D}{\beta}\right)^{-D/(D-1)}, \quad x_{ex} := \frac{D}{D-1}\log\left(-\frac{\alpha D}{\beta}\right), \tag{36}$$

and $f(x_{ex}) = f_{ex}$ and $g(x_{ex}) = 0$. For convenience, we summarise these properties also in Table 1.

From Main Result 1 and these properties of f and g, we instantly get that there is a unique local defect front solution $Z^{\ell}_{f,ld}$ pinned to the left of the defect if $\alpha, \beta > 0$ and $0 < 4\tilde{\gamma}_1/\gamma_2 < \alpha + \beta$ and this solution is stable only if $\gamma_2 > 0$. A similar statement hold for $\alpha, \beta < 0$. For $\alpha\beta < 0$ it directly follows that the situation is more complicated. In particular, the existence condition $\gamma_2 f(x_d) = 4\tilde{\gamma}_1$ (3) for local defect front solutions $Z^{\ell}_{f,ld}$ pinned to the left of the defect can have up to two solutions if $|\alpha D| > |\beta|$. Consequently, there can be two local defect front solutions pinned to the left of the defect with different pinning distances for the same parameter set. From (4) it follows that one of these front solutions will be a stable solution, while the other one is unstable. We summarise the results from Main Result 1 for local defect front solutions $Z^{\ell}_{f,ld}$ pinned to the left of the defect for the different parameter combinations in Table 2, and also refer to Figs. 4 and 5 for particular examples.

For $\gamma_1 \equiv 0$ it immediately follows from (3)—see also Table 2—that local defect front solutions $Z^{\ell}_{f,ld}$ pinned to the left of the defect with pinning distance $x_d = \Theta(1)$ exist only for $\alpha\beta < 0$. Since the local defect front solutions studied in [24], see also Theorem 2, required $\gamma_1 \equiv 0$ and $\alpha, \beta > 0$, we can conclude that these front solutions necessarily have pinning distances $x_d \gg 1$. However, see also Remark 5.

Table 1 Properties of $f(x) := \alpha e^{-x} + \beta e^{-x/D}$ and $g(x) := -f'(x) = \alpha e^{-x} + \frac{\beta}{D} e^{-x/D}$ for $x \in [0, \infty)$

	$f(x)$	$f(0)$	$\mathcal{R}(f)$	f_{ex}	$g(x)$
$\alpha > 0, \beta > 0$	$\searrow$	> 0	$(0, \alpha + \beta]$	–	$\searrow, > 0$
$\alpha < 0, \beta < 0$	$\nearrow$	< 0	$[\alpha + \beta, 0)$	–	$\nearrow, < 0$
$\alpha > 0, \beta < 0, \alpha D < \lvert\beta\rvert$	$\nearrow$	< 0	$[\alpha + \beta, 0)$	–	< 0
$\alpha > 0, \beta < 0, \alpha < \lvert\beta\rvert < \alpha D$	$\searrow\nearrow$	< 0	$[f_{ex}, 0)$	< 0	$g(x_{ex}) = 0$
$\alpha > 0, \beta < 0, \alpha > \lvert\beta\rvert$	$\searrow\nearrow$	> 0	$[f_{ex}, \alpha + \beta]$	< 0	$g(x_{ex}) = 0$
$\alpha < 0, \beta > 0, \lvert\alpha D\rvert < \beta$	$\searrow$	> 0	$(0, \alpha + \beta]$	–	> 0
$\alpha < 0, \beta > 0, \lvert\alpha\rvert < \beta < \lvert\alpha D\rvert$	$\nearrow\searrow$	> 0	$(0, f_{ex}]$	> 0	$g(x_{ex}) = 0$
$\alpha < 0, \beta > 0, \lvert\alpha\rvert > \beta$	$\nearrow\searrow$	< 0	$[\alpha + \beta, f_{ex}]$	> 0	$g(x_{ex}) = 0$

$\mathcal{R}(f)$ stands for the range of the function f, $\searrow$ means that the function is monotonically decreasing, while $\nearrow$ means it is monotonically increasing. Similarly, $\searrow\nearrow$ means that the function f is first decreasing and then increasing and f attains its minimum f_{ex} at x_{ex}, i.e. $f_{ex} = f(x_{ex})$, see (36). Likewise, $\nearrow\searrow$ means that the function f is first increasing and then decreasing and it attains it maximum f_{ex} at x_{ex}

Table 2 Number of local defect front solutions $Z^{\ell}_{f,ld}$ pinned to the left of the defect with pinning distances $x_d = \Theta(1)$, and their stability properties, as derived from Main Result 1

	$\#Z^{\ell}_{f,ld} = 0$	$\#Z^{\ell}_{f,ld} = 1$	$\#Z^{\ell}_{f,ld} = 2$
$\alpha, \beta > 0$ or	$4\tilde{\gamma}_1/\gamma_2 \leq 0$ or	$0 < 4\tilde{\gamma}_1/\gamma_2 < f(0)$	–
$(\alpha < 0, \beta > 0$ and $\lvert\alpha D\rvert < \beta)$	$4\tilde{\gamma}_1/\gamma_2 \geq f(0)$	$\gamma_2 > 0$: stable	
$\alpha, \beta < 0$ or	$4\tilde{\gamma}_1/\gamma_2 \geq 0$ or	$f(0) < 4\tilde{\gamma}_1/\gamma_2 < 0^*$	–
$(\alpha > 0, \beta < 0$ and $\alpha D < \lvert\beta\rvert)$	$4\tilde{\gamma}_1/\gamma_2 \leq f(0)$	$\gamma_2 < 0$: stable	
$\alpha > 0, \beta < 0$ and	$4\tilde{\gamma}_1/\gamma_2 \geq 0$ or	$f(0) \leq 4\tilde{\gamma}_1/\gamma_2 < 0^*$	$f_{ex} < 4\tilde{\gamma}_1/\gamma_2 < f(0)$
$\alpha < \lvert\beta\rvert < \alpha D$	$4\tilde{\gamma}_1/\gamma_2 < f_{ex}$	$\gamma_2 < 0$: stable	$\gamma_2 > 0$: x_d^1 stable
			$\gamma_2 < 0$: x_d^2 stable
$\alpha > 0, \beta < 0$ and	$4\tilde{\gamma}_1/\gamma_2 \geq f(0)$ or	$0 \leq 4\tilde{\gamma}_1/\gamma_2 < f(0)$	$f_{ex} < 4\tilde{\gamma}_1/\gamma_2 < 0^*$
$\alpha > \lvert\beta\rvert$	$4\tilde{\gamma}_1/\gamma_2 < f_{ex}$	$\gamma_2 > 0$: stable	$\gamma_2 > 0$: x_d^1 stable
(Figs. 4 and 5)			$\gamma_2 < 0$: x_d^2 stable
$\alpha < 0, \beta > 0$ and	$4\tilde{\gamma}_1/\gamma_2 > f_{ex}$ or	$0 < 4\tilde{\gamma}_1/\gamma_2 \leq f(0)$	$f(0) < 4\tilde{\gamma}_1/\gamma_2 < f_{ex}$
$\lvert\alpha\rvert < \beta < \lvert\alpha D\rvert$	$4\tilde{\gamma}_1/\gamma_2 \leq 0$	$\gamma_2 > 0$: stable	$\gamma_2 > 0$: x_d^2 stable
			$\gamma_2 < 0$: x_d^1 stable
$\alpha < 0, \beta > 0$ and	$4\tilde{\gamma}_1/\gamma_2 > f_{ex}$ or	$f(0) < 4\tilde{\gamma}_1/\gamma_2 \leq 0^*$	$0 < 4\tilde{\gamma}_1/\gamma_2 < f_{ex}$
$\lvert\alpha\rvert > \beta$	$4\tilde{\gamma}_1/\gamma_2 \leq f(0)$	$\gamma_2 < 0$: stable	$\gamma_2 > 0$: x_d^2 stable
			$\gamma_2 < 0$: x_d^1 stable

Note that $f(0) = \alpha + \beta$ and f_{ex} is defined in (36). In the right-most column, the pinning distance is the defining difference between the two different local defect front solutions $Z^{\ell}_{f,ld}$ and we label the smaller pinning distance as x_d^1 and the larger one as x_d^2. So, $0 < x_d^1 < x_d^2$. The * indicates the cases where local defect front solutions $Z^{\ell}_{f,ld}$ exist for $\tilde{\gamma}_1\gamma_2 < 0$, i.e. the cases where global defect front solutions $Z_{f,gd}$ also exist [54]

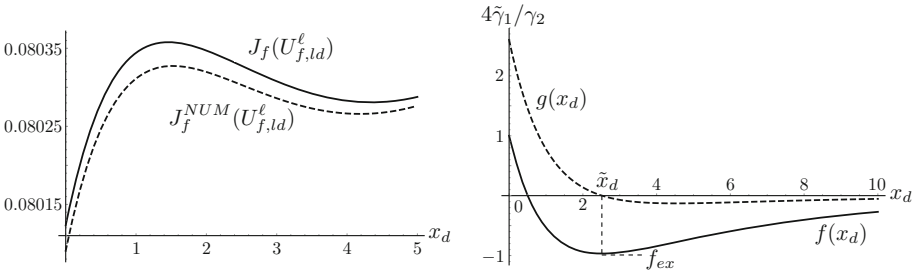

Fig. 4 An example of $J_f(U^{\ell}_{f,ld})$ (35), $f(x_d)$ and $g(x_d)$ for $sgn(\alpha) \neq sgn(\beta) = -1$, $|\alpha D| > |\beta|$ and $\alpha + \beta > 0$. In particular, $(\alpha, \beta, D, \gamma_1, \gamma_2, \varepsilon) = (3, -2, 5, 0.01, -5, 0.01)$. Left panel: the action functional $J_f(U^{\ell}_{f,ld})$ (35) and the numerically evaluated action functional $J_f^{NUM}(U^{\ell}_{f,ld})$ (37) obtained from the asymptotically profile of a local defect front solution $Z^{\ell}_{f,ld}$ pinned to the left of the defect as function of the still undetermined pinning distance (and as derived in Sect. 3.1). The shape of the curve, as well as the location of the critical points are in good agreement, while the difference between the two curves appears to be, as expected, $\mathcal{O}(\varepsilon^2\sqrt{\varepsilon})$. Right panel: the functions $f(x_d)$ and $g(x_d)$. For $f_{ex} < 4\tilde{\gamma}_1/\gamma_2 < 0$ (see (36) for the definition of f_{ex}), there exist two different local defect front solutions $Z^{\ell}_{f,ld}$ pinned to the left of the defect. If $\gamma_2 < 0$, then the pinned front solution closest to the defect, i.e. with smallest pinning distance x_d, is unstable, while the larger one is stable

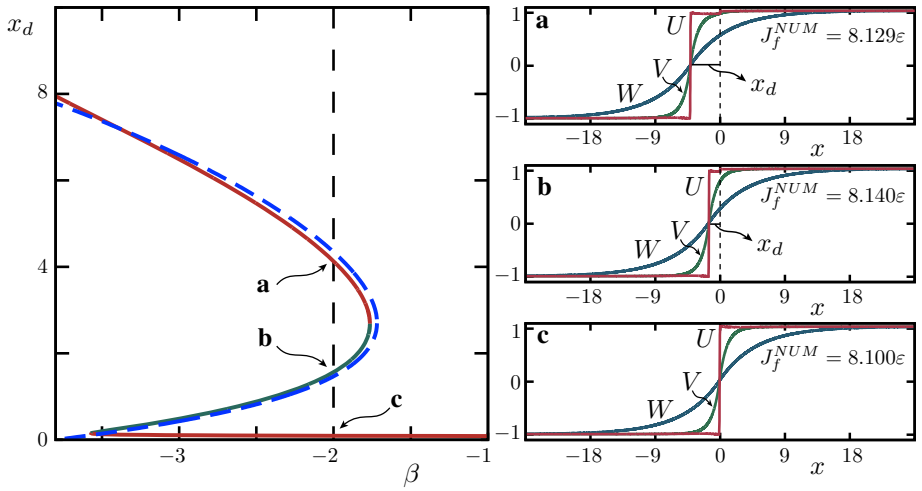

Fig. 5 Left panel: bifurcation diagram of the pinning distance x_d of pinned defect front solutions for varying β obtained by numerically simulating (10) on a domain of length $2L = 54$. The other system parameters are kept fixed at $(\alpha, D, \varepsilon\tilde{\gamma}_1, \gamma_2) = (3, 5, \varepsilon, -5)$ with $\varepsilon = 0.02$. So, besides ε, the system parameters are similar to Fig. 4. The red curves represent numerically stable pinned defect front solutions, while the green curve represent numerically unstable pinned defect front solutions. The dashed blue curve shows the asymptotically predicted pinning distances x_d for the local defect front solutions $Z^{\ell}_{f,ld}$ obtained from the existence condition (3) of Main Result 1. We observe excellent agreement between the asymptotic curve and the numerical curve, and also the stability results coincide. Right panels: the associated profiles of the pinned defect front solutions for $\beta = -2$. We have the co-existence of a stable global defect front solution (panel **c**) and two local defect front solutions (panels **a**, **b**). The local defect front solution with the larger pinning distance is stable (panel **a**), while the other one is unstable (panel **b**). Observe that the unstable local defect front solution in panel **b** indeed has the largest action functional value (Color figure online)

3.2.1 Numerical Results

Global defect front solutions $Z_{f,gd}$ exist only for $\gamma_1\gamma_2 < 0$ [54]. So, from Table 2 it follows that $\alpha > 0$, $\beta < 0$ and $\alpha D > |\beta|$ is the most interesting parameter setting (since in this case we can have the co-existence of two local defect front solutions $Z^{\ell}_{f,ld}$ pinned to the left of the defect and a global defect front solution $Z_{f,gd}$). Therefore, we numerically investigate (10) for this parameter setting to further validate the asymptotic leading order results for pinned defect front solutions as stated in Main Result 1 and as derived in [54]. To determine the ε-dependent numerical profiles, we adapt the path following procedure for the homogeneous version of (10) outlined in [52]. This procedure is inspired by the predictor-corrector method of pseudo-arclength continuation [19,33,49]. From these profiles, we also compute the numerical action functional $J^{NUM}_{f,p}(u)$ by replacing the improper integrals of (15) and (17) by integrals from $-L$ to 0 and 0 to L. Here, $2L$ represents the length of the domain used in the numerical integration. So,

$$J^{NUM}_{f,p}(u) = \int_{-L}^{0} L(u; \bar{u}_{\gamma_1})dx + \int_{0}^{L} L(u; \hat{\bar{u}}_{\gamma_2})dx\,. \tag{37}$$

See [52] for more details regarding the numerical techniques. We observe an excellent agreement between the numerically observed pinning distances and the leading order pinning distances computed from the existence condition (3) of Main Result 1, see the left panels of Figs. 4 and 5. Since $\gamma_2 < 0$ and $\tilde{\gamma}_1 > 0$, the stability condition (4) of Main Result 1 gives that—for fixed system parameters—the local defect front solution $Z^{\ell}_{f,ld}$ with the larger pinning distance is stable, while the other one is unstable, see also Table 2. This agrees with Fig. 4 as the extremum of $J_f(U^{\ell}_{f,ld})$ with the larger pinning distance is a minimum. It also coincides with the numerically observed stability properties of the pinned front solutions—obtained from the spectrum of the discretised PDE—shown in Fig. 5. Furthermore, since $\gamma_2 < 0 < \gamma_1$, the global defect front solution $Z_{f,gd}$ is expected to be stable [54] and this is again confirmed by the numerical results, see again Fig. 5.

4 Pinned Pulse Solutions

In this section, we focus on pinned pulse solutions supported by (1) and we derive the part of Main Result 1 related to the existence and stability of local defect pulse solutions $Z^{r}_{p,ld}$ pinned to the right of the defect. We follow the same procedure as for pinned front solutions and we combine GSPT techniques with the action functional approach. However, for the clarity of the presentation, and since the computations are similar in spirit (though algebraically more involved) as the computations for pinned front solutions, the derivation of the profile of a local defect pulse solution $Z^{r}_{p,ld}$—with unknown pulse half-width x^* and unknown pinning distance x_d—and the computation of its action functional J_p (15) is placed in "Appendix B". In addition, we show that the action functional approach also reproduces some of the previously obtained results of [54] related to the existence of global defect pulse solutions $Z_{p,gd}$ and the non-existence of local defect pulse solutions $Z^{m}_{p,ld}$ with the defect pinned in between the two interfaces [54]. Finally, in Sect. 4.2, we confirm our asymptotic findings by numerically investigating (10).

4.1 The Derivation of the Second Part of Main Result 1

We need to compute the action functional $J_p(U^{r}_{p,ld})$ (15) associated to a local defect pulse solution $Z^{r}_{p,ld}$ pinned to the right of the defect to derive the parts of Main Result 1 related to local defect pulse solutions. We state the action functional below and refer to "Appendix B" for its proof.

Lemma 1 *The action functional $J_p(U^{r}_{p,ld})$ (15) associated to a local defect pulse solution $Z^{r}_{p,ld}$ pinned to the right of the defect is given by*

$$
\begin{aligned}
J_p(U^r_{p,ld}) = &\left(-2\alpha\left(1-e^{-2x^*}\right) - 2\beta D\left(1-e^{-2x^*/D}\right) + 4\gamma_2 x^* + \frac{4\sqrt{2}}{3}\right)\varepsilon \\
&- \left(\alpha\left(1-e^{-2x^*}\right) + \frac{\beta}{D}\left(1-e^{-2x^*/D}\right)\right)\varepsilon^2 \\
&+ 2\alpha\beta\frac{1}{D^2-1}\left(-\left(1-e^{-2x^*}\right) + D^3\left(1-e^{-2x^*/D}\right)\right)\varepsilon^2 \\
&+ \frac{1}{2}\alpha^2\left(3-3e^{-2x^*} - 2x^*e^{-2x^*}\right)\varepsilon^2 \\
&+ \frac{1}{2}\beta^2\left(3D - 3De^{-2x^*/D} - 2x^*e^{-2x^*/D}\right)\varepsilon^2 \\
&- \frac{1}{2}\gamma_1\left(\alpha e^{-x_d}\left(1-e^{-2x^*}\right) + \beta D e^{-x_d/D}\left(1-e^{-2x^*/D}\right)\right)\varepsilon^2 \\
&+ \frac{1}{2}\alpha\gamma_2\left(e^{-x_d} - e^{-(x_d+2x^*)} - 4x^*\right)\varepsilon^2 \\
&+ \frac{1}{2}\beta\gamma_2\left(De^{-x_d/D} - De^{-(x_d+2x^*)/D} - 4x^*\right)\varepsilon^2 + \mathcal{O}(\varepsilon^2\sqrt{\varepsilon}),
\end{aligned}
\tag{38}
$$

with the pinning distance x_d and the half-width of the pulse x^* both positive and $\Theta(1)$ with respect to ε.

Proof of Lemma 1. See "Appendix B". □

To derive the results of Main Result 1 related to local defect pulse solutions, we differentiate the action functional $J_p(U^r_{p,ld})$ (38) with respect to the unknown pulse half-width x^* and with respect to the unknown pinning distance x_d. Next, we equate the resulting expressions to zero. This gives

$$
\begin{aligned}
\frac{\partial}{\partial x^*}J_p(U^r_{p,ld}) = 0 &\implies 4\left(-\alpha e^{-2x^*} - \beta e^{-2x^*/D} + \gamma_2\right)\varepsilon = \mathcal{O}(\varepsilon^2) \\
&\implies 4\left(-f(2x^*) + \gamma_2\right)\varepsilon = \mathcal{O}(\varepsilon^2),
\end{aligned}
$$

and

$$
\begin{aligned}
&\frac{\partial}{\partial x_d}J_p(U^r_{p,ld}) = 0 \implies \\
&\quad\frac{1}{2}(\gamma_1-\gamma_2)\left(\alpha e^{-x_d}\left(1-e^{-2x^*}\right) + \beta e^{-x_d/D}\left(1-e^{-2x^*/D}\right)\right)\varepsilon^2 = \mathcal{O}(\varepsilon^2\sqrt{\varepsilon}) \\
&\qquad\implies \frac{1}{2}(\gamma_1-\gamma_2)\left(f(x_d) - f\left(x_d+2x^*\right)\right)\varepsilon^2 = \mathcal{O}(\varepsilon^2\sqrt{\varepsilon}).
\end{aligned}
$$

The first condition coincides, to leading order, with the first existence condition of (5), while the second condition coincides, to leading order, with the second existence condition of (5). The local defect pulse solutions that are minimisers of $J_p(U^r_{p,ld})$ (38) correspond to stable pulse solutions. Since $J_p(U^r_{p,ld})$ is a function of two unknowns, the second derivative test—see, for instance, Theorems 2.1 and 3.1 in Chapter 8 in [16]—determines these minimisers. However, since $J_p(U^r_{p,ld})$ is to leading order independent of x_d, the second derivative test simplifies and the minimisers of $J_p(U^r_{p,ld})$ are determined given by the critical points of $J_p(U^r_{p,ld})$ such that both $\frac{\partial^2 J}{\partial(x^*)^2}$ and $\frac{\partial^2 J}{\partial(x_d)^2}$ are positive. So, a local defect pulse solution $Z^r_{p,ld}$ with half-width x^* and pinning distance x_d is stable if it is at a critical point of $J_p(U^r_{p,ld})$

and if

$$\frac{\partial^2 J}{\partial (x^*)^2} > 0 \implies 8\left(\alpha e^{-2x^*} + \frac{\beta}{D} e^{-2x^*/D}\right)\varepsilon > 0 \implies g(2x^*) > 0\,,$$

and

$$\frac{\partial^2 J}{\partial (x_d)^2} > 0 \implies$$
$$\frac{1}{2}(\gamma_2 - \gamma_1)\left(\alpha e^{-x_d}\left(1 - e^{-2x^*}\right) + \frac{\beta}{D} e^{-x_d/D}\left(1 - e^{-2x^*/D}\right)\right) > 0\,,$$
$$\implies (\gamma_2 - \gamma_1)\left(g(x_d) - g(x_d + 2x^*)\right) > 0\,.$$

This completes the derivation of the second part of Main Result 1.

4.2 Pinned Pulse Solutions

We further investigate the results of Main Result 1 related to local defect pulse solutions, and we combine these results with the results of [54] related to global defect pulse solutions. So, we aim to get a broad picture of pinned pulse solutions supported by (1).

4.2.1 Numerical Results: Pulse Widths

The action functional $J_p(U^r_{p,ld})$ (38) for a local defect pulse solution $Z^r_{p,ld}$ pinned to the right of the defect is—to leading order—independent of the pinning distance x_d, and, consequently,

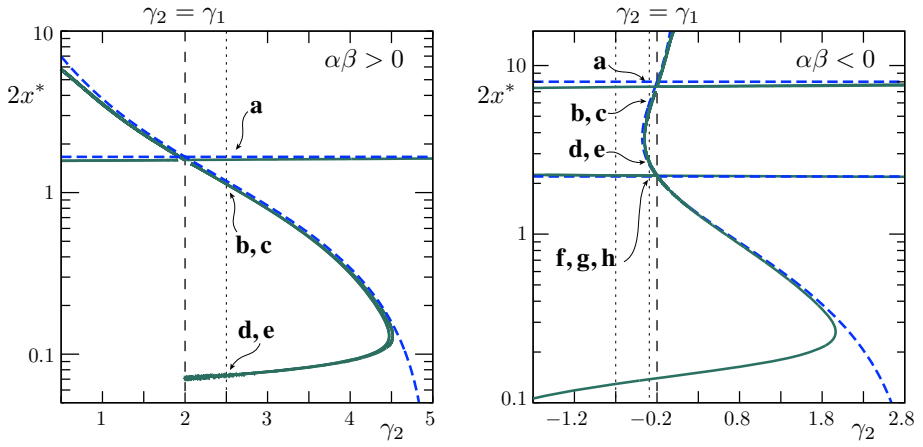

Fig. 6 Bifurcation diagrams of the observed pulse widths $2x^*$ of pinned pulse solutions for varying γ_2 and for two different parameter sets. We observe an excellent agreement between the pulse widths obtained from numerically integrating (10) (green solid curves) and the asymptotically leading order widths determined by (5) of Main Result 1 (blue dashed curves) for pulse widths that are not too small. In the left panel the system parameters are kept fixed at $(\alpha, \beta, D, \gamma_1, \varepsilon) = (3, 2, 5, 2, 0.02)$ such that $\alpha\beta > 0$ and $2L = 24$, while in the right panel the system parameters are set at $(\alpha, \beta, D, \gamma_1, \varepsilon) = (4, -1, 5, -0.2, 0.05)$ such that $\alpha\beta < 0$ and $2L = 48$. The vertical dashed black lines indicate the homogeneous system were $\gamma_1 = \gamma_2$. The pinned pulse profiles associated to $\gamma_2 = 2.5$ (dotted line) in the bifurcation diagram in the left panel are shown in Fig. 7, and the pinned pulse profiles associated to $\gamma_2 = -0.3$ (dotted line) in the bifurcation diagram in the right panel are shown in Fig. 8 (Color figure online)

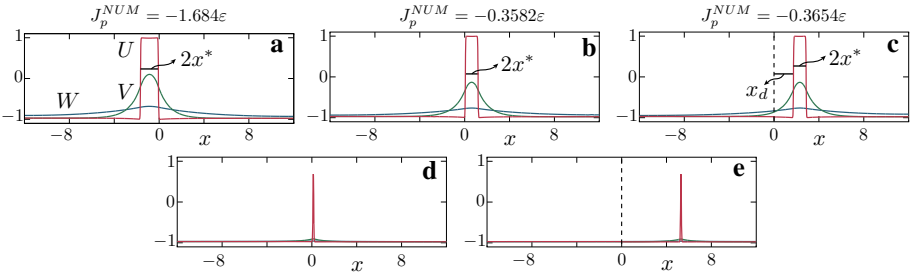

Fig. 7 The pinned pulse profiles associated to $\gamma_2 = 2.5$ in the bifurcation diagram in the left panel of Fig. 6 obtained by numerically integrating (10) over a domain of length $2L = 24$. The other parameters are kept fixed at $(\alpha, \beta, D, \gamma_1, \varepsilon) = (3, 2, 5, 2, 0.02)$. The profiles of panels **b** and **c** have the same leading order widths. The profiles of panels **a** and **c** are numerically stable, while the scatter solution [62] of panel **b** is numerically unstable. The small pulse profiles shown in panels **d** and **e** have not been analysed by the asymptotic methods of this manuscript

similar to the action functional for a homogeneous stationary pulse solution (with $\gamma = \gamma_2$), see Lemma 1 in [52]. As a result, the first existence condition (5) of Main Result 1 determining the width of the local defect pulse solution is the same as the existence condition for a stationary pulse solution in the homogeneous case (with $\gamma = \gamma_2$), see also [23]. In other words, the defect does not—to leading order—destroy the width of a stationary pulse solution. Combining the results of Main Result 1 and [54], and by using the symmetry (8), gives that the widths of both local and global pinned pulse solutions are to leading order determined by $f(2x^*) = \gamma_i$. So, to leading order, the widths of pinned pulse solutions to the right or left of the defect are independent from the pinning distance of the pulse to the defect. This is also observed numerically for pulses with widths that are not too small, i.e. in regions in parameter space where our asymptotic analysis is valid, see the bifurcation diagrams in Fig. 6. The profiles of the particular defect pulse solutions associated to Fig. 6, for a fixed value of γ_2, are shown in Fig. 7 (for $\alpha\beta > 0$) and Fig. 8 (for $\alpha\beta < 0$). Moreover, since $f(2x^*) = \gamma_i$ can have up to two solutions for a fixed parameter set, see Table 1 and [23], a pinned pulse solution can have up to four different leading order widths for a given parameter set $(\alpha, \beta, D, \gamma_1, \gamma_2)$. See, for instance, Fig. 8.

Furthermore, it is clear that for fixed x^* the action functional $J_p(U^r_{p,ld})$ (38) is smaller than the action functional $J_p(U^\ell_{p,ld})$[7] associated to a local defect pulse solution pinned to the left of the defect if and only if $\gamma_1 > \gamma_2$. Consequently,

$$\min_{x^*} J_p(U^\ell_{p,ld}) > \min_{x^*} J_p(U^r_{p,ld}) \quad \text{if and only if} \quad \gamma_1 > \gamma_2\,.$$

That is, a pinned pulse solution $Z^r_{p,ld}$ pinned to the right of the defect is favourable compared to a pinned pulse solution $Z^\ell_{p,ld}$ pinned to the left of the defect if and only if $\gamma_1 > \gamma_2$ (since only critical points that are local minima are stable). See also upcoming Fig. 9. This is consistent with the results for global defect pulse solutions $Z_{p,gd}$ presented in [54]: a global defect pulse solution $Z^r_{p,gd}$ pinned immediately to the right of the defect and with leading order width $2x^*$ exists if $\gamma_1 > \gamma_2$ and if $x^* > 0$ solves $f(2x^*) = \gamma_2$.

[7] This action functional can be directly obtained from (38) by interchanging the role of γ_1 and γ_2.

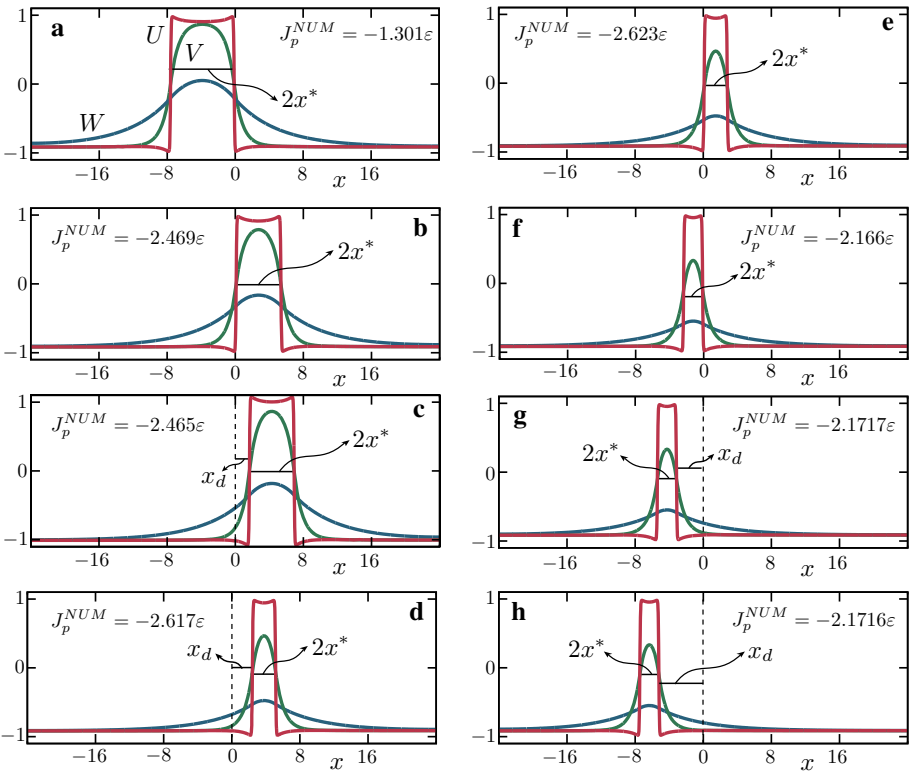

Fig. 8 The pinned pulse profiles associated to $\gamma_2 = -0.3$ in the bifurcation diagram in the right panel of Fig. 6 obtained by numerically integrating (10) over a domain of length $2L = 48$. The other parameters are kept fixed at $(\alpha, \beta, D, \gamma_1, \varepsilon) = (4, -1, 5, -0.2, 0.05)$. The profiles of panels **b** and **c** have the same leading order width. Similarly, the profiles of panels **d** and **e** have the same leading order width, and also the profiles of panels **f**, **g** and **h** have the same leading order width

4.2.2 Local Defect Pulse Solutions $Z^m_{p,ld}$ Pinned Around the Defect

Local defect pulse solutions correspond to pulse solutions with their interfaces located away from the defect. So, there are potentially three different types of local defect pulse solutions: the defect is to the left of both interfaces, the defect is to the right of both interfaces, and the defect is in between both interfaces. In [54], it was shown that local defect pulse solutions with the defect pinned in between both interfaces do not exist. This result can also be explained by using the current approach. The leading order term of an action functional $J_p(U^m_{p,ld})$ for a local defect pulse solution $Z^m_{p,ld}$ with the defect located in between the two interfaces is slightly different from the leading order term of the action functional $J_p(U^r_{p,ld})$ (38) (and from the leading order term of the action functional $J_p(U^\ell_{p,ld})$). This difference comes from the final term $\gamma_i(u_0 - \hat{\hat{u}}_{\gamma_i,0})$ in the integral of the leading order part of the action functional over the slow field in between the interfaces, see (19). Integrating this term for a local defect pulse solution pinned completely to the left or right of the defect—as well as for a homogeneous pulse solution—gives $4\gamma_i x^*$ (with $2x^*$ the leading order pulse width), while integrating this term for $Z^m_{p,ld}$ gives $2\gamma_2 x_2^* - 2\gamma_1 x_1^*$, where $x_1^* < 0 < x_2^*$ denote the location of the two

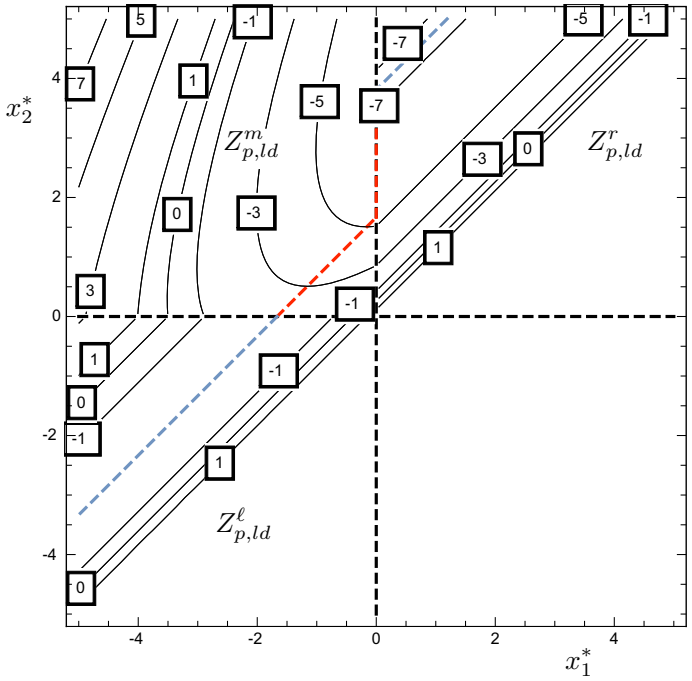

Fig. 9 Contour plot of the leading order part of the action functionals $J_p(U^{r,\ell,m}_{p,ld})$ (38) and (39) (divided by ε) of local defect pulse solutions $Z^{r,\ell,m}_{p,ld}$ as function of the interface locations x_1^* and x_2^*—such that the leading order pulse width is $2x^* = x_2^* - x_1^*$—for $(\alpha, \beta, D, \gamma_1, \gamma_2) = (3, 2, 5, 2, 1)$. The level curves associated to the action functionals $J_p(U^{r,\ell}_{p,ld})$ in first and third quadrants are constant along the lines $x_2^* - x_1^* = K$, $K \in \mathbb{R}$, since these action functionals $J_p(U^{r,\ell}_{p,ld})$ depend only on $2x^* = x_2^* - x_1^*$. The minimum in each of these two quadrants is indicated by the blue dashed curve and they are attained for $x_2^* - x_1^* = K^*_{1,2}$ with $f(K^*_{1,2}) = \gamma_{1,2}$. In particular, $K_1^* \approx 1.6663$ and $K_2^* \approx 3.8096$. Since $\gamma_2 < \gamma_1$, we have—as expected—that $K_2^* > K_1^*$ and $\min\{J_p(U^r_{p,ld})\} < \min\{J_p(U^\ell_{p,ld})\}$. In addition, the leading order part of the action functional $J_p(U^m_{p,ld})$ (39) in the second quadrant becomes minimal for $(x_1^*, x_2^*) \to (0, K_2^*)$. The red dashed curve in the second quadrant indicates the minimum of the action functional $J_p(U^m_{p,ld})$ for a given x_2^* fixed. Note that the action functional $J_p(U^m_{p,ld})$ decreases along the red curve for increasing x_1^* (Color figure online)

interfaces and with $x_2^* - x_1^*$ the leading order pulse width. In the end, this leads to the following action functional $J_p(U^m_{p,ld})$—which we present without proof, but we refer to [52] for more details—for a local defect pulse solution $Z^m_{p,ld}$ with the defect pinned in between the two interfaces

$$J_p(U^m_{p,ld}) = \left(-2\alpha\left(1 - e^{-(x_2^* - x_1^*)}\right) - 2\beta D\left(1 - e^{-(x_2^* - x_1^*)/D}\right) + 2\left(\gamma_2 x_2^* - \gamma_1 x_1^*\right) + \frac{4\sqrt{2}}{3}\right)\varepsilon + \mathcal{O}(\varepsilon\sqrt{\varepsilon})\,. \tag{39}$$

Unlike the leading order term of the action functional $J_p(U^r_{p,ld})$ (38) (and of $J_p(U^{r,\ell}_{p,ld})$), the action functional $J_p(U^m_{p,ld})$ depends on two variables. Upon introducing $2x^* := x_2^* - x_1^* >$

0—such that x^* again represents the pulse half-width—we rewrite (39) as

$$J_p(U^m_{p,ld}) = \left(-2\alpha \left(1 - e^{-2x^*}\right) - 2\beta D \left(1 - e^{-2x^*/D}\right) + 4\min\{\gamma_1, \gamma_2\}x^* + \frac{4\sqrt{2}}{3} \right) \varepsilon + 2\varepsilon(\gamma_2 - \gamma_1)y + \mathcal{O}(\varepsilon\sqrt{\varepsilon}),$$

with $y := x_2^*$ for $\gamma_2 > \gamma_1$ and $y := x_1^*$ for $\gamma_1 > \gamma_2$. By construction, only the linear term $2(\gamma_2 - \gamma_1)y$ of the leading order part of $J_p(U^m_{p,ld})$ depends on the variable y and this term is positive for both $\gamma_2 > \gamma_1$ and $\gamma_1 > \gamma_2$ (since $x_1^* < 0 < x_2^*$). Consequently, for $\gamma_2 > \gamma_1$, $y \to 0$ (which implies that $x_2^* \to 0$) is a necessary condition for $J_p(U^m_{p,ld})$ to be minimal, while $y \to 2x^*$ (which implies $x_1^* \to 0$) is a necessary condition for $J_p(U^m_{p,ld})$ to be maximal. Similarly, for $\gamma_1 > \gamma_2$, $y \to 0$ (which implies that $x_1^* \to 0$) is a necessary condition for $J_p(U^m_{p,ld})$ to be minimal, while $y \to -2x^*$ (which implies $x_2^* \to 0$) is a necessary condition for $J_p(U^m_{p,ld})$ to be maximal. In other words, for both $\gamma_2 > \gamma_1$ and $\gamma_1 > \gamma_2$ local defect pulse solutions $Z^m_{p,ld}$ with the defect in between the two interfaces move towards the boundary of the slow field, see also Fig. 9. So, as was already shown in [54], local defect pulse solutions $Z^m_{p,ld}$ with the defect in between the two interfaces do not exist as they move towards global defect pulse solutions $Z_{p,gd}$.

In addition, the part of the leading order term of the action functional $J_p(U^m_{p,ld})$ that depends on the pulse half-width x^* is identical to the leading order term of the action functionals $J_p(U^{r,\ell}_{p,ld})$ (38). Consequently, they have the same critical points $\{x^* | f(2x^*) = \gamma_i\}$ and thus also the same pulse half-widths and stability properties. For instance, for $\gamma_2 > \gamma_1$, $J_p(U^m_{p,ld})$ is minimal for $y = 0, \{x^* | f(2x^*) = \gamma_1\}$ and $g(2x^*) > 0$ and maximal for $y = 2x^*, \{x^* | f(2x^*) = \gamma_2\}$ and $g(2x^*) < 0$. So, again, smaller γ_i's are favourable.

4.2.3 Numerical Results: Pinning Distances

For $\alpha\beta > 0$ and $|\gamma_1 - \gamma_2| = \Theta(1)$, the first existence condition of (5) of Main Result 1 related to the width of a local defect pulse solution $Z^r_{p,ld}$ pinned to the right of the defect is solvable if $\alpha\gamma_2 > 0$ and $0 < |\gamma_2| < |\alpha + \beta|$. Furthermore, since f is monotonically decreasing or increasing, see Table 1, the second existence condition of (5) yields that—similar to the front case—the pinning distance $x_d \gg 1$. However, see Remark 5. From the stability conditions (6) of Main Result 1—with $x_d \gg 1$—it follows that these local defect pulse solutions $Z^r_{p,ld}$ pinned to the right of the defect are stable only if $\alpha, \beta > 0$ and $\gamma_2 > \gamma_1$. For $\alpha, \beta < 0$ all pinned pulse solutions will be unstable—independent of the defect—since the first stability condition of (6) is never satisfied. Combining this stability result for local defect pulse solutions $Z^r_{p,ld}$ with the results for global defect pulse solutions $Z_{p,gd}$ from [54], we obtain that for $\alpha, \beta > 0$ and $0 < \gamma_1 < \gamma_2 < \alpha + \beta$, (1) supports a stable global defect pulse solution $Z^\ell_{p,gd}$ pinned to the left of the defect and a stable local defect pulse solution $Z^r_{p,ld}$ pinned to the right of the defect (with asymptotically large pinning distance x_d). These stable solutions are separated by an unstable scatter solution $Z^r_{p,gd}$ [62] pinned immediately to the right of the defect, see Figs. 6 and 7. The numerically computed action functional values J_p^{NUM} (37) for the profiles in these figures confirm the asymptotic—and numerical—stability results. That is, the scatter solution $Z^r_{p,gd}$ has the largest action functional value. This unstable scatter solution can be further understood by observing that $J_p(U^r_{p,ld})$ (38) also approaches a critical point—at least from one side—as $x_d \to 0$, and, similarly, $J_p(U^m_{p,ld})$ (39) approaches a critical point—from the other side—as $x_1^* \to 0$.

As for the front case, the results of Main Result 1 related to local defect pulse solutions are more interesting for $\alpha\beta < 0$, see also Remark 2. In this case, stable and unstable local

Table 3 Pulse width $2x^*$, pinning distance x_d, pinning region, and stability properties (S = stable, U = unstable) of pinned pulse solutions obtained from Main Result 1, symmetry (8) and [54] for $(\alpha, \beta, D, \gamma_1, \gamma_2) = (4, -1, 5, -0.2, -0.3)$, as well as their relation to the profiles of Fig. 8 obtained from simulating (10) on a domain of length $2L = 48$

	$2x^*$	x_d	Region	Stab.	Figure 8	Num. stab.	J_p^{NUM}
$Z_{p,gd}^{\ell,1}$	2.20	–	$x < 0$	U	f	U	-2.166ε
$Z_{p,gd}^{\ell,2}$	8.01	–	$x < 0$	U	a	U	-1.301ε
$Z_{p,gd}^{r,1}$	2.61	–	$x > 0$	S	e	S	-2.623ε
$Z_{p,gd}^{r,2}$	5.83	–	$x > 0$	U	b	U	-2.469ε
$Z_{p,ld}^{\ell,1}$	2.20	2.88	$x < 0$	S	g	S	-2.172ε
$Z_{p,ld}^{\ell,2}$	8.01	2.01	$x < 0$	U	–	–	–
$Z_{p,ld}^{r,1}$	2.61	2.76	$x > 0$	U	d	U	-2.617ε
$Z_{p,ld}^{r,2}$	5.83	2.20	$x > 0$	U	c	U	-2.465ε

defect pulse solutions $Z_{p,ld}$ with different widths can be pinned in the same γ-region, see, for instance, Figs. 8, 10 and 11. Combining the result of this manuscript with the results for global defect pulse solutions $Z_{p,gd}$ of [54], and since the first existence condition $f(2x^*) = \gamma_i$ of Main Result 1 can have up to two solutions, shows that there can actually be a myriad of different pinned defect pulse solutions, especially for $0 < |\gamma_{1,2}| < |\alpha + \beta|$ and $|\alpha D| > |\beta|$, see also Table 1. For instance, for $(\alpha, \beta, D, \gamma_1, \gamma_2) = (4, -1, 5, -0.2, -0.3)$—the parameter values used in Figs. 6, 8, 10 and 11—the asymptotic results of this manuscript and [54] predict the existence of (at least) eight different pinned pulse solutions. Two of these eight pinned solutions are stable, while the other six are unstable. The asymptotic results for this particular parameter set are summarised in Table 3. Numerical simulations of (10) for the same parameter set on a domain of length $2L = 48$ yield the same stable pinned pulse solutions, as well as six unstable pinned pulse solutions (and some small pulse profiles similar to the ones shown in panels "d" and "e" of Fig. 7). However, one of the unstable pinned pulse solutions from the asymptotic results of Main Result 1 is not found numerically on this domain of integration. This is due to the relative small size of the domain and we remark that we did find this solution by simulating on a larger domain, see Fig. 10 and also Remark 5. In addition, one of the numerically computed unstable pinned pulse solutions—shown in panel "h" of Fig. 8—is not found by the asymptotic results of Main Result 1. We postulate that this stems from the fact that the pinning distance for this pinned pulse solution is—asymptotically—much larger than one and a higher order analysis is needed to also find the pinning distance for this solution, see again Remark 5. Actually, we believe that there are potentially three more of these pinned pulse solutions that are pinned far away from the defect and that are not captured by the asymptotic results of this manuscript.

To further justify the above claims, we reinvestigate the pinned pulse solutions with leading order width $2x^* \approx 8.01$ for the same parameter set but on a larger domain—$2L = 72$ instead of $2L = 48$. Besides the unstable global defect pulse solution $Z_{p,gd}^{\ell,2}$ we also found on the smaller domain, see Table 3, we discover two addition pinned pulse solutions with leading order width $2x^* \approx 8.01$: the *missing* unstable local defect pulse solution labelled $Z_{p,ld}^{\ell,2}$ in

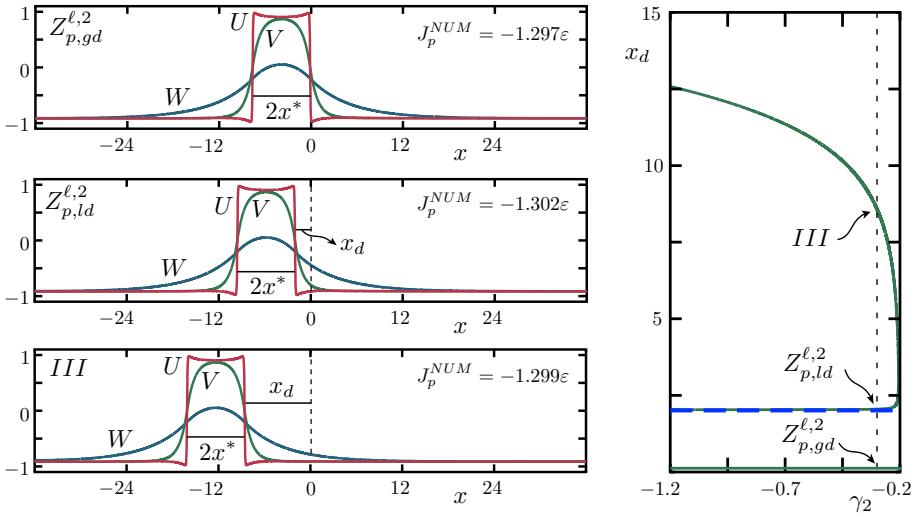

Fig. 10 Left panels: the profiles of the three unstable pinned pulse solutions with leading order width $2x^* \approx 8.01$ obtained by numerically integrating (10) over a domain of length $2L = 72$ and with $(\alpha, \beta, D, \gamma_1, \gamma_2, \varepsilon) = (4, -1, 5, -0.2, -0.3, 0.05)$. Right panel: bifurcation diagram of the numerically observed pinning distances x_d (green solid curves) for these three pinned pulse solutions for varying γ_2. For $|\gamma_2 - \gamma_1|$ not too small, we observe an excellent agreement between the numerically computed pinning distance of the local defect pulse solution $Z^{\ell,2}_{p,ld}$ and the leading order pinning distance determined by Main Result 1 (blue dashed curves). The pinned pulse solutions on the lower branch of the bifurcation diagram correspond to the global defect pulse solution $Z^{\ell,2}_{p,gd}$ in Table 3, see also panel **a** of Fig. 8. Furthermore, the pinned pulse solution in panel III, and the upper branch of the bifurcation diagram, are not captured by the analysis of this manuscript since the pinning distance for these pulses is asymptotically much larger than one, see also Remark 5 (Color figure online)

Table 3 with pinning distance $x_d \approx 2.88$ and a defect pulse solution pinned far away from the defect, see the three panels on the left of Fig. 10.

In Fig. 11, we show the bifurcation diagram of the pinning distances x_d associated to the pinned defect pulse solutions shown in panels "f–h" of Fig. 8—so with leading order pulse width $2x^* \approx 2.20$, see also $Z^{\ell,1}_{p,gd}$ and $Z^{\ell,1}_{p,ld}$ in Table 3—for varying γ_2, while the other parameters are kept fixed, i.e. $(\alpha, \beta, D, \gamma_1) = (4, -1, 5, -0.2)$. We observe that as long as $|\gamma_2 - \gamma_1|$ is not too small, the asymptotically predicted pinning distances x_d (indicated by the blue dashed line in Fig. 11) of Main Result 1 agree perfectly with the numerically observed pinning distances x_d of the local defect pulse solutions. Moreover, both the asymptotical and numerical results predict that the middle branch of pinned pulse solutions is stable. The unstable upper branches in Fig. 11 relate to the pinned pulse solutions with asymptotically large pinning distances (e.g. panel "h" of Fig. 8 and panel III of Fig. 11) and that these branches connect with the middle branches for $|\gamma_2 - \gamma_1|$ small—a region in parameter space where the results of Main Result 1 do not apply. See also the panel on the right of Fig. 10 where we observe similar behavior for the pinned pulse solutions with leading order pulse width $2x^* \approx 8.01$. The onset of these local defect solutions with asymptotically large pinning distances is unclear to us at this stage and whether these solutions fall in the category of *bifurcations from infinity* [45, e.g.] seems to deserve further investigation in the future.

Remark 5 Main Result 1 predicts that, under the conditions of Theorem 2, the pinning distance of a local defect front and pulse solution is much larger than one. However, the numerically

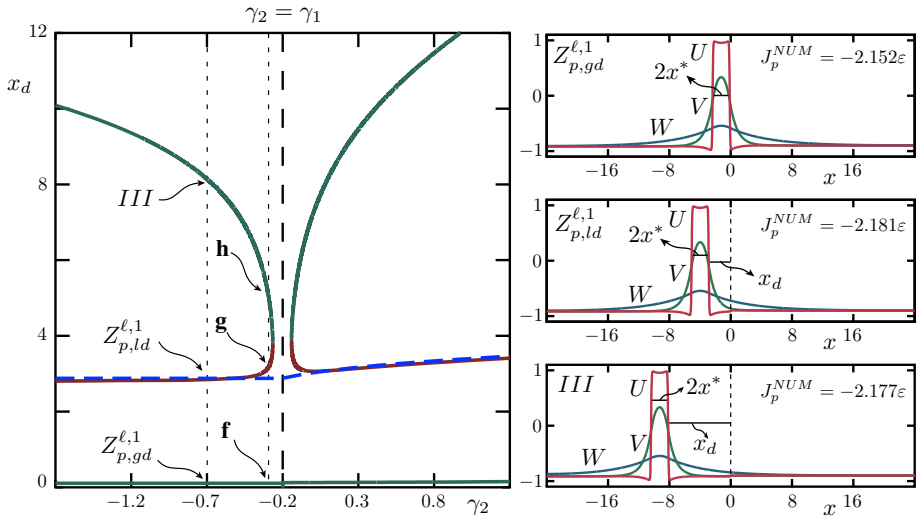

Fig. 11 Left panel: bifurcation diagram of the observed pinning distance x_d for varying γ_2 and $(\alpha, \beta, D, \gamma_1, \varepsilon) = (4, -1, 5, -0.2, 0.05)$ for pinned pulse solutions with leading order width $2x^* \approx 2.20$ and associated to the profiles shown in panels **f–h** of Fig. 8 (as long as $\gamma_2 < \gamma_1$). This bifurcation diagram is obtained by numerically integrating (10) over a domain of length $2L = 48$. Right panel: the associated profiles of the pinned pulse solutions for $\gamma_2 = -0.7$. The profiles associated to the branches to the right of $\gamma_2 = \gamma_1$ are actually pinned to the right of the defect. For $|\gamma_2 - \gamma_1|$ not too small, we observe an excellent agreement between the pinning distances obtained from numerically integrating (10) (red solid curves) and the asymptotically leading order pinning distances determined by (5) of Main Result 1 (blue dashed curves). Moreover, both the numerics and the results of Main Result 1 yield that these local defect pulse solutions $Z_{p,ld}$ with the smaller pinning distances x_d are stable (red curves), while the other ones are unstable (green curves), see also Table 3. The unstable upper branches relate to the pinned pulse solutions with asymptotically large pinning distances (e.g. panel **h** of Fig. 8), and these branches connect with the middle branches for $|\gamma_2 - \gamma_1|$ small (Color figure online)

observed pinning distances of local defect front and pulse solutions under these conditions do not appear to be much greater than one (see, for instance, the panel "c" of Fig. 1, Figures 4 and 5 in [54] and Figure 1 in [24]). We postulate that this stems from the fact that the numerical simulations are necessarily done on a bounded domain and this obviously influences the results on the pinning distances. Moreover, the asymptotic results from Main Result 1 hold only for small enough ε. See also Fig. 12, where we show numerically simulated profiles of local defect pulse solutions for α and β positive—one of the conditions of Theorem 2—but for two different ε-values and on two different domains of integration.

5 Discussion

5.1 Summary

In this manuscript, we studied a heterogeneous three-component FitzHugh–Nagumo model (1) and we derived existence and stability conditions for the simplest, but fundamental, localised pinned solutions—namely pinned front and pulse solutions—that are pinned away from the heterogeneity, see Main Result 1. In certain parameter regimes, we explicitly com-

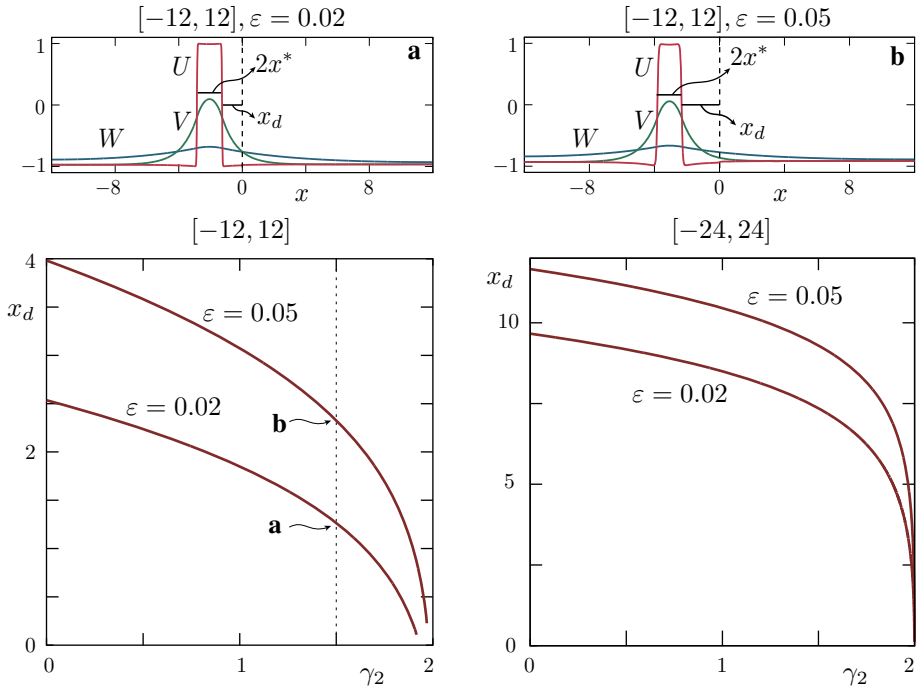

Fig. 12 Top panels: local defect pulse solutions obtained by simulating the time-independent version of (1), i.e. by simulating (10), on a domain of length 24 for $(\alpha, \beta, D, \gamma_1, \gamma_2) = (3, 2, 5, 2, 1.5)$—so $\alpha\beta > 0$—and for two different ε-values. Whilst the pulse widths appear to be the same in both simulations, the pinning distances x_d differ significantly, see also Remark 5. Bottom panels: bifurcation diagrams of γ_2 versus the pinning distance x_d for pinned pulse solutions for the same parameter set (but with γ_2 varying) and for two different ε-values and for two different domain lengths. The domain size, as well as the size of ε, have a leading order influence on the observed pinning distances

puted the relationship between the jump-type heterogeneity (2) and the pinning distance x_d of a pinned localised solution, see, in particular, (3) and (5). In other parameter regimes, e.g. for $\alpha\beta > 0$ for pinned pulse solutions, we showed that the pinning distances x_d are much larger than one, see also Remarks 2 and 5, and higher order computations are needed to explicitly determine these pinning distances. These results were derived by combining GSPT techniques with an action functional approach. This combined approach was pioneered by us in [52] to study stationary localised solutions for the homogeneous three-component FitzHugh–Nagumo model. By appending the homogeneous action functional to deal with the defect, see (15) and (17), we showed that—due to the asymptotic scaling of the defect—the leading order width of the localised solution is not affected by the defect (see, however, Remark 1). In contrast, the pinning distance is determined at the next order (in ε) of the action functional. In essence, the defect destroys the translation invariance of the homogeneous problem and pinpoints—from the family of stationary localised solutions in the homogeneous case—a set of isolated locations for the localised pinned solutions. In addition, the defect also determines the fate of the translation invariance eigenvalue at zero—and thus the stability—of the localised pinned solutions, see (4) and (6).

5.2 Concluding Remarks and Future Work

5.2.1 Designing a Defect

Localised pinned solutions to (1) have been studied in detail before, see, in particular, [24,54]. However, this is the first time that (1) has been studied in this generality and that the pinning distance x_d has been computed explicitly. Actually, to the best of our knowledge this is the first time that this pinning distance has been computed analytically for local defect solutions for such systems of heterogeneous nonlinear reaction–diffusion equations. A direct consequence of explicitly characterising the pinning distance x_d in terms of the system parameters and the strength of the defect is that it opens the path to solving the inverse problem of controlling the pinned solutions. That is, for a given width and location, can we find suitable system parameters and a heterogeneity such that (1) supports a stable localised pinned solution satisfying these prescribed conditions. For instance, say $(\alpha, \beta) = (3, -1)$ are given and we want to *design* a stable local defect pulse solution pinned to the right of the defect with width $2x^* = 3$ and pinning distance $x_d = 2.3$. Then, (5) of Main Result 1 holds for $D \approx 4.94$ and consequently $\gamma_2 = 3e^{-3} - e^{-3/D} \approx -0.395$ (5). To ensure this pinned solution is also stable, i.e. such that (6) holds, it is required that $\gamma_1 < \gamma_2$ and $\gamma_1 \not\approx \gamma_2$.

5.2.2 Extensions Within the Action Functional Framework

The homogeneous version of (1) was originally developed for both α and β positive, see also Remark 2. In contrast, the results of this manuscript give explicit information regarding the pinning distances x_d of pinned localised solutions for α and β of opposite sign only. For α and β positive, the results only imply that the pinning distances x_d are much larger than one. It is expected that an even higher order computation of the action functional will also provide the crucial information regarding the explicit pinning distances x_d of pinned localised solutions for α and β positive. The exploration of the next order term of the action functional is part of future work.

The homogeneous version of (1) also supports stable stationary symmetric 2-pulse solutions [23,53]—and, under the right parameter conditions, also stationary asymmetric 2-pulse solutions or stationary symmetric 3-pulse solutions [52]—so it can be expected that (1) also supports these more exotic types of localised solutions. It is interesting to see if the explicit pinning distances of these more exotic solutions—as well as their stability—can also be explicitly determined by the action functional approach of this manuscript.

The heterogeneous model (1) has one small jump-type heterogeneity (2). However, there is *a priori* no reason to restrict to one jump and different types of heterogeneities have been investigated numerically before [41,50,54, e.g.]. For instance, in [54] (1) with a bump-type heterogeneity, i.e. $\gamma(x) = \gamma_1$ for $x \notin [-A, A]$ and $\gamma(x) = \gamma_2$ for $x \in [-A, A]$, was numerically simulated and it was observed that—under the right conditions on the parameters—local defect pulse solutions with the expected widths still form, see, in particular, the left panel of Figure 8 in [54]. The approach of the action functional used in this manuscript can be easily extended to handle several of these jump-type heterogeneities and is interesting to see if, for instance, the numerical observations of [54] can be shown analytically with the current approach. This bump-type heterogeneity is particularly interesting since a pinned solution in the region $[-A, A]$ (with $A = \Theta(1)$) cannot have an asymptotically large pinning distance (as is the case for the jump-type heterogeneity for α and β both positive).

5.2.3 Interaction Dynamics

Since we now understand—to a certain extend—pinned front and pulse solutions of (1), a next natural question to ask is the following. Suppose the homogeneous problem supports a stable stationary localised solution. What happens if you introduce a small jump heterogeneity far away from the position of the localised solution? Will the solution move towards the defect, or will it move away from it? That is, can we also understand the interaction dynamics of the heterogeneous model and can we, for example, derive the *laws of motion* that describe how front-like or pulse-like initial conditions of (1) evolve? For the homogeneous model these laws of motion are rigorously derived in [55] by using a Renormalization Group (RG) method [44]. By projecting the equations on the eigenspace associated to the small eigenvalues it is shown that an N-front-like initial condition evolves according to a N-dimensional system of ODEs. For instance, a pulse-like initial condition with initial width x_w^0 evolves according to

$$\dot{x}_w = 3\sqrt{2}\varepsilon^2(f(x_w) - \gamma), \qquad x_w(0) = x_w^0,$$

with f as given in (3). Actually, the derived systems of ODEs is a gradient flow with functional G, and the action functional approach can be seen as a direct way of computing (a scaled version of) this functional G, see Remark 4.3 in [55] and [52] for more details. It is interesting to see how the presence of the defect influences the dynamics of front-like and pulse-like initial conditions and whether the GSPT techniques and the action functional approach of this manuscript can be combined with the RG method of [55] to explicitly derive similar systems of ODEs describing the evolution in the defect case. Alternatively, one can try to adapt the formal approach of [38] in which the interface dynamics for similar defect models was derived. This approach is based on using the singular limit of the PDE to rewrite it into a free-boundary problem of mixed PDE-ODE-type and subsequently use a center manifold reduction to derive the interface dynamics, see [38] for more details.

5.2.4 Collision Dynamics

The importance of various types of defect solutions, such as scatter solutions, originated from numerical explorations of the collision dynamics between travelling pulse solutions and defects [41,50,62, e.g.], since understanding the structure of defect solutions would help understanding the dynamics of travelling pulse solutions when colliding with the heterogeneity. In the current setting with τ and θ $\mathcal{O}(1)$, the homogeneous version of (1) does not support travelling pulse solutions [23]. However, for τ and/or θ large (in particular $\mathcal{O}(\varepsilon^{-2})$) the homogeneous version does support stable and unstable travelling pulse solutions and these solutions travel with speed $c = \mathcal{O}(\varepsilon^2)$ [23,53,55]. In addition, the homogeneous version also supports so-called breathing pulse solutions [23]. In [54], several numerical simulations were performed in this parameter regime and it appeared that, under the right parameter conditions, an initially breathing pulse solution could evolve to a travelling pulse solution after colliding with the defect, see, in particular, Figure 10 in [54]. It would be interesting to see whether this collision dynamics can be studied analytically and whether we can develop an understanding on how a defect influences travelling pulse solutions and breathing pulse solutions. One of the complications arising in this parameter regime stems from the fact that the essential spectrum of the linearised operator needed to determine stability lies asymptotically close to the imaginary axis and additional point eigenvalues (compared to the τ, θ $\mathcal{O}(1)$-case) potentially pop out of this essential spectrum, see [53] for more detail. Unfortunately, the action functional approach used in the current setting is not directly suitable to study these travelling pulse

solutions, not even in the homogeneous case, see [52] for more details. However, an existence result for travelling pulse solutions supported by a mono-stable two-component FitzHugh–Nagumo model was established in [6] using a variational approach. Finally, observe that the general results of [24] are not applicable in this situation, since the underlying hypotheses in [24] are not met.

Acknowledgements PvH thanks the National Changhua University of Education in Taiwan, the National Center for Theoretical Sciences in Taiwan, and Tohoku University in Japan for their hospitality. CNC is grateful for the warm hospitality of Queensland University of Technology in Australia. YN and TT also thank Queensland University of Technology in Australia and the National Tsing-Hua University in Taiwan for their hospitality. The authors also acknowledge support from the Mathematics Research Promotion Center in Taiwan and they note that part of this research was finalised during the first joint Australia-Japan workshop on dynamical systems with applications in life sciences at Queensland University of Technology in Australia.

Appendix A: Trivial Defect Solutions

From Lemma 1.7 in [24], we know that (1) supports two trivial defect solutions $Z_{td}^{\pm} = (U_{td}^{\pm}, V_{td}^{\pm}, W_{td}^{\pm})$ near $\pm(1, 1, 1)$. We use a regular expansion

$$Z_{td}^{\pm} = (U_{td}^{\pm}, V_{td}^{\pm}, W_{td}^{\pm})(x) = \pm(1, 1, 1) + \varepsilon(U_{td,1}^{\pm}, V_{td,1}^{\pm}, W_{td,1}^{\pm})(x) + \mathcal{O}(\varepsilon^2)\,, \tag{40}$$

to determine the next order terms of these trivial defect solutions. Because of the different asymptotic scaling in the diffusion coefficients in (1)/(10)/(12), we expect that near the defect the profile of the U-component changes faster—in the sense that we expect its gradient (in space) to be steeper—than the profiles of the V and W components. Therefore, and as eluded to in Sect. 2, we split our spatial domain into four different regions $I_s^{\pm}$ and $I_f^{\pm}$. The two outer slow regions $I_s^{\pm}$ are away from the defect at $x = 0$ and are given by $I_s^- = (-\infty, -\sqrt{\varepsilon}]$, respectively, $I_s^+ = [\sqrt{\varepsilon}, \infty)$. In these slow regions, the spatial scaling as stated in (1) and (10)—the slow scaling—is used to accommodate the changes in the two slow V and W components, while the fast U-component does not change significantly (as it is already close to one of its asymptotic end states). The two inner fast regions $I_f^{\pm}$ near the defect deal with the changes in the fast U-component (due to the heterogeneity) and are given by $I_f^- = (-\sqrt{\varepsilon}, 0]$, respectively, $I_f^+ = (0, \sqrt{\varepsilon})$. These fast regions are asymptotically small in x. Therefore, the two slow V and W components do not change significantly in these regions. To understand the changes in U over the fast regions, we use the fast scaling $\xi := x/\varepsilon$ and study (12). The crux behind the asymptotic $\sqrt{\varepsilon}$-scaling of the two slow regions and two fast regions is that the slow regions $I_s^{\pm}$ span—to leading order—the whole spatial domain in the slow scaling x, while the fast regions $I_f^{\pm}$ span—to leading order—the whole spatial domain in the fast scaling ξ (since $I_f^- = (-1/\sqrt{\varepsilon}, 0]$ and $I_f^+ = (0, 1/\sqrt{\varepsilon})$ in the fast ξ-variable). Observe that similar spatial scalings are used to study the homogeneous version of (1), see [23,53, e.g.].

We first compute the next order terms $(U_{td,1}^-, V_{td,1}^-, W_{td,1}^-)$ of the trivial defect solution Z_{td}^-. Subsequently, the next order terms of the trivial defect solution Z_{td}^+ are obtained by applying both symmetries (7) and (8) to the Z_{td}^--profile. In the first slow region I_s^-, implementing the

regular expansion (40) into (10) gives

$$I_s^- : \begin{cases} \mathcal{O}(\varepsilon) = -2U_{td,1}^- + (\alpha + \beta - \gamma_1)\,, \\ \mathcal{O}(\varepsilon) = \left(V_{td,1}^-\right)_{xx} + U_{td,1}^- - V_{td,1}^-\,, \\ \mathcal{O}(\varepsilon) = D^2\left(W_{td,1}^-\right)_{xx} + U_{td,1}^- - W_{td,1}^-\,. \end{cases} \tag{41}$$

The U-equation shows that the first order correction term $U_{td,1}^-$ of the fast component in this region is constant. In particular, for $x \in I_s^-$ we get

$$U_{td,1}^-(x) = \frac{1}{2}(\alpha + \beta - \gamma_1)\,.$$

This allows us to solve the leading order parts of the slow equations of (41) explicitly and we obtain

$$V_{td,1}^-(x) = C_{s,V}^- e^x + \frac{1}{2}(\alpha + \beta - \gamma_1)\,, \quad W_{td,1}^-(x) = C_{s,W}^- e^{\frac{x}{D}} + \frac{1}{2}(\alpha + \beta - \gamma_1)\,,$$

for $x \in I_s^-$ and with $C_{s,V}^-$ and $C_{s,W}^-$ integration constants that are determined later (the two other integration constant have been set to zero to ensure that the profiles stay bounded as $x \to -\infty$). Similarly, we obtain that the first order correction terms in the second slow region I_s^+ are given by

$$\begin{aligned} U_{td,1}^-(x) &= \frac{1}{2}(\alpha + \beta - \gamma_2)\,, \quad V_{td,1}^-(x) = C_{s,V}^+ e^{-x} + \frac{1}{2}(\alpha + \beta - \gamma_2)\,, \\ W_{td,1}^-(x) &= C_{s,W}^+ e^{-\frac{x}{D}} + \frac{1}{2}(\alpha + \beta - \gamma_2)\,, \end{aligned}$$

with $C_{s,v}^+$ and $C_{s,W}^+$ two different integration constants.

We use the fast scaling ξ in the fast regions $I_f^\pm$, and substituting the regular expansion (40) (in ξ) into (12) gives

$$I_f^\pm : \begin{cases} \mathcal{O}(\varepsilon) = \left(U_{td,1}^-\right)_{\xi\xi} - 2U_{td,1}^- + (\alpha + \beta - \gamma_{1,2})\,, \\ \mathcal{O}(\varepsilon) = \left(V_{td,1}^-\right)_{\xi\xi}\,, \\ \mathcal{O}(\varepsilon) = D^2\left(W_{td,1}^-\right)_{\xi\xi}\,. \end{cases}$$

The leading order part of the U-equations is solved by

$$U_{td,1}^-(\xi) = \frac{1}{2}(\alpha + \beta - \gamma_{1,2}) + C_{f,U}^\pm e^{\sqrt{2}\xi} + D_{f,U}^\pm e^{-\sqrt{2}\xi}\,,$$

for $\xi \in I_f^\pm$ and with $C_{f,U}^\pm$ and $D_{f,U}^\pm$ four different integration constants. The equations for the slow components give

$$V_{td,1}^-(\xi) = C_{f,V}^\pm + D_{f,V}^\pm \xi\,, \quad W_{td,1}^-(\xi) = C_{f,W}^\pm + D_{f,W}^\pm \xi\,, \quad \xi \in I_f^\pm.$$

The solutions in the different regions—and their derivatives—should match at the boundaries of the particular slow and fast fields. Matching the fast U-component between the fast and slow fields gives—to leading order—$D_{f,U}^- = C_{f,U}^+ = 0$. To ensure that the profile U, and its derivative, match over the defect point $x = 0$, we get $C_{f,U}^- = -D_{f,U}^+ = -\frac{1}{4}(\gamma_2 - \gamma_1)$. To ensure the boundedness of the profiles of the slow components, we get $D_{f,V}^\pm = D_{f,W}^\pm = 0$

and matching at the defect point results in $C^-_{f,V} = C^+_{f,V}$ and $C^-_{f,W} = C^+_{f,W}$. Finally, matching the profiles of the V-component and their derivatives at the boundaries between the fast and slow regions gives $C^+_{f,V} = C^-_{s,V} = -C^+_{s,V} = -\frac{1}{4}(\gamma_2 - \gamma_1)$. Similarly, $C^+_{f,W} = C^-_{s,W} = -C^+_{s,W} = -\frac{1}{4}(\gamma_2 - \gamma_1)$.

In summary, the trivial defect solution $Z^-_{td} = (U^-_{td}, V^-_{td}, W^-_{td})(x)$ (40) is, to leading order, given by $(-1, -1, -1)$, and the first order correction terms are given by

$$U^-_{td,1}(x) = \begin{cases} \frac{1}{2}(\alpha+\beta-\gamma_1), & \text{in } I^-_s, \\ \frac{1}{4}(\gamma_1-\gamma_2)e^{\sqrt{2}x/\varepsilon} + \frac{1}{2}(\alpha+\beta-\gamma_1), & \text{in } I^-_f, \\ \frac{1}{4}(\gamma_2-\gamma_1)e^{-\sqrt{2}x/\varepsilon} + \frac{1}{2}(\alpha+\beta-\gamma_2), & \text{in } I^+_f, \\ \frac{1}{2}(\alpha+\beta-\gamma_2), & \text{in } I^+_s, \end{cases}$$

$$V^-_{td,1}(x) = \begin{cases} \frac{1}{4}(\gamma_1-\gamma_2)e^{x} + \frac{1}{2}(\alpha+\beta-\gamma_1), & \text{in } I^-_s, \\ -\frac{1}{4}(\gamma_1+\gamma_2) + \frac{1}{2}(\alpha+\beta), & \text{in } I^-_f, \\ -\frac{1}{4}(\gamma_1+\gamma_2) + \frac{1}{2}(\alpha+\beta), & \text{in } I^+_f, \\ \frac{1}{4}(\gamma_2-\gamma_1)e^{-x} + \frac{1}{2}(\alpha+\beta-\gamma_2), & \text{in } I^+_s, \end{cases}$$

and

$$W^-_{td,1}(x) = \begin{cases} \frac{1}{4}(\gamma_1-\gamma_2)e^{x/D} + \frac{1}{2}(\alpha+\beta-\gamma_1), & \text{in } I^-_s, \\ -\frac{1}{4}(\gamma_1+\gamma_2) + \frac{1}{2}(\alpha+\beta), & \text{in } I^-_f, \\ -\frac{1}{4}(\gamma_1+\gamma_2) + \frac{1}{2}(\alpha+\beta), & \text{in } I^+_f, \\ \frac{1}{4}(\gamma_2-\gamma_1)e^{-x/D} + \frac{1}{2}(\alpha+\beta-\gamma_2), & \text{in } I^+_s. \end{cases}$$

By applying both symmetries (7) and (8) to the above profile Z^-_{td}, we get that, to leading order, Z^+_{td} (40) is given by $(1, 1, 1)$, and the first order correction terms are given by

$$U^+_{td,1}(x) = \begin{cases} -\frac{1}{2}(\alpha+\beta+\gamma_1), & \text{in } I^-_s, \\ \frac{1}{4}(\gamma_1-\gamma_2)e^{\sqrt{2}x/\varepsilon} - \frac{1}{2}(\alpha+\beta+\gamma_1), & \text{in } I^-_f, \\ \frac{1}{4}(\gamma_2-\gamma_1)e^{-\sqrt{2}x/\varepsilon} - \frac{1}{2}(\alpha+\beta+\gamma_2), & \text{in } I^+_f, \\ -\frac{1}{2}(\alpha+\beta+\gamma_2), & \text{in } I^+_s, \end{cases}$$

$$V^+_{td,1}(x) = \begin{cases} \frac{1}{4}(\gamma_1-\gamma_2)e^x - \frac{1}{2}(\alpha+\beta+\gamma_1)\,, & \text{in } I_s^-\,, \\ -\frac{1}{4}(\gamma_1+\gamma_2) - \frac{1}{2}(\alpha+\beta)\,, & \text{in } I_f^-\,, \\ -\frac{1}{4}(\gamma_1+\gamma_2) - \frac{1}{2}(\alpha+\beta)\,, & \text{in } I_f^+\,, \\ \frac{1}{4}(\gamma_2-\gamma_1)e^{-x} - \frac{1}{2}(\alpha+\beta+\gamma_2)\,, & \text{in } I_s^+\,, \end{cases}$$

and

$$W^+_{td,1}(x) = \begin{cases} \frac{1}{4}(\gamma_1-\gamma_2)e^{x/D} - \frac{1}{2}(\alpha+\beta+\gamma_1)\,, & \text{in } I_s^-\,, \\ -\frac{1}{4}(\gamma_1+\gamma_2) + \frac{1}{2}(\alpha+\beta)\,, & \text{in } I_f^-\,, \\ -\frac{1}{4}(\gamma_1+\gamma_2) + \frac{1}{2}(\alpha+\beta)\,, & \text{in } I_f^+\,, \\ \frac{1}{4}(\gamma_2-\gamma_1)e^{-x/D} - \frac{1}{2}(\alpha+\beta+\gamma_2)\,, & \text{in } I_s^+\,. \end{cases}$$

Appendix B: Proof of Lemma 1

To prove Lemma 1 regarding the action functional of a local defect pulse solution $Z^r_{p,ld}$ pinned to the right of the defect, we first need to determine the profile of $Z^r_{p,ld}$. With a slight abuse of notation, we split the spatial domain in four slow regions $I_s^{1,4,6,8}$ and four fast regions $I_s^{2,3,5,7}$:

$$\begin{aligned} &I_s^1 := x \in (-\infty, -\sqrt{\varepsilon}]\,, && I_f^2 := x \in (-\sqrt{\varepsilon}, 0]\,, \\ &I_f^3 := x \in (0, \sqrt{\varepsilon})\,, && I_s^4 := x \in [\sqrt{\varepsilon}, x_d - \sqrt{\varepsilon}]\,, \\ &I_f^5 := x \in (x_d - \sqrt{\varepsilon}, x_d + \sqrt{\varepsilon})\,, && I_s^6 := x \in [x_d + \sqrt{\varepsilon}, x_d + 2x^* - \sqrt{\varepsilon}] \\ &I_f^7 := x \in (x_d + 2x^* - \sqrt{\varepsilon}, x_d + 2x^* + \sqrt{\varepsilon})\,, && I_s^8 := x \in [x_d + 2x^* + \sqrt{\varepsilon}, \infty)\,, \end{aligned} \tag{42}$$

with the pinning distance x_d and the pulse width $2x^*$ both positive and $\Theta(1)$ with respect to ε. Since the defect (2) is small, it has no leading order influence on the profile of a local defect pulse solution $Z^r_{p,ld}$. So, $Z^r_{p,ld}$ is to leading order similar to the leading order profile of the homogeneous pulse solution. In particular, upon using the regular expansion $Z^r_{p,ld} = (U^r_{p,ld,0}, V^r_{p,ld,0}, W^r_{p,ld,0}) + \varepsilon(U^r_{p,ld,1}, V^r_{p,ld,1}, W^r_{p,ld,1}) + \mathcal{O}(\varepsilon^2)$, we get that

$$U^r_{p,ld,0}(x) = \begin{cases} -1\,, & \text{in } I_s^1 \cup I_f^2 \cup I_f^3 \cup I_s^4\,, \\ \tanh\left(\frac{x-x_d}{\sqrt{2}\varepsilon}\right), & \text{in } I_f^5\,, \\ 1\,, & \text{in } I_s^6\,, \\ -\tanh\left(\frac{x-x_d-2x^*}{\sqrt{2}\varepsilon}\right), & \text{in } I_f^7\,, \\ -1\,, & \text{in } I_s^8\,, \end{cases}$$

$$V^r_{p,ld,0}(x) = \begin{cases} -1 + \left(e^{x-x_d} - e^{x-x_d-2x^*}\right), & \text{in } I^1_s \cup I^2_f \cup I^3_f \cup I^4_s, \\ -e^{-2x^*}, & \text{in } I^5_f, \\ 1 - \left(e^{x-x_d-2x^*} + e^{-(x-x_d)}\right), & \text{in } I^6_s, \\ -e^{-2x^*}, & \text{in } I^7_f, \\ -1 + \left(e^{-(x-x_d-2x^*)} - e^{-(x-x_d)}\right), & \text{in } I^8_s, \end{cases}$$

and

$$W^r_{p,ld,0}(x) = \begin{cases} -1 + \left(e^{(x-x_d)/D} - e^{(x-x_d-2x^*)/D}\right), & \text{in } I^1_s \cup I^2_f \cup I^3_f \cup I^4_s, \\ -e^{-2x^*/D}, & \text{in } I^5_f, \\ 1 - \left(e^{(x-x_d-2x^*)/D} + e^{-(x-x_d)/D}\right), & \text{in } I^6_s, \\ -e^{-2x^*/D}, & \text{in } I^7_f, \\ -1 + \left(e^{-(x-x_d-2x^*)/D} - e^{-(x-x_d)/D}\right), & \text{in } I^8_s, \end{cases}$$

see [23,52,54, e.g.]. To determine the next order correction terms, we use that—as for pinned front solutions—the fast component is still slaved to the slow components in the slow fields, see the first equation of (32). In particular, for x in the slow fields we have $U^r_{p,ld,1} = -\frac{1}{2}(\alpha V^r_{p,ld,0} + \beta W^r_{p,ld,0} + \gamma(x))$. So,

$$U^r_{p,ld,1}(x) = \begin{cases} \frac{1}{2}(\alpha+\beta-\gamma_1) + \frac{1}{2}\alpha\left(e^{-2x^*}-1\right)e^{x-x_d} + \frac{1}{2}\beta\left(e^{-2x^*/D}-1\right)e^{(x-x_d)/D}, & \text{in } I^1_s, \\ \frac{1}{2}(\alpha+\beta-\gamma_2) + \frac{1}{2}\alpha\left(e^{-2x^*}-1\right)e^{x-x_d} + \frac{1}{2}\beta\left(e^{-2x^*/D}-1\right)e^{(x-x_d)/D}, & \text{in } I^4_s, \\ -\frac{1}{2}(\alpha+\beta+\gamma_2) + \frac{1}{2}\alpha\left(e^{x-x_d-2x^*} + e^{-(x-x_d)}\right) & \\ \quad + \frac{1}{2}\beta\left(e^{(x-x_d-2x^*)/D} + e^{-(x-x_d)/D}\right), & \text{in } I^6_s, \\ \frac{1}{2}(\alpha+\beta-\gamma_2) - \frac{1}{2}\alpha\left(e^{2x^*}-1\right)e^{-(x-x_d)} & \\ \quad - \frac{1}{2}\beta\left(e^{2x^*/D}-1\right)e^{-(x-x_d)/D}, & \text{in } I^8_s. \end{cases} \tag{43}$$

By the second and third equations of (32), the above expressions allow us to compute—up to integration constants—the first order correction terms of the slow components in the slow fields. We get

$$V^r_{p,ld,1}(x) = \begin{cases} \frac{1}{2}(\alpha+\beta-\gamma_1) + \frac{1}{8}\alpha(2x-1)\left(1-e^{-2x^*}\right)e^{x-x_d} \\ \quad -\frac{1}{2}\beta\frac{D^2}{D^2-1}\left(1-e^{-2x^*/D}\right)e^{(x-x_d)/D} + C_1^v e^x\,, & \text{in } I_s^1, \\ \frac{1}{2}(\alpha+\beta-\gamma_2) + \frac{1}{8}\alpha(2x-1)\left(1-e^{-2x^*}\right)e^{x-x_d} \\ -\frac{1}{2}\beta\frac{D^2}{D^2-1}\left(1-e^{-2x^*/D}\right)e^{(x-x_d)/D} + D_1^v e^x + D_2^v e^{-x}\,, & \text{in } I_s^4, \\ -\frac{1}{2}(\alpha+\beta+\gamma_2) + \frac{1}{8}\alpha\left(e^{x-x_d-2x^*} + e^{-(x-x_d)}\right. \\ \quad \left. -2x\left(e^{x-x_d-2x^*} - e^{-(x-x_d)}\right)\right) \\ +\frac{1}{2}\beta\frac{D^2}{D^2-1}\left(e^{(x-x_d-2x^*)/D} + e^{-(x-x_d)/D}\right) + E_1^v e^x + E_2^v e^{-x}\,, & \text{in } I_s^6, \\ \frac{1}{2}(\alpha+\beta-\gamma_2) + \frac{1}{8}\alpha(1+2x)\left(1-e^{2x^*}\right)e^{-(x-x_d)} \\ \quad +\frac{1}{2}\beta\frac{D^2}{D^2-1}\left(1-e^{2x^*/D}\right)e^{-(x-x_d)/D} + F_2^v e^{-x}\,, & \text{in } I_s^8, \end{cases} \tag{44}$$

and

$$W^r_{p,ld,1}(x) = \begin{cases} \frac{1}{2}(\alpha+\beta-\gamma_1) + \frac{1}{8}\beta\left(\frac{2x}{D}-1\right)\left(1-e^{-2x^*/D}\right)e^{(x-x_d)/D} \\ \quad +\frac{1}{2}\alpha\frac{1}{D^2-1}\left(1-e^{-2x^*}\right)e^{x-x_d} + C_1^w e^{x/D}\,, & \text{in } I_s^1, \\ \frac{1}{2}(\alpha+\beta-\gamma_2) + \frac{1}{8}\beta\left(\frac{2x}{D}-1\right)\left(1-e^{-2x^*/D}\right)e^{(x-x_d)/D} \\ +\frac{1}{2}\alpha\frac{1}{D^2-1}\left(1-e^{-2x^*}\right)e^{x-x_d} + D_1^w e^{x/D} + D_2^w e^{-x/D}\,, & \text{in } I_s^4, \\ -\frac{1}{2}(\alpha+\beta+\gamma_2) + \frac{1}{8}\beta\left(e^{(x-x_d-2x^*)/D} + e^{-(x-x_d)/D}\right. \\ \quad \left. -2\frac{x}{D}\left(e^{(x-x_d-2x^*)/D} - e^{-(x-x_d)/D}\right)\right) \\ -\frac{1}{2}\alpha\frac{1}{D^2-1}\left(e^{x-x_d-2x^*} + e^{-(x-x_d)}\right) + E_1^w e^{x/D} + E_2^w e^{-x/D}\,, & \text{in } I_s^6, \\ \frac{1}{2}(\alpha+\beta-\gamma_2) + \frac{1}{8}\beta\left(1+\frac{2x}{D}\right)\left(1-e^{2x^*/D}\right)e^{-(x-x_d)/D} \\ \quad -\frac{1}{2}\alpha\frac{1}{D^2-1}\left(1-e^{2x^*}\right)e^{-(x-x_d)} + F_2^w e^{-x/D}\,, & \text{in } I_s^8. \end{cases} \tag{45}$$

Similar to the front case, the slow components—and their derivatives—do not change in the fast fields. Therefore, we require that they match up at the boundaries of the slow fields. This results in twelve conditions that determine the twelve unknown integration constants of (44) and (45). In the end, we find that

$$C_1^v = \frac{1}{4}(\gamma_1-\gamma_2) + \frac{1}{8}\left(e^{-2x^*}-1\right)\left(3\alpha+2\alpha x_d - 4\beta\frac{1}{D^2-1}\right)e^{-x_d} + \frac{1}{2}\alpha x^* e^{-(x_d+2x^*)}\,,$$

$$D_1^v = \frac{1}{8}\left(e^{-2x^*}-1\right)\left(3\alpha+2\alpha x_d - 4\beta\frac{1}{D^2-1}\right)e^{-x_d} + \frac{1}{2}\alpha x^* e^{-(x_d+2x^*)}\,,$$

$$
\begin{aligned}
D_2^v &= \frac{1}{4}(\gamma_2-\gamma_1)\,,\\
E_1^v &= \frac{1}{8}\left(3\alpha+2\alpha x_d+4\alpha x^*-4\beta\frac{1}{D^2-1}\right)e^{-(x_d+2x^*)}\,,\\
E_2^v &= \frac{1}{4}(\gamma_2-\gamma_1)+\frac{1}{8}\left(3\alpha-2\alpha x_d-4\beta\frac{1}{D^2-1}\right)e^{x_d}\,,\\
F_2^v &= \frac{1}{4}(\gamma_2-\gamma_1)+\frac{1}{8}\left(1-e^{2x^*}\right)\left(3\alpha-2\alpha x_d-4\beta\frac{1}{D^2-1}\right)e^{x_d}+\frac{1}{2}\alpha x^* e^{x_d+2x^*}\,,
\end{aligned}
$$

and, similarly,

$$
\begin{aligned}
C_1^w &= \frac{1}{4}(\gamma_1-\gamma_2)+\frac{1}{8}\left(e^{-2x^*/D}-1\right)\left(4\alpha\frac{D^2}{D^2-1}+3\beta+2\beta\frac{x_d}{D}\right)e^{-x_d/D}\\
&\quad+\frac{1}{2}\beta\frac{x^*}{D}e^{-(x_d+2x^*)/D}\,,\\
D_1^w &= \frac{1}{8}\left(e^{-2x^*/D}-1\right)\left(4\alpha\frac{D^2}{D^2-1}+3\beta+2\beta\frac{x_d}{D}\right)e^{-x_d/D}+\frac{1}{2}\beta\frac{x^*}{D}e^{-(x_d+2x^*)/D}\,,\\
D_2^w &= \frac{1}{4}(\gamma_2-\gamma_1)\,,\\
E_1^w &= \frac{1}{8}\left(4\alpha\frac{D^2}{D^2-1}+3\beta+2\beta\frac{x_d}{D}+4\beta\frac{x^*}{D}\right)e^{-(x_d+2x^*)/D}\,,\\
E_2^w &= \frac{1}{4}(\gamma_2-\gamma_1)+\frac{1}{8}\left(4\alpha\frac{D^2}{D^2-1}+3\beta-2\beta\frac{x_d}{D}\right)e^{x_d/D}\,,\\
F_2^w &= \frac{1}{4}(\gamma_2-\gamma_1)+\frac{1}{8}\left(1-e^{2x^*/D}\right)\left(4\alpha\frac{D^2}{D^2-1}+3\beta-2\beta\frac{x_d}{D}\right)e^{x_d/D}\\
&\quad+\frac{1}{2}\beta\frac{x^*}{D}e^{(x_d+2x^*)/D}\,.
\end{aligned}
$$

What remains to determine are the next order correction terms of the fast component in the fast fields. We first look into the fast fields $I_f^{2,3}$ around the defect. The fast equation in these fields, in the fast variable ξ, are given by the first equation of (12)—with $\gamma(x)=\gamma_1$ in I_f^2 and $\gamma(x)=\gamma_2$ in I_f^3. Plugging in the regular expansions for the local defect pulse solution $Z_{p,ld}^r$—and recalling that the slow components are constant in the fast fields—we get at the $\mathcal{O}(\varepsilon)$-level:

$$
\begin{aligned}
\left(U_{p,ld,1}^r\right)_{\xi\xi} &= 2U_{p,ld,1}^r-\alpha\left(1+\left(e^{-2x^*}-1\right)e^{-x_d}\right)\\
&\quad-\beta\left(1+\left(e^{-2x^*/D}-1\right)e^{-x_d/D}\right)+\begin{cases}\gamma_1\,, & \text{in } I_f^2\,,\\ \gamma_2\,, & \text{in } I_f^3\,.\end{cases}
\end{aligned}
$$

The solutions to these equations are given by

$$U^r_{p,ld,1} = \begin{cases} A_2 e^{\sqrt{2}\xi} + B_2 e^{-\sqrt{2}\xi} + \frac{1}{2}\alpha\left(1 + \left(e^{-2x^*} - 1\right)e^{-x_d}\right) \\ \qquad + \frac{1}{2}\beta\left(1 + \left(e^{-2x^*/D} - 1\right)e^{-x_d/D}\right) - \frac{1}{2}\gamma_1\,, & \text{in } I_f^2, \\ A_3 e^{\sqrt{2}\xi} + B_3 e^{-\sqrt{2}\xi} + \frac{1}{2}\alpha\left(1 + \left(e^{-2x^*} - 1\right)e^{-x_d}\right) \\ \qquad + \frac{1}{2}\beta\left(1 + \left(e^{-2x^*/D} - 1\right)e^{-x_d/D}\right) - \frac{1}{2}\gamma_2\,, & \text{in } I_f^3\,. \end{cases}$$

Matching $U^r_{p,ld,1}$ at the left boundary of I_f^2 with $U^r_{p,ld,1}$ (43) at the right boundary of I_s^1 gives $B_2 = 0$. Similarly, matching at the right boundary of I_f^3 with the left boundary of I_s^4 gives $A_3 = 0$. Matching $U^r_{p,ld,1}$, as well as its derivative, at $\xi = 0$ gives $-A_2 = B_3 = \frac{1}{4}(\gamma_2 - \gamma_1)$. Finally, the fast correction terms over the jump regions $I_f^{5,7}$ can, as for a local defect front solution, be set to zero since the fast equations over these fields have no $\mathcal{O}(\varepsilon)$-correction terms.

To compute the action functional $J_p(Z^r_{p,ld})$ (38) and finalise the proof of Lemma 1, we split the action functional integral (15) according to the four slow and four fast regions (42)

$$J_p = \underbrace{\int_{I_s^1} \cdot\, dx}_{:=J_p^1} + \underbrace{\int_{I_f^2} \cdot\, dx}_{:=J_p^2} + \underbrace{\int_{I_f^3} \cdot\, dx}_{:=J_p^3} + \underbrace{\int_{I_s^4} \cdot\, dx}_{:=J_p^4} + \underbrace{\int_{I_f^5} \cdot\, dx}_{:=J_p^5} + \underbrace{\int_{I_s^6} \cdot\, dx}_{:=J_p^6} + \underbrace{\int_{I_f^7} \cdot\, dx}_{:=J_p^7} + \underbrace{\int_{I_s^8} \cdot\, dx}_{:=J_p^8}\,. \tag{46}$$

By using the observations of Sect. 2.2 and the profile of a local defect pulse solution $Z^r_{p,ld}$ constructed above, we compute the eight integrals $J_p^i = \varepsilon J^i_{p,1} + \varepsilon^2 J^i_{p,2} + \mathcal{O}(\varepsilon^2\sqrt{\varepsilon})$, $i = 1, 2, \ldots, 8$ of (46)[8]. We start with the integrals over the slow fields. The integral over the first slow field I_s^1 gives $J_p^1 = \varepsilon J^1_{p,1} + \varepsilon^2 J^1_{p,2} + \mathcal{O}(\varepsilon^2\sqrt{\varepsilon})$ with, by (19) and (20),

$$\begin{aligned} J^1_{p,1} &= \int_{I_s^1} L_1(U^r_{p,ld}; \bar{u}_{\gamma_1})dx \\ &= \int_{I_s^1} -\frac{1}{2}\alpha\left(e^{x-x_d} - e^{x-x_d-2x^*}\right) + \frac{1}{2}\beta\left(e^{(x-x_d)/D} - e^{(x-x_d-2x^*)/D}\right)dx \\ &= -\frac{1}{2}\left(\alpha e^{-x_d}\left(1 - e^{-2x^*}\right) + \beta D e^{-x_d/D}\left(1 - e^{-2x^*/D}\right)\right) \\ &\quad + \frac{1}{2}\left(\alpha e^{-x_d}\left(1 - e^{-2x^*}\right) + \beta e^{-x_d/D}\left(1 - e^{-2x^*/D}\right)\right)\sqrt{\varepsilon} \\ &\quad - \frac{1}{4}\left(\alpha e^{-x_d}\left(1 - e^{-2x^*}\right) + \frac{\beta}{D}e^{-x_d/D}\left(1 - e^{-2x^*/D}\right)\right)\varepsilon + \mathcal{O}(\varepsilon\sqrt{\varepsilon})\,, \end{aligned}$$

[8] We do not show all the details of the computations since these are very similar to the computations for the front case.

and

$$\begin{aligned}
J^1_{p,2} &= \int_{I^1_s} L_2(U^r_{p,ld};\bar{u}_{\gamma_1})dx \\
&= -\frac{1}{2}\alpha\beta\frac{1}{D^2-1}\left(e^{-x_d}-e^{-(x_d+2x^*)}-D^3e^{-x_d/D}+D^3e^{-(x_d+2x^*)/D}\right) \\
&\quad+\frac{1}{8}\alpha^2\left((3+x_d)\left(1-e^{-2x^*}\right)e^{-x_d}-2x^*e^{-(x_d+2x^*)}\right) \\
&\quad+\frac{1}{8}\beta^2\left((3D+x_d)\left(1-e^{-2x^*/D}\right)e^{-x_d/D}-2x^*e^{-(x_d+2x^*)/D}\right) \\
&\quad+\frac{1}{8}\gamma_1\left(\alpha\left(-1-2e^{-x_d}+2e^{-(x_d+2x^*)}\right)+\beta D\left(-1-2e^{-x_d/D}+2e^{-(x_d+2x^*)/D}\right)\right) \\
&\quad+\frac{1}{8}\gamma_2(\alpha+\beta D)+\mathcal{O}(\sqrt{\varepsilon}).
\end{aligned}$$

Similarly, the integral over the second slow field I^4_s gives

$$\begin{aligned}
J^4_{p,1} &= -\frac{1}{2}\left(\alpha\left(1-e^{-x_d}\right)\left(1-e^{-2x^*}\right)+\beta D\left(1-e^{-x_d/D}\right)\left(1-e^{-2x^*/D}\right)\right) \\
&\quad+\frac{1}{2}\left(\alpha\left(1+e^{-x_d}\right)\left(1-e^{-2x^*}\right)+\beta\left(1+e^{-x_d/D}\right)\left(1-e^{-2x^*/D}\right)\right)\sqrt{\varepsilon} \\
&\quad-\frac{1}{4}\left(\alpha\left(1-e^{-x_d}\right)\left(1-e^{-2x^*}\right)+\frac{\beta}{D}\left(1-e^{-x_d/D}\right)\left(1-e^{-2x^*/D}\right)\right)\varepsilon+\mathcal{O}(\varepsilon\sqrt{\varepsilon}),
\end{aligned}$$

and

$$\begin{aligned}
J^4_{p,2} &= \frac{1}{2}\alpha\beta\frac{1}{D^2-1}\left(-\left(1-e^{-x_d}\right)\left(1-e^{-2x^*}\right)+D^3\left(1-e^{-x_d/D}\right)\left(1-e^{-2x^*/D}\right)\right) \\
&\quad+\frac{1}{8}\alpha^2\left(3\left(1-e^{-x_d}\right)\left(1-e^{-2x^*}\right)-x_de^{-x_d}\left(1-e^{-2x^*}\right)-2x^*e^{-2x^*}\left(1-e^{-x_d}\right)\right) \\
&\quad+\frac{1}{8}\beta^2\left(3D\left(1-e^{-x_d/D}\right)\left(1-e^{-2x^*/D}\right)-x_de^{-x_d/D}\left(1-e^{-2x^*/D}\right)\right) \\
&\quad-\frac{1}{4}\beta^2x^*e^{-2x^*/D}\left(1-e^{-x_d/D}\right)+\frac{1}{8}\gamma_1\left(\alpha\left(1-e^{-x_d}\right)+\beta D\left(1-e^{-x_d/D}\right)\right) \\
&\quad-\frac{1}{8}\gamma_2\left(\alpha\left(1-e^{-x_d}\right)\left(3-2e^{-2x^*}\right)+\beta D\left(1-e^{-x_d/D}\right)\left(3-2e^{-2x^*/D}\right)\right)+\mathcal{O}(\sqrt{\varepsilon}).
\end{aligned}$$

The integral over the third slow region I^6_s gives

$$\begin{aligned}
J^6_{p,1} &= -\alpha\left(1-e^{-2x^*}\right)-\beta D\left(1-e^{-2x^*/D}\right)+4\gamma_2x^* \\
&\quad+\left(\alpha\left(1+e^{-2x^*}\right)+\beta\left(1+e^{-2x^*/D}\right)-4\gamma_2\right)\sqrt{\varepsilon} \\
&\quad+\left(-\frac{1}{2}\alpha\left(1-e^{-2x^*}\right)-\frac{1}{2}\frac{\beta}{D}\left(1-e^{-2x^*/D}\right)\right)\varepsilon+\mathcal{O}(\varepsilon\sqrt{\varepsilon}),
\end{aligned}$$

and

$$
\begin{aligned}
J^6_{p,2} = \alpha\beta\frac{1}{D^2-1}\left(-\left(1-e^{-2x^*}\right)+D^3\left(1-e^{-2x^*/D}\right)\right)\\
+\frac{1}{4}\alpha^2\left(3-3e^{-2x^*}-2x^*e^{-2x^*}\right)\\
+\frac{1}{4}\beta^2\left(3D-3De^{-2x^*/D}-2x^*e^{-2x^*/D}\right)\\
-\frac{1}{8}\gamma_1\left(\alpha e^{-x_d}\left(1-e^{-2x^*}\right)+\beta De^{-x_d/D}\left(1-e^{-2x^*/D}\right)\right)\\
+\frac{1}{8}\gamma_2\left(\alpha\left(4-16x^*+e^{-x_d}-4e^{-2x^*}-e^{-(x_d+2x^*)}\right)\right)\\
+\frac{1}{8}\gamma_2\left(\beta\left(4D-16x^*+De^{-x_d/D}-4De^{-2x^*/D}-De^{-(x_d+2x^*)/D}\right)\right)+\mathcal{O}(\sqrt{\varepsilon}).
\end{aligned}
$$

The integral over the last slow field I^8_s gives

$$
\begin{aligned}
J^8_{p,1} = -\frac{1}{2}\left(\alpha\left(1-e^{-2x^*}\right)+\beta D\left(1-e^{-2x^*/D}\right)\right)\\
+\frac{1}{2}\left(\alpha\left(1-e^{-2x^*}\right)+\beta\left(1-e^{-2x^*/D}\right)\right)\sqrt{\varepsilon}\\
-\frac{1}{4}\left(\alpha\left(1-e^{-2x^*}\right)+\frac{\beta}{D}\left(1-e^{-2x^*/D}\right)\right)\varepsilon+\mathcal{O}(\varepsilon\sqrt{\varepsilon}),
\end{aligned}
$$

and

$$
\begin{aligned}
J^8_{p,2} = \frac{1}{2}\alpha\beta\frac{1}{D^2-1}\left(-\left(1-e^{-2x^*}\right)+D^3\left(1-e^{-2x^*/D}\right)\right)\\
+\frac{1}{8}\alpha^2\left(3-3e^{-2x^*}-2x^*e^{-2x^*}\right)\\
+\frac{1}{8}\beta^2\left(3D-3De^{-2x^*/D}-2x^*e^{-2x^*/D}\right)\\
+\frac{1}{8}\gamma_1\left(\alpha e^{-(x_d+2x^*)}+\beta De^{-(x_d+2x^*)/D}\right)\\
-\frac{1}{8}\gamma_2\left(\alpha\left(2-2e^{-2x^*}+e^{-(x_d+2x^*)}\right)\right)\\
-\frac{1}{8}\gamma_2\left(\beta D\left(2-2e^{-2x^*/D}+e^{-(x_d+2x^*)/D}\right)\right)+\mathcal{O}(\sqrt{\varepsilon}).
\end{aligned}
$$

Next, we compute the integrals over the four fast fields. The leading order computation of the action functional over the fast fields yields $\frac{4\sqrt{2}}{3}\varepsilon$—see [52] and (30)—and to determine the next order term we use (23). Around the defect point we get

$$
\begin{aligned}
J^2_p &= \varepsilon\int_{I^2_f}\bar{L}_0(U^r_{p,ld};\bar{u}_{\gamma_1})d\xi+\varepsilon^2\int_{I^2_f}\bar{L}_1(U^r_{p,ld};\bar{u}_{\gamma_1})d\xi\\
&= -\frac{1}{2}\varepsilon^2\int_{-1/\sqrt{\varepsilon}}^{0}\left(\alpha\left(e^{-x_d}-e^{-x_d-2x^*}\right)+\beta\left(e^{-x_d/D}-e^{-(x_d+2x^*)/D}\right)\right)d\xi\\
&\quad+\mathcal{O}(\varepsilon^2\sqrt{\varepsilon})\\
&= -\frac{1}{2}\left(\alpha\left(e^{-x_d}-e^{-x_d-2x^*}\right)+\beta\left(e^{-x_d/D}-e^{-(x_d+2x^*)/D}\right)\right)\varepsilon\sqrt{\varepsilon}+\mathcal{O}(\varepsilon^2\sqrt{\varepsilon}),
\end{aligned}
$$

and

$$J_p^3 = -\frac{1}{2}\left(\alpha\left(e^{-x_d} - e^{-x_d-2x^*}\right) + \beta\left(e^{-x_d/D} - e^{-(x_d+2x^*)/D}\right)\right)\varepsilon\sqrt{\varepsilon} + \mathcal{O}(\varepsilon^2\sqrt{\varepsilon})\,.$$

The integral over the first fast jump, see also [52] and (30), gives

$$\begin{aligned} J_p^5 &= \varepsilon\int_{I_f^5}\bar{L}_0(U_{p,ld}^r;\bar{u}_{\gamma_2})d\xi + \varepsilon^2\int_{I_f^5}\bar{L}_1(U_{p,ld}^r;\bar{u}_{\gamma_2})d\xi \\ &= \frac{2\sqrt{2}}{3}\varepsilon + \varepsilon^2\int_{-1/\sqrt{\varepsilon}}^{1/\sqrt{\varepsilon}}\left(\frac{1}{2}\alpha\left(-e^{-2x^*}\tanh(\xi/\sqrt{2}) - 1\right)\right. \\ &\quad \left. + \frac{1}{2}\beta\left(-e^{-2x^*/D}\tanh(\xi/\sqrt{2}) - 1\right) + \gamma_2(\tanh(\xi/\sqrt{2}) + 1)\right)d\xi + \mathcal{O}(\varepsilon^2\sqrt{\varepsilon}) \\ &= \frac{2\sqrt{2}}{3}\varepsilon + (-\alpha - \beta + 2\gamma_2)\,\varepsilon\sqrt{\varepsilon} + \mathcal{O}(\varepsilon^2\sqrt{\varepsilon})\,. \end{aligned}$$

Similarly,

$$J_p^7 = \frac{2\sqrt{2}}{3}\varepsilon + (-\alpha - \beta + 2\gamma_2)\varepsilon\sqrt{\varepsilon} + \mathcal{O}(\varepsilon^2\sqrt{\varepsilon})\,.$$

So, adding the contributions of the slow and fast fields to the action functional together gives the action functional $J_p(U_{p,ld}^r)$ (38) of a local defect pulse solution $Z_{p,ld}^r$ pinned to the right of the defect. As expected, the $\mathcal{O}(\varepsilon\sqrt{\varepsilon})$-terms of the action functional from the slow and fast fields cancel out. This completes the proof of Lemma 1. □

References

1. Benson, D., Sherrat, J., Maini, P.: Diffusion driven instability in an inhomogeneous domain. Bull. Math. Biol. **55**, 365–384 (1993)
2. Bode, M., Liehr, A.W., Schenk, C.P., Purwins, H.G.: Interaction of dissipative solitons: particle-like behaviour of localized structures in a three-component reaction–diffusion system. Physica D **161**, 45–66 (2002)
3. Brazhnik, P., Tyson, J.: Steady-state autowave patterns in a two-dimensional excitable medium with a band of different excitability. Physica D **102**, 300–312 (1997)
4. Carr, J., Pego, R.L.: Metastable patterns in solutions of $u_t = \varepsilon^2 u_{xx} - f(u)$. Commun. Pure Appl. Math. **42**, 523–576 (1989)
5. Chen, C.N., Choi, Y.S.: Standing pulse solutions to FitzHugh–Nagumo equations. Arch. Ration. Mech. Anal. **206**, 741–777 (2012)
6. Chen, C.N., Choi, Y.S.: Traveling pulse solutions to FitzHugh–Nagumo equations. Calc. Var. Partial Differ. Equ. **54**, 1–45 (2015)
7. Chen, C.N., Hu, X.: Maslov index for homoclinic orbits of Hamiltonian systems. Ann. I. H. Poincare-An. **24**, 589–603 (2007)
8. Chen, C.N., Hu, X.: Stability criteria for reaction–diffusion systems with skew-gradient structure. Commun. Partial Differ. Equ. **33**, 189–208 (2008)
9. Chen, C.N., Hu, X.: Stability analysis for standing pulse solutions to FitzHugh–Nagumo equations. Calc. Var. Partial Differ. Equ. **49**, 827–845 (2014)
10. Chen, C.N., Kung, S.Y., Morita, Y.: Planar standing wavefronts in the FitzHugh–Nagumo equations. SIAM J. Math. Anal. **46**, 657–690 (2014)
11. Chen, C.N., Séré, E.: Multiple front standing waves in the Fitzhugh–Nagumo equations. arXiv:1804.01727 (2018)
12. Chen, C.N., Tanaka, K.: A variational approach for standing waves of FitzHugh–Nagumo type systems. J. Differ. Equ. **257**, 109–144 (2014)

13. Chen, C.N., Tzeng, Sy: Existence and multiplicity results for heteroclinic orbits of second order Hamiltonian systems. J. Differ. Equ. **158**, 211–250 (1999)
14. Chen, C.N., Tzeng, Sy: Periodic solutions and their connecting orbits of Hamiltonian systems. J. Differ. Equ. **177**, 121–145 (2001)
15. Chirilus-Bruckner, M., Doelman, A., van Heijster, P., Rademacher, J.D.M.: Butterfly catastrophe for fronts in a three-component reaction–diffusion system. J. Nonlinear Sci. **25**, 87–129 (2015)
16. Corwin, L., Szczarba, R.H.: Multivariable Calculus, Monographs and Textbooks in Pure and Applied Mathematics, vol. 64. Marcel Dekker, Inc., New York City (1982)
17. Derks, G.: Stability of fronts in inhomogeneous wave equations. Acta Appl. Math. **137**, 61–78 (2014)
18. Derks, G., Doelman, A., Knight, C., Susanto, H.: Pinned fluxons in a Josephson junction with a finite-length inhomogeneity. Eur. J. Appl. Math. **23**, 201–244 (2012)
19. Doedel, E.J.: Lecture notes on numerical analysis of nonlinear equations. In: Krauskopf, B., Osinga, H.M., Galán-Vioque, J. (eds.) Numerical Continuation Methods for dynamical systems, Und. Com. Sys., pp. 1–49. Springer, Berlin (2007)
20. Doelman, A., Gardner, R.A., Kaper, T.J.: Stability analysis of singular patterns in the 1D Gray–Scott model: a matched asymptotics approach. Physica D **122**, 1–36 (1998)
21. Doelman, A., Gardner, R.A., Kaper, T.J.: Large stable pulse solutions in reaction–diffusion equations. Indiana Univ. Math. J. **50**, 443–507 (2001)
22. Doelman, A., Gardner, R.A., Kaper, T.J.: A stability index analysis of 1-D patterns of the Gray–Scott model. Mem. Am. Math. Soc. **155**, xii+64 (2002)
23. Doelman, A., van Heijster, P., Kaper, T.: Pulse dynamics in a three-component system: existence analysis. J. Dyn. Differ. Equ. **21**, 73–115 (2009)
24. Doelman, A., van Heijster, P., Xie, F.: A geometric approach to stationary defect solutions in one space dimension. SIAM J. Appl. Dyn. Syst. **15**, 655–712 (2016)
25. Fenichel, N.: Geometric singular perturbation theory for ordinary differential equations. J. Differ. Equ. **31**, 53–98 (1979)
26. Fusco, G., Hale, J.K.: Slow-motion manifolds, dormant instability, and singular perturbations. J. Dyn. Differ. Equ. **1**, 75–94 (1989)
27. Goldobin, E., Vogel, K., Crasser, O., Walser, R., Schleich, W., Koelle, D., Kleiner, R.: Quantum tunneling of semifluxons in a 0–π–0 long Josephson junction. Phys. Rev. B **72**, 054 527 (2005)
28. Gurevich, S.V., Amiranashvili, S., Purwins, H.G.: Breathing dissipative solitons in three-component reaction–diffusion system. Phys. Rev. E **74**, 066 201 (2006)
29. Holmes, M.H.: Introduction to Perturbation Methods. Springer Science & Business Media, Berlin (2012)
30. Ikeda, H., Ei, S.I.: Front dynamics in heterogeneous diffusive media. Physica D **239**, 1637–1649 (2010)
31. Jones, C.K.R.T.: Geometric singular perturbation theory. In: Johnson, R. (ed.) Dynamical Systems (Montecatini Terme, 1994), Lecture Notes in Mathematics, vol. 1609, pp. 44–118. Springer, Berlin (1995)
32. Kaper, T.J.: An introduction to geometric methods and dynamical systems theory for singular perturbation problems. In: O'Malley, R.E., Cronin, J. (eds.) Analyzing Multiscale Phenomena Using Singular Perturbation Methods (Baltimore, MD, 1998), Proceedings of Symposia in Applied Mathematics, vol. 56, pp. 85–131. American Mathematical Society, Providence, RI (1999)
33. Keller, H.B.: Numerical solution of bifurcation and nonlinear eigenvalue problems. In: Rabinowitz, P. (ed.) Applications of Bifurcation Theory, vol. 38, pp. 359–384. Academic Press, New York (1977)
34. Knight, C., Derks, G., Doelman, A., Susanto, H.: Stability of stationary fronts in a non-linear wave equation with spatial inhomogeneity. J. Differ. Equ. **254**, 408–468 (2013)
35. Marangell, R., Jones, C., Susanto, H.: Localized standing waves in inhomogeneous Schrödinger equations. Nonlinearity **23**, 2059–2080 (2010)
36. Marangell, R., Susanto, H., Jones, C.: Unstable gap solitons in inhomogeneous nonlinear Schrödinger equations. J. Differ. Equ. **253**, 1191–1205 (2012)
37. McLaughlin, D., Scott, A.: Perturbation analysis of fluxon dynamics. Phys. Rev. A **18**, 1652–1680 (1978)
38. Nishi, K., Nishiura, Y., Teramoto, T.: Dynamics of two interfaces in a hybrid system with jump-type heterogeneity. Jpn. J. Ind. Appl. Math. **30**, 351–395 (2013)
39. Nishiura, Y., Teramoto, T., Ueda, K.I.: Dynamic transitions through scattors in dissipative systems. Chaos **13**, 962–972 (2003)
40. Nishiura, Y., Teramoto, T., Ueda, K.I.: Scattering and separators in dissipative systems. Phys. Rev. E **67**, 056 210 (2003)
41. Nishiura, Y., Teramoto, T., Yuan, X., Ueda, K.I.: Dynamics of traveling pulses in heterogeneous media. Chaos **17**, 037 104 (2007)
42. Or-Guil, M., Bode, M., Schenk, C.P., Purwins, H.G.: Spot bifurcations in three-component reaction–diffusion systems: the onset of propagation. Phys. Rev. E **57**, 6432–6437 (1998)
43. Pegrum, C.: Can a fraction of a quantum be better than a whole one? Science **312**, 6432–6437 (2006)

44. Promislow, K.: A renormalization method for modulational stability of quasi-steady patterns in dispersive systems. SIAM J. Math. Anal. **33**, 1455–1482 (2002)
45. Rabinowitz, P.H.: On bifurcation from infinity. J. Differ. Equ. **14**, 462–475 (1973)
46. Rademacher, J.D.M.: First and second order semi-strong interaction in reaction–diffusion systems. SIAM J. Appl. Dyn. Syst. **12**, 175–203 (2013)
47. Robinson, C.: Sustained resonance for a nonlinear system with slowly-varying coefficients. SIAM J. Math. Anal. **14**, 847–860 (1983)
48. Schenk, C.P., Or-Guil, M., Bode, M., Purwins, H.G.: Interacting pulses in three-component reaction–diffusion systems on two-dimensional domains. Phys. Rev. Lett. **78**, 3781–3784 (1997)
49. Seydel, R.: Practical Bifurcation and Stability Analysis. Interdisciplinary Applied Mathematics, vol. 5. Springer, New York (2010)
50. Teramoto, T., Yuan, X., Bär, M., Nishiura, Y.: Onset of unidirectional pulse propagation in an excitable medium with asymmetric heterogeneity. Phys. Rev. E **79**, 046 205 (2009)
51. Vanag, V.K., Epstein, I.R.: Localized patterns in reaction–diffusion systems. Chaos **17**, 037 110 (2007)
52. van Heijster, P., Chen, C.N., Nishiura, Y., Teramoto, T.: Localized patterns in a three-component FitzHugh–Nagumo model revisited via an action functional. J. Dyn. Differ. Equ. **30**, 521–555 (2016)
53. van Heijster, P., Doelman, A., Kaper, T.: Pulse dynamics in a three-component system: stability and bifurcations. Physica D **237**, 3335–3368 (2008)
54. van Heijster, P., Doelman, A., Kaper, T., Nishiura, Y., Ueda, K.I.: Pinned fronts in heterogeneous media of jump type. Nonlinearity **24**, 127–157 (2011)
55. van Heijster, P., Doelman, A., Kaper, T.J., Promislow, K.: Front interactions in a three-component system. SIAM J. Appl. Dyn. Syst. **9**, 292–332 (2010)
56. van Heijster, P., Sandstede, B.: Planar radial spots in a three-component FitzHugh–Nagumo system. J. Nonlinear Sci. **21**, 705–745 (2011)
57. van Heijster, P., Sandstede, B.: Coexistence of stable spots and fronts in a three-component FitzHugh–Nagumo system. RIMS Kokyuroku Bessatsu **B31**, 135–155 (2012)
58. van Heijster, P., Sandstede, B.: Bifurcations to travelling planar spots in a three-component FitzHugh–Nagumo system. Physica D **275**, 19–34 (2014)
59. Ward, M.J., McInerney, D., Houston, P., Gavaghan, D., Maini, P.: The dynamics and pinning of a spike for a reaction–diffusion system. SIAM J. Appl. Math. **62**, 1297–1328 (2002)
60. Wei, J., Winter, M.: Spikes for the Gierer–Meinhardt system with discontinuous diffusion coefficients. J. Nonlinear Sci. **19**, 301–339 (2009)
61. Yadome, M., Nishiura, Y., Teramoto, T.: Robust pulse generators in an excitable medium with jump-type heterogeneity. SIAM J. Appl. Dyn. Syst. **13**, 1168–1201 (2014)
62. Yuan, X., Teramoto, T., Nishiura, Y.: Heterogeneity-induced defect bifurcation and pulse dynamics for a three-component reaction–diffusion system. Phys. Rev. E **75**, 036 220 (2007)